



**DISSIPATIVE INSTABILITY
IN PARTIALLY IONISED
PROMINENCE PLASMA**

Marios Alexandrou

**Submitted for the degree of
Doctor of Philosophy
Department of Solar Physics
School of Maths and Statistics
July 2015**

**Supervisors: Dr Istvan Ballai &
Professor Robertus Erdélyi
University of Sheffield**

ACKNOWLEDGEMENTS

I would like to thank my supervisor, Dr. Istvan Ballai, who helped me throughout these long years in my good times and my difficult times, always believing in me. Without his help I would not have made it for sure. Cheers Istvan.

Cheers to Chris Nelson for all his help compiling the thesis.

I would also like to thank my family: my father Emilios, my mother Anthoulla and my brother Linos for all their support , material and psychological.

Cheers to my friends Pavlos and George whose precious time outs made the working days bearable.

This thesis is specially dedicated to my mother Anthoulla, the best mother anyone could ever wish for, a mother who was there for me in my personal tragedies and helped me stand up and stay up. Thank you for believing in me and for showing me how to get through this difficult path with dignity and courage.

ABSTRACT

Solar prominences are among the most enigmatic structures in the solar atmosphere whose study is made difficult by their complex evolution and the multitude of important effects appearing in them. Beside a natural curiosity, their importance stems from the recognition that almost 80% of the observed coronal mass ejections (CMEs) - believed to drive the space weather- have a cold chromospheric core believed to originate from a prominence, which is why the study of the generation and evolution of prominences is necessary. The difficulty in studying prominences arises from the complex dynamics occurring in these magnetic features, but also because of their intrinsic structure and properties. Significant advancement in the study of prominences was made when high-resolution observations of waves, oscillations, and flows became available. Scientists were able to connect theoretical models with observations through seismological techniques in order to derive quantities and understand properties (e.g. structure of the magnetic field, transport mechanisms acting in prominences, internal structure, etc.) that cannot be measured directly or indirectly. One of the fundamental properties of solar prominences is that due to their relatively low temperature, the plasma is not fully ionised and its description therefore needs special attention, especially when compared to the fully ionised coronal plasma that surrounds prominences. The ionisation degree of prominences is not well known, but there is plentiful evidence that this cannot be neglected when one studies the dynamics and stability of these structures. The aim of the following thesis is to investigate the generation of dissipative instability at the boundary between the viscous corona and the partially ionised prominence plasma, or at the interface between various prominence fine structure in the incompressible limit. The importance of the partial ionisation is investigated in terms of the ionisation fraction or ionisation degree. By matching the solutions for the transversal component of the velocity and total pressure at the interface between the prominence and its surrounding, we derive dispersion relations whose imaginary parts

describe the evolution of the instability. Results are obtained in the limit of weak dissipation. Using simple analytical methods, we detect the spectrum of equilibrium flows for which dissipative instabilities appear. While viscosity tends to destabilize the plasma, the effect of partial ionisation (through the Cowling resistivity) will act towards stabilizing the interface. For ionisation degrees closer to a neutral gas the interface will be unstable for larger values of equilibrium flow. The same principle is assumed when studying the appearance of instability at the interface between prominences and dark plumes. The unstable mode appearing in this case has a very small growth rate and dissipative instability cannot explain the appearance of flows in plumes. The same principles will be applied when studying the generation of dissipative instability in the case of waves propagating in a magnetic slab. The present study improves our understanding of the complexity of dynamical processes in solar prominences, and the role partial ionisation can have on the stability of the plasma. Our results clearly show that the problem of partial ionisation introduces new aspects of plasma stability with consequences on the evolution of solar prominences.

Contents

1	Introduction	1
1.1	The sun	1
1.2	The solar atmosphere	7
1.2.1	The photosphere	8
1.2.2	The chromosphere	10
1.2.3	The transition region	12
1.2.4	The corona	13
1.3	Prominences	15
1.3.1	Physical parameters of solar prominences	18
1.4	Prominence oscillations	19
1.5	Theoretical models for oscillating prominences	23
1.5.1	Isothermal plasma slab of finite width	24
1.5.2	Single fibril model	25
1.5.3	Models treating equilibrium configurations as a line-current	26
1.6	Motivation for prominence study	26
1.7	Overview of this thesis	28
2	Magnetohydrodynamics	31
2.1	MHD equations	33
2.2	MHD waves	37
2.2.1	Linearised ideal MHD equations	38
2.2.2	MHD waves	39
2.2.3	Waves in a uniform atmosphere	43
2.3	Waves in structured media	44

2.3.1	Waves at a single interface	45
2.3.2	Waves in magnetic slabs	48
3	MHD equations in partially ionized plasma	53
3.1	Partially ionized plasma	53
3.2	Continuity equation	56
3.3	Momentum equation	56
3.4	The energy equation	59
3.5	Equation of state	60
3.6	Ohm's law	60
3.7	Induction equation	62
3.8	Summary of single-fluid MHD equations for partially ionised plasma	63
4	Dissipative instability in partially ionised prominence plasmas¹	66
4.1	Introduction	66
4.2	Governing equations and basic assumptions	69
4.2.1	Equilibrium	69
4.2.2	Basic assumptions	70
4.2.3	Governing linearised equations	74
4.3	Dispersion relation of surface waves propagating at the tangential discontinuity	76
4.3.1	Instability conditions	79
4.4	Dissipative instabilities in the two-fluid approach	85
4.5	Conclusions	93
5	Dissipative instability in a partially ionised prominence plasma slab²	95
5.1	The equilibrium configuration	96
5.2	Dispersion relation of surface waves propagating in the slab	100
5.3	Dissipative instability	102
5.4	Conclusions	115
6	Conclusions	117
6.1	Future possible research avenues	120

List of Figures

1.1	The Sun seen in the 304 Å bandpass (courtesy of NASA/SDO/AIA and the AIA science team)	2
1.2	The interior of the Sun featuring the core, the radiative zone and the convective zone (courtesy of NASA/SDO/AIA and the AIA science team).	4
1.3	Temperature and density diagrams of the interior of the Sun shown on the left and on the right, respectively (where height is given as a fraction of solar radius, R_{\odot}). Both diagrams are adopted from the Dalsgaard Model S for the solar interior. Vertical lines show the heights of each layer of the solar interior	4
1.4	The proton-proton fusion taking place in the solar core, releasing most of the Sun's energy (Adopted from a diagram in Horizons by M. Seeds (1991)).	5
1.5	The Sun is rotating with a mean period of 25.38 days (mean frequency 456 nHz). The period varies with latitude and depth (Glatzmaier, 1981).	6
1.6	The photosphere of the Sun seen in white light - the only visible surface of the sun observed from the earth (courtesy of SOHO science team).	8
1.7	The chromosphere of the Sun seen in H_{α} emission line (courtesy of NOAA). The dark patches seen here on the surface of the Sun are cool and dense prominences that appear dark because they are cooler than their surrounding.	11

LIST OF FIGURES

1.8	The temperature and density profiles of the solar atmosphere. Here the very steep temperature gradients in the transition region are clearly seen. (Given by the VALC model of Vernazza et al. (1981))	12
1.9	The solar corona - looks like the faint halo which surrounds the Moon during a total solar eclipse (obtained with EIT instrument onboard SoHO)	14
1.10	An active prominence in an active region and a nearby solar flare seen in H_α (courtesy of TRACE)	16
2.1	The variation of plasma-beta (defined by Eq. (2.24)) in the solar atmosphere. The plot has been adapted from Gary (2001)	40
2.2	Analysis of the 3 MHD waves in a polar diagram. Adopted from Denmark Solar System school. Lectures On Space Plasma Physics 2007.	44
2.3	Sketch of the kink and sausage modes supported by a magnetic waveguide.	49
2.4	Sketch of the surface and body modes supported by a magnetic waveguide.	50
2.5	The dispersive diagram of modes arising in a coronal magnetic slab. Note that no surface modes are able to propagate in these structures (adapted from Edwin and Roberts 1982)	51
4.1	The interface between the corona (labeled with index “1”) and the solar prominence (labeled with index “2”) is situated at $z = 0$ in a two-dimensional $(x - z)$ Cartesian reference system. Regions 1 and 2 correspond to $z < 0$ and $z > 0$, respectively. The equilibrium flow is denoted by v_0 for region 2 and is parallel to the interface. In region 1 equilibrium flow is static. Magnetic fields differ in magnitude in the two regions but they are both parallel to the interface	71

4.2	Variation of the imaginary part of the frequency for the backward propagating wave with the flow speed and the ionisation fraction. The flow changes in the interval $10-60 \text{ km s}^{-1}$ and the ionisation fraction varies between 0.5 (fully ionised plasma) and 1 (neutral gas). The horizontal curve drawn at the $Im(\omega) = 0$ helps to visualize the transition of $Im(\omega)^-$ from the positive to the negative domain. . . .	82
4.3	Contour plot of the variation of the imaginary part of the frequency for <i>backward</i> propagating waves. The region below the zero level curve corresponds to a stable regime and waves will have a classical damping, while the interface described by the quantities in the region above the curve is unstable.	83
4.4	We denote by the indices 1 and 2 the regions corresponding to $z < 0$ and $z > 0$, respectively which correspond to two partially ionised plasmas of different ionisation fraction. The equilibrium flows are denoted by v_{01} and v_{02} and they are parallel to the interface. Magnetic fields are identical in the two regions and parallel to the interface.	86
4.5	The variation of imaginary part of the frequency belonging to the ion fluid with the background flow for three different values of collisional frequency (here quantified by the parameter α). The solid line corresponds to $\alpha = 0.1$, the dashed line to $\alpha = 0.5$, and the dash-dotted line to $\alpha = 1$. Waves are unstable for those values of v_0 and α for which the imaginary part of the frequency becomes positive. . .	92
5.1	Magnetic slab of thickness z_0 lying along the x -axis lies between two semi-infinite planes, with interfaces situated at $z = 0$ and $z = z_0$. The magnetic field in the three regions are taken to be identical and parallel to the x axis. The first model represents a partially ionised prominence slab fibril (shown as P) immersed into the fully ionised and viscous solar corona (shown as C in Fig. 5.1). The second and third models consist of a partially ionised prominence fibril (shown as F in Fig. 5.1) sandwiched by an interfibril partially ionised prominence plasma (shown as IF). The latest two models engage opposite directions in their equilibrium flows.	97

5.2	The variation of the Kelvin-Helmholtz speed with the dimensionless quantity kz_0 for model 1 on logarithmic scale for three different values of the density contrast between the solar prominence and neighboring solar corona.	105
5.3	Similar to Fig 5.1, but here the variation of v_{KH} with the dimensionless quantity kz_0 refers to models 2 and 3.	105
5.4	Contour plot of the variation of $Im(\omega)$ in the case of sausage (solid lines) and kink (dashed) modes in terms of background equilibrium flow and the value of the dimensionless parameter kz_0 for model 1. Here $\mu = 0.95$	108
5.5	Contour plot of the variation of $Im(\omega)$ in the case of sausage (solid lines) and kink (dashed) modes in terms of ionisation degree and the value of the dimensionless parameter kz_0 for model 1. Here $v_0 = 30 \text{ km s}^{-1}$. The region where instability occurs is shown by the <i>plus</i> symbols.	109
5.6	Contour plot of the variation of $Im(\omega)$ in the case of sausage modes in terms of the ionisation degree of the external medium and the value of the dimensionless parameter kz_0 for model 2. The region where instability occurs is shown by the <i>plus</i> symbols.	111
5.7	Contour plot of the variation of $Im(\omega)$ in the case of kink modes in terms of the ionisation degree of the external medium and the value of the dimensionless parameter kz_0 for model 2. The region where instability occurs is shown by the <i>plus</i> symbol.	112
5.8	The same as in Fig. (5.5) but now the contour plots show the variation of $Im(\omega)$ in the case of sausage modes in terms of the ionisation degree of the external medium and the value of the dimensionless parameter kz_0 for model 3.	113
5.9	The same as in Fig. (5.5) but now the contour plots show the variation of $Im(\omega)$ in the case of kink modes in terms of the ionisation degree of the external medium and the value of the dimensionless parameter kz_0 for model 3.	114

Chapter 1

Introduction

1.1 The sun

The Sun (Fig. 1.1) has always been worshipped throughout the history of mankind. Associated or even identified with gods through ancient legends of Greeks, Chinese, Japanese and many others, the Sun has always been the most spectacular celestial object, being respected and feared due to its role in maintaining life on Earth.

Our Sun has also been an object of observation since eclipses started to be recorded and predicted by the Chinese as early as 2000 BC and by the Greeks later on. In the years that followed, ancient Greek scientists recorded the first visions of sunspots with naked eye (Theophrastus of Athens, a pupil of Aristotle), and elementary predictions of planetary motions were made.

The knowledge about our Sun has gone through a series of changes in the last millennia. In the beginning it was believed that the Sun was orbiting around the Earth and besides, faulty predictions of the distance between Earth and Sun were determined. In the mid-centuries Copernicus suggested that the known 6 planets orbit around the Sun, while Kepler defined his laws of planetary motion. Shortly after, Galileo - using the recently invented telescope - had clearer visions of sunspots.

In 1666 Newton formulated the classical gravitational law and applied it to the planetary motions around the Sun. Euler measured exactly the distance from Sun to Earth at 93 million miles. Later on, in the nineteenth century, eclipses were studied systematically and prominences were recorded.

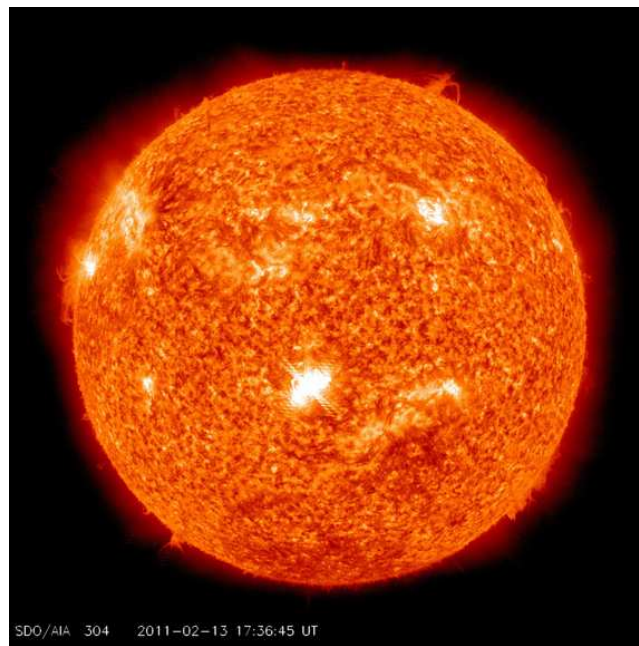


Figure 1.1: The Sun seen in the 304 Å bandpass (courtesy of NASA/SDO/AIA and the AIA science team)

The use of telescopes during eclipses changed considerably the amount and quality of the knowledge about our Sun. In this way astronomers were able to see clearly the outer layers of the solar atmosphere (the chromosphere and corona).

The sunspots were now related to geomagnetic storms while the first solar flare was recorded by Carrington and Hodgson in 1859. The Sun was already considered as a gaseous sphere and a new element, called *Helium*, was discovered at an eclipse, followed by the invention of the spectroheliograph by Hale in 1889.

In the early twentieth century sunspots were identified with strong magnetic fields. The coronagraph was invented in order to be able to observe the corona without an eclipse. Furthermore, emission lines were deduced to be arising from ionized normal elements (hydrogen and other heavier elements) by the extremely hot corona.

The second half of the 20th century witnessed many astonishing developments and discoveries, like the existence of the later called Alfvén waves, the necessity of heating of the solar upper atmosphere, the cool temperature of the sunspots due to inhibition of convection, the invention of magnetograph, the discovery of solar wind,

and of course the amazing pictures and invaluable information provided by solar telescopes on space satellite missions in high resolution.

The Sun is a hot, dense, auto-gravitational sphere of plasma at the center of our solar system. It is an ordinary star of spectral type $G2V$ with absolute magnitude 4.8. The Sun is 4.5 billion years old and has a mass of 1.99×10^{30} kg meaning more than 333,000 times the mass of the Earth. The Sun's diameter is almost 1.4 million km which is 109 times larger than the Earth's diameter. The central $0.25R_{\odot}$ of the Sun (barely one 50th of the Sun's volume) carries half of the solar mass - meaning non-homogeneous density which has a mean value of roughly a quarter of the Earth's mean density.

The surface gravity is 28 times larger than the corresponding Earth's surface gravity and thus the escape velocity comes out to be about 55 times larger than the escape velocity from Earth. The Sun is rotating with a mean period of 25.38 days and it has a mean distance from the Earth of about 150 million km (often also called 1 Astronomical Unit, 1AU). The surface temperature averages to 5785 K, while every second the Sun is losing one billion kg of its mass.

The Sun can be divided into two main regions, the interior and the exterior. Unlike the exterior, the interior is not directly observable. However, a variety of methods can be used to study internal structure, such as measurement of neutrino fluxes and global oscillations for helio-seismology (the study of oscillations at the solar surface). The solar interior is composed of approximately 90% hydrogen, 10% helium and a very small percentage in the form of heavier atoms, such as oxygen, carbon and nitrogen and other elements. The majority of this stellar material is a highly ionised gas due to the high temperature within the interior and has densities similar to liquids on Earth. Although the ionised gas is almost entirely composed of positively and negatively charged particles, it is electrically neutral and the particles exhibit a collective behavior. This material state is known as a plasma state and it is the most extended form of matter in the universe. The interior can be further divided into three regions (see Fig. 1.2). At the centre is the core (confined to the central $0.25 R_{\odot}$), where the majority of the Sun's energy is produced. Half of the mass of the Sun is contained within the core, which has temperatures of the order 15 million K and densities of $1.5 \times 10^5 \text{ kg m}^{-3}$, which is about 150 times the density of water (see Fig. 1.3).

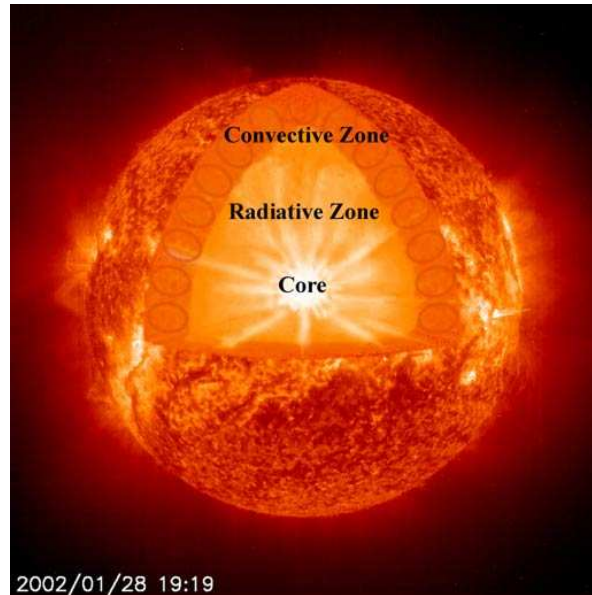


Figure 1.2: The interior of the Sun featuring the core, the radiative zone and the convective zone (courtesy of NASA/SDO/AIA and the AIA science team).

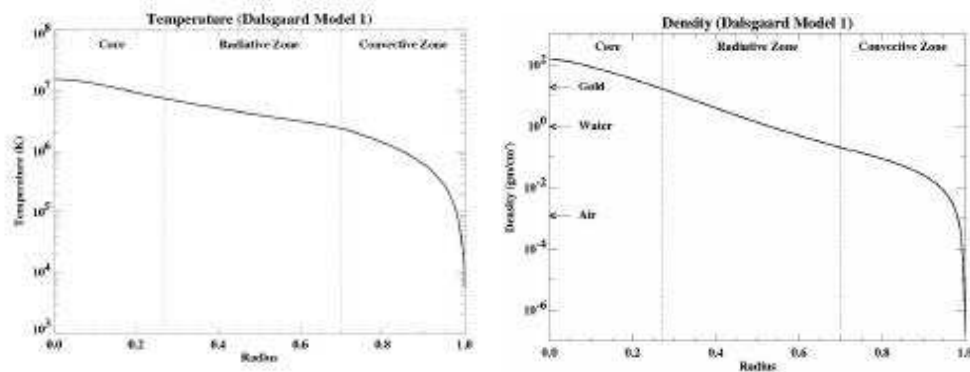


Figure 1.3: Temperature and density diagrams of the interior of the Sun shown on the left and on the right, respectively (where height is given as a fraction of solar radius, R_{\odot}). Both diagrams are adopted from the Dalsgaard Model S for the solar interior. Vertical lines show the heights of each layer of the solar interior .

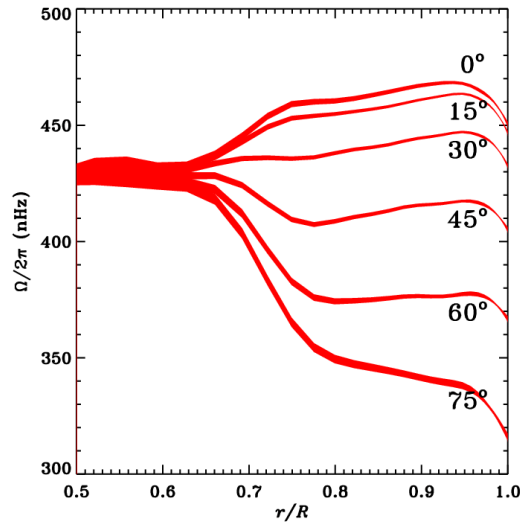


Figure 1.5: The Sun is rotating with a mean period of 25.38 days (mean frequency 456 nHz). The period varies with latitude and depth (Glatzmaier, 1981).

Sun.

The photons are absorbed and re-emitted by electrons and neutrons, simultaneously releasing energy to the surrounding plasma. Because of the high density, the process is repeated so many times during these 10 million years, that the initially high-energy gamma rays enlarge their wavelength due to collisions, until they reach the surface where they become our familiar visible light.

The temperature in the radiative zone varies from 8 million K (inner radiative zone) to half a million K (outer radiative zone), while the corresponding density varies from $20,000 \text{ kg m}^{-3}$ to 200 kg m^{-3} .

Finally, the convective zone extends from the radiative zone out to the surface and here the energy is transported by convection. There is though, an intermediate extremely thin layer between radiative and convective zones, the tacholine (Spiegel and Zahn, 1992), where it is believed that the Sun's magnetic field is generated (Aschwanden, 2008) through a dynamo process.

According to this theory, in the convective zone the rotation of the Sun has variable period depending on the latitude. So, the period of the rotation increases by up to 9 days as we move from the Sun's equator out to the poles (see Fig. 1.5). Combining

this with the convective zone's relatively low temperatures, which accommodates fewer fully ionized elements, heavier elements may sustain their electrons, which by turn switches the main energy transfer mechanism from radiative to convective.

In this process, assuming very steep density and temperature gradients, convective instability occurs and as a result large 'blobs' of plasma are displaced vertically that can enlarge enough to lower the density and induce buoyancy. Once the 'blobs' reach the surface of the Sun, the energy escapes into the solar system.

The rising plasma "blobs" then cool down and sink back into the convective zone, being replaced by hotter convectively unstable plasma 'blobs' from below. The temperature in the convective zone varies from 500,000 K to 6,600 K. The corresponding densities vary from 20 kg m^{-3} to $8 \times 10^{-5} \text{ kg m}^{-3}$.

1.2 The solar atmosphere

The solar atmosphere is the visible, exterior region and is composed of four distinct layers. Considerable parts of these layers are dominated and connected by the magnetic field which provides a wide variety of fine structure in the atmosphere. Each of the external layers, known as the photosphere, chromosphere, transition region and the corona, have their own array of distinct magnetic features. Nowadays, these solar regions are rigorously studied in great detail using space-born and Earth-based telescopes, e.g. the Transition Region and Coronal Explorer (TRACE), Solar and Heliospheric Observatory (SOHO), Hinode, the Solar Dynamic Observatory (SDO) and the Interface Region Imaging Spectrograph (IRIS) that are continuously corroborated with terrestrial imaging and spectral instruments that are able to observe the atmosphere with a relatively high spatial and temporal resolution in visible, EUV, X-ray and radio wavelengths.

Each atmospheric layer has characteristic wavelengths associated with certain spectral lines, allowing the regions to be viewed individually. However, these layers are not separate from each other and are magnetically coupled. The layers are interwoven by the complex network of magnetic field lines originating from below the surface, reaching high up in to the corona and extending far out into interplanetary space.

One of the tasks of the observing instruments is to study oscillatory phenomena

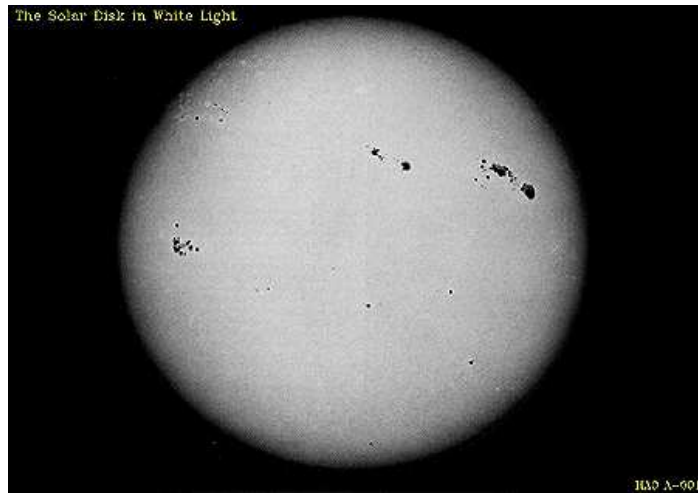


Figure 1.6: The photosphere of the Sun seen in white light - the only visible surface of the sun observed from the earth (courtesy of SOHO science team).

that occur across the surface and throughout the atmosphere. The oscillations are of interest as they provide information about the physical state of the local plasma and the dynamical events that occur within the internal regions (e.g. convection) and the atmosphere (e.g., nanoflares, flares, coronal mass ejections). We can describe the oscillatory motions of the magnetic structures by using the equations of magnetohydrodynamics (MHD) (see Section 2.1).

1.2.1 The photosphere

The photosphere (see Fig. 1.6) is the lowest layer in the solar atmosphere and its name can be derived from the Greek language meaning ball of light. This name was attributed due to the fact that photosphere is the only visible surface of the Sun observed from the Earth.

Visible light is only part of the emission from photosphere since electromagnetic waves from all the frequency spectrum are detected to be emitted. The photosphere is an extremely thin layer (500 km thick) of relatively dense plasma which emits most of the solar radiation. Temperatures vary from 5800 K (low photosphere) to 4300 K at the top.

The photosphere has a highly non-uniform magnetic structure. Regions where

1.2. THE SOLAR ATMOSPHERE

patterns of magnetic elements are arranged, are called active regions, which give way to areas of large magnetic flux (corresponding to fields of a few thousand G).

In the photosphere we can distinguish irregularly shaped granules which are small (about 1000 km long) cellular features that cover all the surface of the Sun except for the areas which are covered by sunspots. Granules are the tops of convection cells where hot plasma emerges from the interior towards the bright areas, spreads throughout the surface, cools down, and then sinks back again along the dark lanes. Each granule lasts for about 20 minutes. The granulation scene is continually changing as old granules are pushed aside to give way to newly uprisen ones. The flow inside a granule may reach supersonic speeds (relative to the position of the granule) of more than 7 km s^{-1} and create sonic 'booms' and other noise which produce waves on the Sun's surface.

A distinctive feature of the solar photosphere is sunspots. Sunspots are seen as dark spots on the surface of the Sun. Temperatures in the dark centers of sunspots drop down to 3700 K (compared to 5700 K for the surrounding photospheric plasma). They normally live for a few days, although very large ones may last for some weeks. Sunspots are highly magnetic regions on the solar photosphere with magnetic fields thousands of times stronger than the Earth's magnetic field. Most of the times, sunspots are appearing as two sets of spots. One set will have positive sign (where the field emerges) while the other set will have negative sign (where the field returns into the solar interior). In the darker parts of the sunspots - the umbra - the field is strongest, while in the lighter part - the penumbra - the magnetic field is weaker and more horizontal. Sunspots are also the location where massive magnetic fluxes emerge to the surface (see, e.g. Sobotka, 2003; Solanski, 2003).

Magnetic field (although weaker than in sunspots) can also emerge in, e.g. faculae which are bright regions that one can easily observe near the solar limb, or the edge of the disk. They are magnetic regions as well as the sunspots, whose magnetic field though is concentrated in much smaller bundles than in sunspots. Where the sunspots make the Sun look darker, the faculae in contrary make the sun look brighter.

Magnetic pores are also seen on the photosphere and they are basically small sunspots with simpler magnetic structure. They may reach the chromosphere and as they do so they become larger (see, e.g. Sobotka, 2003; Thomas and Weiss, 2004).

Magnetic pores have diameters upto 16 Mm. The pores are regions of intense magnetic field (~ 1700 G) and can be seen in the photosphere, but as they expand as they reach chromospheric territories. Pores' behavior is very dynamic because of the constant buffeting from the convective motion of granules at the photospheric level (Sobotka, 2003). There have recently been observations of photospheric structures experiencing a vortex style motion, which could act as a driver for a wide variety of waves and oscillations (Bonet et al. 2008). These waves and oscillations may have the ability to propagate upwards across the lower solar atmospheric layers along the length of the pore, which is acting as an MHD waveguide. Most of these waves though, will be reflected at the transition region due to the steep temperature gradients in sound or Alfvén speeds. Some of them though, will manage to get into the corona. The transmitted fraction of the waves may be related to MHD wave heating or magneto-seismology of the solar corona (see, e.g. Klimchuk, 2006; Erdélyi and Ballai, 2007). One of the interesting new discoveries associated with magnetic elements in the lower layers of the solar atmosphere is the proof of the existence of torsional Alfvén waves (Jess et al. 2009), which have been known to be difficult to detect. Due to the steep decay in density, upward propagating waves can easily steepen into shock waves that could provide the heating of the lower parts of the atmosphere.

1.2.2 The chromosphere

On top of the photosphere we find the chromosphere (a typical image of the chromosphere is shown in Fig. 1.7). The name has also Greek origin and it means ball of color. It has an average thickness of 2 Mm and presents a steady temperature gradient starting at 4,000 K at the base and ending at 20,000 K at the top. Recent detailed observations have suggested that the chromosphere is not a homogeneous layer with constant thickness surrounding the Sun. It is now believed to be compressed or expanded in specific areas, due to the interactions of the chromosphere with the underlying photosphere or the over-lying transition region. In other words the existence or the absence of an active region or a sunspot on a specific region of the photosphere not only affects the surrounding temperature, density and pressure but also the height at which chromosphere will start above the specific region. Moving outwards we de-



Figure 1.7: The chromosphere of the Sun seen in H_α emission line (courtesy of NOAA). The dark patches seen here on the surface of the Sun are cool and dense prominences that appear dark because they are cooler than their surrounding.

tect that mean density and pressure are decreasing. At chromospheric temperatures the light emitted by hydrogen has a reddish color (H_α emission, i.e. the Balmer emission line in the spectrum of hydrogen). This reddish emission may also be observed in prominences that are visible above the solar limb during total eclipses of the sun. If now we observe the Sun through a spectrograph or a filter which can isolate the H_α emission, a rich scene of solar figures can be seen, like the chromospheric network of magnetic field elements, bright plage around sunspots, prominences projecting above the limb and dark filaments on disk. One key characteristic of the chromosphere (and technically speaking about regions below the chromosphere) is that it contains plasma that is not fully ionised. Dynamics in this sort of plasma constitutes the working environment of the research presented in this Thesis.

The chromosphere is an arena of dynamic activity. In just a few minutes one can observe the changes in solar flares, prominence and filament eruptions, and the plasma flow in magnetic loops following the end of a solar flare. We may see the chromosphere by detecting the light that ionized calcium - Ca II - emits, in the violet region of the solar spectrum at a wavelength of 393.4 nanometers (the Calcium K-line).

Recent high-resolution observations have shown the importance and complexity of waves within the chromosphere. Spicules, usually observed as vertical extensions

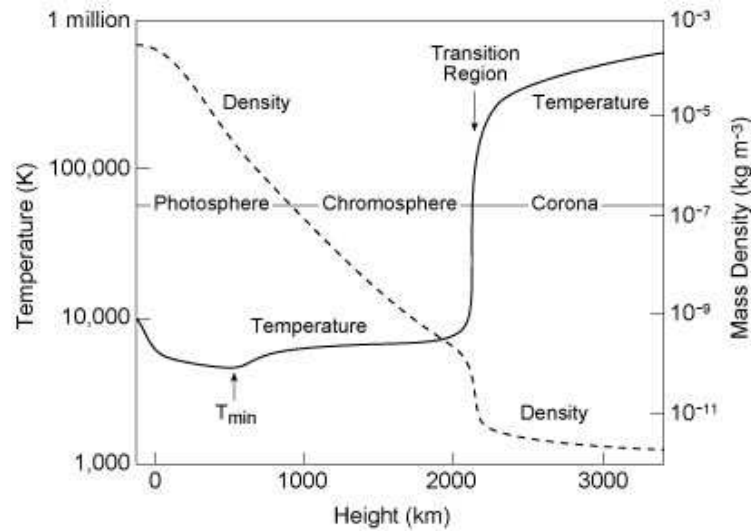


Figure 1.8: The temperature and density profiles of the solar atmosphere. Here the very steep temperature gradients in the transition region are clearly seen. (Given by the VALC model of Vernazza et al. (1981))

away from the Sun provide one of the suspects for supplying enough energy into the corona to ensure the rapid heating which occurs there. As well as this, more horizontal structures, such as mottles, have been found to be energetic, standing sausage waves.

Besides, waves propagating upwards around sunspots and pores have been shown to penetrate into the lower transition region, with the capacity to release huge amounts of energy (see, e.g. De Pontieu et al. 2004, Freij et al. 2014).

Thus we can deduce that the chromosphere is a very dynamic layer of the solar atmosphere and in a complex, though still not clear way, it collaborates with the photosphere to transfer energy into the corona, contributing to the mystery of coronal heating.

1.2.3 The transition region

The thin and very irregular transition region is the most interesting, intriguing and confusing region of the solar atmosphere primarily because of the huge temperature gradients which exponentially lift the temperature from 20,000 K to 1,000,000 K

(see Fig. 1.8) while, at the same time, clear observations of this region and proper theoretical formulation is still far from accomplished. The very high temperatures provoke the full ionisation of Hydrogen which in turn is difficult to observe. On the contrary, ions such as C IV, O IV, and Si IV are easily detected in the light emitted by the Transition Region. The light that these ions emit is in the ultraviolet part of the solar spectrum, and this is only accessible from space. The very steep temperature gradients make the investigation of the role of the transition region in the energy flow process of the solar atmosphere very difficult to model.

The transition region is the location of various energetic phenomena that have been observed recently in the form of small-scale ‘sparkles’ which are suspected to be leftovers of reconnection events of small magnitude, referred to as nano-flares, taking place in the transition region, and these could be responsible for transferring energy to heat the surrounding plasma to temperatures of millions of Kelvin. Blinkers (see, e.g. Harrison, 1997) are larger-scale events in the transition region, with diameter of several millions of km. The steep variation of the temperature makes the transition region a filter region too, some of the waves coming from the lower regions being reflected, thus forming a chromospheric resonant cavity. Equally, perturbations coming from the solar corona in the form of global shocks (as a result of, e.g. a CME) can generate secondary running waves along the transition region.

1.2.4 The corona

The solar corona (see Fig.1.9) is the outer and the most extended layer of the solar atmosphere, starting from the transition region and extending out into the solar system till the Earth and beyond. It can be seen only during eclipses (looks like the faint halo which surrounds the Moon during a total solar eclipse) or using a coronagraph which is an instrument to hide exactly the solar disc as the Moon is doing during an eclipse. Corona is yet another Greek word which means crown as the halo mentioned above.

The mean density and pressure in the solar corona are very low but the temperatures are estimated to be in excess of 1 million K (see Fig. 1.8). X-ray and (E)UV observations by high resolutions space satellites (SOHO, TRACE, HINODE, SDO, etc.) have given us a new picture about the dynamics of the corona. The magnetic



Figure 1.9: The solar corona - looks like the faint halo which surrounds the Moon during a total solar eclipse (obtained with EIT instrument onboard SoHO)

structure of the corona reveals a complex network of magnetic fields which are continuously changing and can be separated into two magnetic zones: (i) open regions of magnetic field, like coronal holes and the solar wind, and (ii) closed magnetic regions, like coronal loops. Since the Skylab mission it is known that the corona consists of a variety of coronal loops with strong emissions, and a large range of lengths, densities, etc. at very high temperature. Since the plasma-beta is much smaller than 1 in the corona, the plasma is controlled by magnetic forces and one may use coronal loops to trace coronal magnetic field lines. The characteristics of coronal loops are ranging in a wide spectrum. The small X-ray bright points which have time scales of around 8 hours are believed to be loop structures while coronal loops are thought to be expanding to form large prominences, sometimes upto 100 Mm above the limb and last from few days upto a few months. Some of the loops are closed with their foot-points being magnetically opposite and are restricted to the chromospheric and photospheric regions, extending as high as 300 Mm, while other loops are open, reaching out, deep in the infinite coronal regions and giving way to the solar wind. Using extrapolation techniques from the photosphere and also using coronal loop seismology, showed that intensities of the magnetic field inside coronal

loops vary between a few G up to 100 G (Priest, 1982). Measuring the widths of emission lines resulted to the conclusion that coronal loops are 5 to 10 times denser than their environment. This conclusion refers mostly to loops in active regions since they are more easily observable, especially shortly after a solar flare.

The very high temperature of the corona constitutes one of the biggest mysteries of the solar system, which remains a problem to be explained in the future. Given the role of the magnetic field, nowadays it is widely recognized that the heating process has to be of magnetic nature, the most promising mechanisms that could provide the required heating being magnetic reconnection and wave dissipation over short lengths scales (for an overview see, e.g. Klimchuk, 2006, Erdélyi and Ballai, 2007).

Magnetic reconnection is the mechanism that stays at the core of energetic events such as flares and coronal mass ejections (CMEs) and it is a mechanism that releases the magnetic tension that is later transformed into heat by (DC) current dissipation. The frequency though of such events is low. In contrast, waves dissipated over short scales through processes such as phase mixing or resonant absorption can transfer their kinetic energy into heat (often labeled as AC mechanisms). It is believed that closed magnetic structures are heated by magnetic reconnection, while the dominant heating mechanism in open structures is wave heating.

1.3 Prominences

Prominences (an illustrative example of a prominence seen in the wings of H_α is shown in Fig. 1.10) play a central role in our investigation and that is why we are going to present their characteristics and properties in detail.

Solar prominences are clouds of relatively cool ($\leq 10^4$ K) and dense gas ($\sim 10^{-12}$ kg m⁻³) being situated in a much tenuous and much hotter corona. These differences in temperature and density support the theory that prominences are of chromospheric nature (see, e.g. Engvold 1998, Lin 2005, Okamoto et al. 2007, Martin et al. 2008; Berger et al. 2008).

Prominences have typical lengths of 10^5 km, heights of 5×10^4 km and widths of 6×10^3 km. Prominences appear bright at the limb but on the disk they form dark ribbons called filaments. The different appearance of prominences can be explained in terms of the background (bright when the background is the interplanetary space

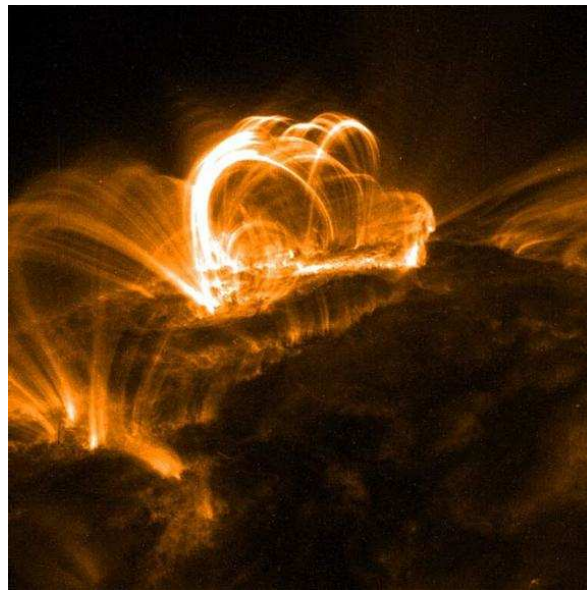


Figure 1.10: An active prominence in an active region and a nearby solar flare seen in H_{α} (courtesy of TRACE)

and dark when the background is the much hotter corona or chromosphere, see also Fig. 1.7). The magnetic fields thread them through, balance the force of gravity and inhibit the heat flow from the surrounding corona, where the temperature is at least two orders of magnitude higher.

It is known that prominences exist above polarity inversion lines dividing two regions of opposite magnetic polarity in the photosphere, therefore they are embedded in a larger coronal arcade that connects the two opposite polarity regions. Prominences can be classified into two categories:

- *Quiescent prominences*, which have a stable structure and can last for many months and they appear in regions far away from active solar regions
- *Active prominences*, that are associated with solar filaments and are dynamic structures with violent motions with lifetimes of minutes or hours

Prominences were first seen by naked eye in the 13th century during an eclipse and they were explained as *clouds on the moon*. Five centuries later and during another eclipse, they were described as *red flames* and in the 19th century with the help

of photography they were correctly assigned as *shiny masses of gas*.

Quiescent prominences show very delicate composure in the body of the filament, revealing that they consist of very thin threads (called fibrils) partially filled with cold plasma. Even though vertical figures of filaments can be seen in limb prominences (Dunn 1960), there is also evidence for the existence of horizontal fine structures within prominences (Schmieder and Mein 1989; Schmieder et al. 1991; Tandberg-Hanssen 1995). For instance, Simon et al. (1986) observed the velocities in quiescent filaments in H_α and C IV. From the H_α emission lines the filament was concluded to be consisting of many small-scale loops whose foot-points occupied various positions but surely not along the filament axis. Demoulin et al. (1987) concluded a thickness of the order of 10^3 and a length of the order of 10^4 km for the threads that compose a filament. Engvold et al. (1987) observed a quiescent prominence seen in projection against the disk, and considering the interface between the prominence and the surrounding corona, it was concluded that the prominence may be composed of thin magnetic flux ropes inclined at an angle of 20 degrees to the prominence long axis.

More recent high resolution H_α observations from ground-based Swedish Solar Telescope and Dutch Open Telescope both in Palma, have given detailed description of the fibrils to have an average width of 210 km and the length varying from 3500 to 28000 km (see, e.g. Lin et al. 2005; Heinzel and Anzer, 2006). From the theoretical aspect, even though several models were set up to explain the vertical filamentary structure of prominences, only a few models (Ballester and Priest, 1989; Degenhardt and Deinzer, 1993) were proposed to represent the horizontal fibril structure of solar prominences. Ballester and Priest (1989) proposed a model for the horizontal fibril structure of prominences, representing fibrils with slender flux tubes containing hot plasma throughout most of their length, and cool plasma near the summits (the regions of the prominence with lower temperature).

A prominence can be formed in as little as a day and it can last as long as a few months (quiescent prominences) or as little as a few minutes in the case of active prominences (Priest, 1982). Active prominences are found in active regions and are associated with solar flares. They can behave in a violent way according to their type which can be surges, sprays (erupting filaments) and loop prominences. The magnetic field is high (100 G) and the temperature is much higher than in a quiescent

prominence.

Near the end of their existence, prominences may have an instability which may cause eruption and sometimes together with coronal mass ejection or even solar flares. Quiescent prominences have very simple structure and may last for a few months. It all starts as a small active region filament located either along the magnetic inversion line between the two polarity regions of an active region or at the end of an active region where it meets the surrounding region of opposite polarity (Priest, 1982).

As the active region dissolves, the prominence becomes longer and thicker and turns into a quiescent prominence; it never stops moving, and it is heading towards the nearest pole.

1.3.1 Physical parameters of solar prominences

In comparison with active prominences, the quiescent ones have low temperatures (about 7000 K), weak magnetic field (5-10 G) and densities of the order of approximately $10^{-12} \text{ kg m}^{-3}$. Their size can reach 60 to 600 Mm in length, 15 to 100 Mm in height and 6 to 20 Mm in width. The magnetic field may vary according to the position and height within the prominence.

Sometimes both kinds of prominences-especially if their height exceeds 50,000 km, can become erupting prominences, with some material escaping the Sun and the rest returning back to the chromosphere. In more than half of the cases, after an eruption a prominence returns back to the initial quiescent form.

Observing solar prominences in the H_{α} , UV, EUV lines, one can detect down-flows and up-flows of plasma (Berger et al. 2008), and even horizontal flows. Velocities vary from 2 km s^{-1} to 35 km s^{-1} . In active prominences though speeds can reach 200 km s^{-1} and sometimes this represents the displacement of plasma during the formation of the prominence. Counter-streaming flows (oppositely directed flows) were also observed (Zirker et al. 1998).

Observations also show that all the parameters within an individual prominence (magnetic flux, temperature, density and pressure) vary with time and position (Patsourakos and Vial, 2002). The same variability is applicable for their lifetime, stability and eruptive behavior - they vary from prominence to prominence even if the

configurations look similar.

Their structure is highly non-uniform and extremely delicate with thousands of fibrils (Tandberg-Hansen, 1967). The magnetic field is not isolated but suffers from the interaction of the common interface with the magnetic field of the surrounding corona.

Finally, prominences have been observed to oscillate with large amplitude oscillations mainly due to the influence of a nearby violent activity, like a solar flare or a Coronal Mass Ejection (CME) that could easily trigger a global coronal wave (sometimes labeled as EIT waves). Quiescent prominences though are also oscillating with smaller amplitudes (Harvey, 1969).

The observed oscillations (as standing or propagating MHD waves), are collaborated with theoretical models in order to derive valuable information about the intrinsic values of prominence parameters, e.g. the magnetic field's magnitude and structure, transport coefficients and the dynamics inside a prominence.

1.4 Prominence oscillations

Oscillations have been detected all around the regions of the sun with the outstanding example of the 5-minute period oscillation of the photosphere.

The whole sun is oscillating with large period oscillations and that can be observed by means of a telescope. The magnetic features in the corona though, are oscillating with a much shorter period. In order to obtain an estimate of physical parameters like temperature, density, magnetic flux and pressure in the complex structure of the corona, observable properties of waves and oscillations are compared to theoretical values and models enabling conclusions about the above mentioned parameters, whose direct computations (observational or theoretical) is very difficult to produce (see, e.g. Roberts et al. 1984; Uchida, 1967).

The first recorded prominence oscillation occurred more than 50 years ago (Moreton and Ramsey, 1960), but due to the difficulty of the inversion of the physical parameters, the specific research did not progress until the 90's. In that decade we were able to use detailed, high-resolution images from the observational point of view, as well as the progress in setting up reliable theoretical models that use the observed quantities like phase speed, period, damping time and flow speed and through an in-

1.4. PROMINENCE OSCILLATIONS

version technique, estimates were drawn about temperature, density, magnetic flux and pressure. The launch of high-resolution satellites has changed dramatically our understanding capabilities of the complex dynamical and energetic phenomena in the solar atmosphere, and solar prominences in particular, see Oliver and Ballester, (2002) and Engvold, (2001) for detailed reviews on prominence oscillations observations and theory.

From the observational aspect, prominence oscillations can be separated in two categories with respect to the amplitude of periodic variations: large amplitude and small amplitude oscillations. The first category arises when the whole prominence is shaken by a wave propagating on the Sun's surface, e.g. coronal global waves that are large scale waves propagating in the low corona being generated by a large flare and/or a CME (see, e.g. Ballai, 2007). In this category falls the so called *winking filament*, which refers to the optical effect of an event in which the line of sight velocity is large enough to make the emission of the material fall outside the sensitivity range of the instrument at the maxima of the oscillatory movement. When these large amplitude waves are generated, the prominence loses the equilibrium state and starts shaking with an amplitude of sometimes more than 20 km s^{-1} in a horizontal vibration (see, e.g. Eto et al. 2002; Okamoto et al. 2004). This may continue for several periods until it is damped.

Due to the large vibrating speed, the emission-transmission wavelength of the prominence is changing, and this helps the observational point of view to become clearer, e.g. in H_{α} filter, the filament is only visible when the prominence is at rest (at maximum displacement), whereas at the center of the oscillation (minimum displacement) the velocity (amplitude of the oscillation) is maximum and the filament becomes invisible. The periods vary from 30 minutes to 2 hours (Jing et al. 2006; Isobe and Tripathi, 2006). Jing et al. (2006), also suggested that a sub-flare at the end of a filament may cause an oscillation. For large amplitude oscillations there is lack of theoretical models to correspond the dynamics and the physical parameters of the oscillating medium. The reason is that these oscillations are very rare. Combining with the fact that high resolution observations became available only in the last 2 decades, the records of such oscillations are just not enough to set up reliable theoretical models. Some attempts have been made to introduce such models (Tripathi et al. 2009) but we still have a long way to progress.

1.4. PROMINENCE OSCILLATIONS

The second class of oscillations is frequently observed and may show spatial structure (can be even confined to a small region or a fibril). The amplitude of these oscillations is smaller, sometimes near the noise level, and seems to be related to proper modes of the structure. The amplitude varies between 0.1 km s^{-1} and 3 km s^{-1} , even though sometimes, larger amplitudes have been recorded (Terradas et al. 2002). For small amplitude oscillations though, because of the great frequency they occur, a variety of models have been designed. Using the linearized MHD equations, the analytical investigation of these modes reduces the solution of the dynamical system to a set of differential equations with boundary solutions.

Short amplitude oscillations may not affect the whole prominence but only a part of it. The small amplitude oscillations can be categorized in five categories according to the magnitude of their period, P , as seen in the following table:

Category	Period	References
Very short period	$P \leq 1 \text{ min}$	Balthasar et al. (1993)
Short period	$1 \text{ min} \leq P \leq 10 \text{ min}$	Tsubaki & Takeuchi (1986); Thomppson & Schmieder (1991); Yi et al. (1991)
Intermediate period	$10 \text{ min} \leq P \leq 40 \text{ min}$	Lin and Engvold (2002)
Long period	$40 \text{ min} \leq P \leq 8 \text{ h}$	Suematsu et al. (1990); Ter- radas et al. (2002)
Ultra long period	$P \geq 8 \text{ h}$	Fullon et al. 2004

Two-dimensional, high-resolution observations (Yi et al. 1991; Yi and Engvold, 1991) have shown that single fibrils or sets of fibrils may oscillate independently with their own periods, with a range of 3 to 20 minutes. Therefore, one of the mysteries of prominence seismology is whether periodic changes in prominences should as a principle depend on their fine fibril structure or not. Most of the observed oscillations and waves in fibrils showed some sort of damping, an effect that received special attention in solar prominences (see further down this chapter).

We should keep in mind though, that the period by itself cannot give exact interpretation of any physical parameter, since various combinations of physical parameters may result to identical periods. That is where phase velocities and wavelengths of the standing and the propagating waves come in the equation. Combining veloc-

1.4. PROMINENCE OSCILLATIONS

ities, wavelengths and periods, one may use inversion techniques to estimate values of physical parameters (Oliver and Ballester, 2002; Terradas et al. 2002; Engvold, 2008).

In addition to the information about periodicities, observations also allow the determination of other parameters of the oscillatory motion, e.g. wavelength and phase speeds. Malville and Schindler (1981) studied a loop prominence and detected periodic changes with a wavelength of 37,000 km, which together with a period of 75 minutes, results in a phase speed of about 8 km s^{-1} . Later, Thompson and Schmieder (1991) detected periodic motions in a filament fibril with periods between 3.5 and 4.5 minutes. Using these values and at the same time computing the wavelength of the observed motion to be approximately 50,000 km, they resulted a phase speed of 200 km s^{-1} . Later, Molowny-Horras et al. (1997) observed periodic velocity variations with period of 7.5 minutes. The linear variation of the Fourier phase with position allowed them to determine wavelengths of the order of 20,000 km, resulting in a phase speed of 44 km s^{-1} . Wavelength analysis of the same data showed the presence of a train of waves with periods of 7.5 minutes and a duration of about 12 minutes. The time occurrence of this train increased linearly with position, which agrees with the assumption of a propagating disturbance.

Yet another observed parameter of the prominence oscillations is damping time—that is the the time until the oscillation completely dissolves. The damping times in prominence oscillations are observed to be always smaller than 10 periods of the corresponding oscillation, and this is of particular interest since it gives partial inside information about the the structure of the oscillating medium, here the prominence plasma (see e.g. Molowny-Horras et al. 1999; Terradas et al. 2002). The large damping times observed in prominences will give us a very good support for our assumptions that the dissipation in prominences is weak.

Landman et al. (1977) observed prominence oscillations with a period of 22 minutes, that remained coherent for just 3-4 cycles. The same property was later seen by Tsubaki and Takeuchi (1986) who observed Doppler oscillations with periods of around 2.7-3.5 minutes, which were damped in roughly 3-4 cycles. Molowny-Horras et al. (1997) used wavelength analysis to determine periodicities of 7.5 minutes and the oscillations lasted for about 12 minutes. In the following year, Molowny-Horras et al. (1998) placed the slit on a filament (rather than on a limb prominence) and

1.5. THEORETICAL MODELS FOR OSCILLATING PROMINENCES

found period motion with periods of 2.7 and 12.5 minutes, with a lifetimes of 10 and 20 minutes, respectively. Terradas et al. (2002) used two-dimensional Doppler maps applied to a limb prominence and found that the 75 minutes periods were present over very large regions of the prominence, leading to the conclusion that what they observed was more likely a global oscillation of the prominence. The oscillations were damped with damping times of the order of 3 periods.

All these determinations of damping times could help scientists to use seismological techniques to determine physical damping mechanisms that act upon waves and oscillations in solar prominences. Significant advances were made to determine which non-ideal mechanisms are responsible for explaining the damping of waves and oscillations in solar prominences.

The first attempts to describe the observed damping involved the use of various transport mechanisms (such as viscosity, thermal and electrical conductivity, optical thin radiation) but neither of these mechanisms proved to explain the damping for the whole range of observed wavelengths (see, e.g. Ballai, 2003; Carrbonell et al. 2004). It was clear that some other mechanisms are needed, the most probable being resonant absorption, damping due to friction between various species of the ionised plasma, or dissipation of perpendicular currents (e.g. Cowling resistivity).

1.5 Theoretical models for oscillating prominences

Theoretical modeling of dynamical phenomena in solar prominences were driven by observations since mid-1960s. Historically, Hyder (1966) was the first who discussed winking filaments, and concluded that the prominence internal magnetic field created a restoring force, leading the oscillation in a vertical direction. It was also found that oscillations are damped due to the viscosity of coronal plasma, through which the prominence moves.

Kleczek and Kuperus (1969), discussed prominence oscillations as transverse motions of the prominence with the magnetic tension driving the oscillation. Later, Roberts (1991) used simplified models for small amplitude oscillations in a prominence, which was assumed to be like a point of mass, suspended on an elastic string, reflecting the local deformation of the magnetic field, which supports the prominence against gravity. The model could explain the vertical oscillations of the prominence

1.5. THEORETICAL MODELS FOR OSCILLATING PROMINENCES

as a whole, and the derived periods were found in agreement to the observed 10-20 minute range. Another model considered a prominence oscillating in a similar fashion of a mass vibrating on a taut string. The frequency which depended on the mass, density, length and natural wave-speed of the string was estimated, and the resulting estimation of the period, which was around 30 minutes, was in agreement with the observed intermediate period oscillations.

More recent and more sophisticated theoretical investigation on small amplitude prominence oscillations, use linearized MHD equations, including a magnetic field, which in turn is establishing magnetic tension and magnetic pressure as restoring forces to the oscillation, in addition to gas pressure. This results to the presence of 3 types of waves, namely the slow magnetoacoustic waves, the fast magnetoacoustic waves, and Alfvén waves. These models solve a set of differential equations together with the correct prominence-corona boundary conditions. The variety of theoretical structures is due to the three different choices of the equilibrium state.

1.5.1 Isothermal plasma slab of finite width

Here the prominence is modeled as a magnetic slab of finite width filled with isothermal plasma. Basically there are two categories of models used:

(1) *Models which do not consider the underlying arcade and external coronal medium:* Oliver et al. (1992) studied the oscillating modes of the Kippenhahn and Schluter (1957) prominence model and concluded that the three MHD modes have different directions of propagation: fast magnetoacoustic modes perform vertical motions, slow magnetoacoustic modes perform motions parallel to the magnetic field (i.e. transverse to the prominence), and Alfvén modes perform motions along the filament axis. Therefore, investigating the polarization of the velocity could help identify each discrete mode. Unfortunately, if the magnetic field possess an additional longitudinal component along the prominence axis (due to boundary conditions), the velocity vector turns into a complex combination of the 3 modes, which become impossible to distinguish (Joarder and Roberts, 1993b). On the other hand, Joarder and Roberts (1993a), based on a Menzel (1951) prominence model, added gravity to the model, which resulted in periods with up to 50% variation from the corresponding periods

1.5. THEORETICAL MODELS FOR OSCILLATING PROMINENCES

without gravity.

(2) *Models in which the external coronal medium has an effect:* Joarder and Roberts, (1992a), worked on a model that assumed adiabatic perturbations of a cool, dense, rectangular slab in a hot corona, with an imposed homogeneous magnetic field parallel to the long axis of the slab. Their analysis recovered many kinds of periods, including long period oscillations (up to 10 hours), intermediate (around one hour) and short period oscillations (a few minutes). The same authors (Joarder and Roberts, 1992b), considered the case where the magnetic field is perpendicular to the slab, a case which was analytically solvable, and the solution gave distinguished modes as internal and external modes. The resulting oscillating periods were consistent with the observed parameters of the coronal and prominence plasma. Oliver et al. (1993b) analyzed the Poland and Anzer (1971) equilibrium model, working on both the internal and external modes, ending up with the conclusion that the fundamental mode was a *hybrid mode* (both internal and external). This *hybrid mode* was labeled as *string mode* by Joarder and Roberts, (1993b), who found that if a magnetic field is imposed on an angle in the finite slab, then the 3 modes are no longer distinct. Regnier et al. (2001), used the Joarder and Roberts, (1993b) model to compare the frequencies between theoretical and observational data, and estimated the angle between the magnetic field and the longitudinal axis. The magnitude of the magnetic field was also calculated in terms of slab density.

1.5.2 Single fibril model

This model is based on the fine structure of the prominence. Using an earlier model, Joarder and Roberts (1992), Joarder et al. (1997), assumed a magnetic field parallel to the fibril, which was regarded as a thin thread with a finite length and width. Distinction between external and internal modes was again achieved. This model will be partly used in our investigation, too.

Diaz et al. (2002), studied the propagation of fast modes in a model that the fibril is considered to be a cylindrically symmetric flux tube, concluding that all sausage modes possess a cut-off frequency, while the fundamental kink and fluting modes do not. In addition, it was shown that the frequency of the sausage modes is invariant to the fibril width. Furthermore, the modes occupying a frequency below the cut-off

value, were found to be of such spatial structure, that perturbations are limited to the dense part of the fibril, leading to the absence of induction of the oscillations to nearby fibrils.

1.5.3 Models treating equilibrium configurations as a line-current

The effect of a finite time needed for perturbations to travel between a prominence and photosphere was studied by Schutgens (1997a). Later, the same author (Schutgens 1997b) concluded that the fundamental mode has a longer period in a normal polarity model, rather than in an inverse polarity model. Furthermore, Schutgens and Tóth (1999), showed that in an inverse polarity prominence, the horizontal oscillations are damped by the emission of slow waves, while the vertical oscillations are damped by the emission of fast waves.

All these models show that the discussion of dynamical phenomena in solar prominences is far from being understood, the complexity of these amazing solar features makes the problem rather difficult to tackle. However, simple models (including key ingredients) are able to recover observed parameters rather well.

1.6 Motivation for prominence study

Decades of study have shown that it is very difficult to characterize prominence properties. They show differences in morphology, lifetime, position on the solar disk, complexity of their magnetic field environments, etc. They are not uniform in shape and show a fine, dynamic structure at the limit of the instrumental resolution. This high variability makes their classification difficult and also results in a wide range of physical conditions deduced from observations that poorly constrain the models of prominence formation and disappearance (Vial, 1998). At the same time, understanding the origin of such variety and attaining better knowledge of these structures and their environment during the different phases of their life, can provide valuable information on the physics of the solar atmosphere. In fact, prominences are commonly found in the solar atmosphere, which indicates that it is easy to find favorable conditions for their formation and stability. This tells us that prominences are manifestations of a common physical process found in the solar atmosphere.

1.6. MOTIVATION FOR PROMINENCE STUDY

The research in prominence physics is driven by several questions, whose answers are still eluding (Parenti, 2014):

- **Stability:** In the quiescent state, prominences are interesting for their puzzling equilibrium condition that allows their mass to be supported in the tenuous corona. Clearly the magnetic field plays a major role, but still we do not have sufficient observational information to identify the different mechanisms and/or magnetic configurations responsible for their stability. The present Thesis aims to address a few questions related to this problem, in particular how the stability of a prominence is influenced by the presence of plasmas flows and by the fact that the plasma is partially ionised.
- **Mass motion:** Mass flows inside a prominence can also have a role in the equilibrium, mass support, and mass refurnishing. Observations reveal a variety of mass motions inside prominences, even though the spatial resolution of instruments may limit their diagnostic capability. However, only a few prominence models include such observed dynamics. The equilibrium flow of the plasma is going to be a fundamental ingredient in our analysis and will play a crucial role in the onset of instabilities.
- **Radiative losses:** Partially-ionized prominence plasma is an interesting laboratory for testing our knowledge of the radiation-transfer mechanisms in an optically-thick medium. In addition, non-local thermodynamic conditions (NLTE) generally exist in these plasmas. Even if the prominence density is high (and so the mean free path of electrons is small), collisions are unable to compete with radiation in populating the energy levels of the atoms, so that the Local Thermodynamic Equilibrium Condition (LTEC) does not hold. The incoming radiation due to the environmental solar emission is, in fact, another element affecting the prominence physical conditions. Proper treatment of radiative transfer in prominences is also important for quantifying the amount of radiative losses: this mechanism acts as a cooling mechanism in the energy equilibrium equation. In quiescent conditions, the prominence radiation is steady, requiring a source of still unknown heating to maintain energy balance in the structure.

- **Magnetic field:** The lack of extensive magnetic-field measurements in prominences limits our knowledge of the physics of the coronal magnetic field and its interaction with the plasma. We often assume that the observed prominence plasma- emission morphology traces the magnetic field lines. One of the paradoxes in prominence studies is that prominences at the limb can show a vertical fine bright structure, while disk observations and the few magnetic field measurements suggest that the field is almost horizontal. Solving this conundrum will help to understand the coronal magnetic environment and to identify the dominant physical process in the solar atmosphere. Here we will restrict our analysis to the horizontal field configuration. This will simplify considerably our mathematical approach.
- **Formation and disappearance:** Prominences as a whole can be very stable for a few months, or can be part of large-scale dynamic and energetic events like solar flares and CMEs (see, e.g. van Driel-Gesztelyi and Culhane, 2009, for a review). These enormous eruptions (about 3×10^{12} kg) perturb the interplanetary medium, and their effects can be seen on Earth. For example, they are the origin of geomagnetic storms, which can affect everyday life through electric blackouts, and since nowadays we depend so much on technology, such solar activity is a concern. It is shown that solar eruptions may influence the technology of satellites for telecommunication and human space activity. That is why Space Weather was developed very fast during the last decade, becoming a new branch of science which aims to forecast the activity of our sun and any resulting consequences for humans. The disappearance of prominences can be ultimately connected to their stability; our analysis will try to find answers to questions on the causes of these instabilities.

1.7 Overview of this thesis

After being introduced to the Sun and its structure, the mysteries and the eternal problem of coronal heating, the properties of prominences and prominence oscillations together with theoretical models which help us understand the structure of the coronal plasma, we are going to investigate the stability of the boundary between

the prominence and the surrounding coronal plasma or the interface between various prominence structures. The boundary separates two sort of plasmas with very different physical properties (temperature, density, ionisation degree, etc.)

The aim of this thesis is to contribute to the theoretical understanding of the dissipative instability at the interfaces between the partially ionized prominence plasma, and the surrounding coronal plasma or at the interface between fibrils/plumes in quiescent prominences. The interface between these two media is going to be considered as a tangential discontinuity, at which continuity conditions have to be imposed.

The outline of the thesis is as follows: In Chapter 2 the basic magnetohydrodynamic (MHD) equations are introduced, as well as the wave equations, which describe the different MHD modes. We also review some theoretical results on magnetic interface and magnetic slab models under specific assumptions.

Since the main model of the Thesis is based on the concept of partially ionised plasma, in Chapter 3 we introduce the governing equations for this sort of plasma, in the case of a single and two-fluid approach and we will review the changes in the wave propagation that appear in partially ionized plasmas.

In Chapter 4 we investigate the dissipative instability at the boundary, between the viscous corona and the partially ionized prominence plasma at the incompressible limit. The importance of the partial ionization is investigated in terms of the ionization factor. The same principle is going to be applied in the case of an interface separating two plasmas described in the two-fluid approximation.

We do that by matching solutions for the transversal component of the velocity and total pressure at the interface of the mentioned boundary, and derive a dispersion relation whose imaginary part describes the evolution of the instability. Results are obtained in the limit of weak dissipation.

In Chapter 5 we extend previous results to the investigation of dissipative instability in a Cartesian slab. Given the dispersion character of the plasma, we will discuss separately the conditions of appearance of dissipative instability for body and kink waves modeling various cases in solar prominences. All these models will assume that one of the media (or both) have an equilibrium flow that is chosen to be directed along the interface, parallel to the ambient magnetic field.

Finally, in Chapter 6 we summarize the results of this work and present the conclusions, giving a brief discussion of future developments and possible applications

of the results.

Chapter 2

Magnetohydrodynamics

The electromagnetic force is generally known to create structures: e.g. stable atoms and molecules, crystalline solids. Furthermore, studying the resulting impact of the electromagnetic force is forming the sciences of chemistry and solid-state physics, which are both developed to understand basically static structures.

The binding energies of such structured systems are bigger in magnitude than the ambient thermal energy. However, imposing a large enough temperature, they decompose due to the increased thermal energy: e.g. crystals melt, molecules dissociate. If the temperature is near or exceeds the corresponding atomic ionization energy, the atoms will then decompose into negatively charged electrons and positively charged ions. These ions not free: they are actually strongly affected by each others' electromagnetic fields. However, since the charges are no longer bound, their system becomes capable of exhibiting collective behavior of great complexity and they form a plasma.

The plasma complexity is both temporal and spatial. The plasma is predominately described by the excitation of a multitude of collective dynamical features. Since interatomic bonds are breaking before ionizing under huge temperatures, most plasmas on earth begin as gases, and actually sometimes the definition of plasma is a gas which is ionized enough, to exhibit plasma-like behavior. Note that plasma-like behavior ensues after an extremely small fraction of the gas has undergone ionization. Therefore, partially ionized gases share most of the characteristic features with fully ionized gases. Plasmas which were produced by ionizing neutral gases, con-

tain in principle equal numbers of positive and negative ions. In this case, the oppositely charged ions are strongly coupled, and tend to electrically neutralize each other on macroscopicly. These plasmas are named quasi-neutral ("quasi" since they are not absolutely neutral and this fact is dynamically affecting certain types of plasma modes). Highly positively or negatively charged plasmas, which may even consist of ions of only one sign, mostly exist in laboratory experiments: their equilibrium is ensured by a strong magnetic field, about which the charged fluid rotates. In a neutral gas the dynamics is described by the collisions of the neutral particles with large force but with short range. In plasma though, the charged particles are attracted to each other or repelled away from each other under the Coulomb force.

Besides, the displacement of the charged particles leaves magnetic field traces behind, which in turn is affecting nearby charged particles with a weak long-range force. This leads to the conclusion that in an ionized gas, charged particles are interacting with each other many times, resulting in the collective behavior of plasma. Of course, for collective behavior to be ensured, the number of collisions between charged and neutral particles should be much smaller than the number of collisions between charged particles.

It is remarkable that 95% of the baryonic content of the known Universe is composed of plasma (Priest, 1982). This number is flattering the science of plasma physics (and plasma physicists), but from the other hand is so difficult to disprove. However, it is essential to show off the prevalence of the plasma state, which is considered as the 4th state of matter. In earlier times of the Universe, everything was plasma. Currently stars, nebulae, and even interstellar space, are filled with plasma. The Solar System is also a host for plasma, since it is penetrated by the solar wind, while the Earth is completely surrounded by plasma trapped within its magnetic field (called plasma sphere).

Plasmas can have at least two definitions:

- **Microscopic definition:** Plasma is a quasi-neutral gas of charged and neutral particles which show collective behavior.
- **Macroscopic definition:** For a valid macroscopic model of magnetized plasma dynamical configurations, size, duration, density, and magnetic field strength should be large enough to establish fluid behavior and to average out the micro-

scopic phenomena (i.e. collective plasma oscillations and cyclotron motions of electrons and ions).

Finally, a plasma is defined as an ionized gas where the Debye-length (λ_D) is much smaller than any other length-scale in the dynamical system. The Debye-length is a measure of the distance, over which negatively charged particles, deviate from positively charged particles (Boyd and Sanderson, 1969). The charge imbalance (due to thermal fluctuations), may create electric fields, which cause the acceleration of charged particles, which leads to instant neutralization. Thus, for the plasma to sustain its ionized state, this neutralization should be restricted to a fraction of the particles, meaning that the deviation of positive and negative particles should be relatively easy due to the small size of the Debye length.

2.1 MHD equations

There are three different popular models in which a plasma can be described. Although apparently these models are independent, one particular model can be derived from another one

- Theory of motion of single charged particles in given magnetic/electric field
- Kinetic theory of a collection of such particles, describing plasmas from microscopic point of view with the help of particle distribution functions
- Fluid theory (magnetohydrodynamics or MHD) describes the plasma in terms of averaged macroscopic functions depending on position and time

For our present purposes, we will concentrate only on the last model as it is the model which requires the least special mathematics to be introduced.

The motion of the plasma is affected and even guided by a magnetic field. Thus a combination of hydrodynamics and electromagnetic theory is required to describe the plasma dynamics. When charged particles (in terms of the sign of their charge) and neutrals are treated separately then the mathematical formalism used is called the "multi-fluid" MHD. In contrast, the plasma can be treated as a single fluid whose dynamics are described by its macroscopic properties (density, temperature, pressure,

magnetic flux etc). In this case we can speak about "single-fluid" MHD. The MHD description of continuous plasmas is based on the combination of simplified form of Maxwell's equations, Ohm's law and the equations of mass continuity, motion and energy. The system of equations can be further simplified if the electromagnetic field is eliminated between Maxwell's and Ohm's laws, and we obtain one single equation called *the induction equation* which relates the plasma velocity and magnetic induction vectors.

In order to formulate the MHD equations, we assume the following:

- Most of the plasma properties are assumed isotropic.
- All the equations must be written in an inertial frame
- All speeds involved in the MHD description are much smaller than the speed of light. This assumption is easy to satisfy as the highest speeds we will deal with are Alfvén waves in the solar corona, whose speed is of the order of a thousand km s^{-1}
- All time scales are longer than inverse cyclotron frequency. In the solar corona $B = 10 \text{ G}$, $n = 5 \times 10^{14} \text{ m}^{-3}$ the cyclotron frequency is of the order of $1.5 \times 10^4 \text{ Hz}$, meaning that waves and oscillations described within the framework of MHD must have periods larger than 10^{-4} s .
- Characteristic times are much longer than the collision times and the characteristic spatial scales are larger than the mean free path, i.e.

$$\lambda \gg l_{ii} = \frac{7.2 \times 10^7 T^2}{n},$$

where the temperature is measured in K and number density in m^{-3} . For the typical conditions in the solar corona this gives a lower threshold of 10^5 - 10^6 m , while in the solar prominence ($T = 10^4 \text{ K}$, $n = 10^{15}$ - 10^{17} m^{-3}) this equates to lengths larger than a few centimeters to meters.

- In a single-fluid plasma description, the estimated quantities of the plasma are the sum of the corresponding quantities of ions, electrons and neutrals.

- Since the variations length-scales are much larger than the typical plasma lengths, we may assume that plasma is treated as a continuum.

Let us consider the gas dynamic equations for the evolution of the plasma parameters, such as density ρ , pressure p or the velocity field \mathbf{v} . The first equation comes from the mass continuity (conservation of mass in the fluid motion), which can be written in two equivalent forms,

$$\frac{\partial \rho}{\partial t} + \nabla \cdot (\rho \mathbf{v}) = 0, \quad (2.1)$$

$$\frac{D\rho}{Dt} + \rho \nabla \cdot \mathbf{v} = 0, \quad (2.2)$$

where

$$\frac{D}{Dt} = \frac{\partial}{\partial t} + \mathbf{v} \cdot \nabla$$

is the Lagrangian time-derivative (moving with the fluid). This equation states that in a closed system no mass can be created and/or annihilated.

Let us consider the case when $\rho = \text{const}$. From the mass conservation equation we obtain that $\nabla \cdot \mathbf{v} = 0$ which constitutes the incompressible limit. Our analysis will extensively use this approximation.

The balance of forces is expressed through the equation of momentum, which has its roots within Newton's second law

$$\rho \frac{D\mathbf{v}}{Dt} = -\nabla p + [\mathbf{j} \times \mathbf{B}] + \rho \mathbf{g} + \mathbf{F}, \quad (2.3)$$

where \mathbf{F} represents any force that is non-inertial (Coriolis force, viscous force, etc.). In this equation \mathbf{j} is the current, \mathbf{B} is the magnetic field induction vector, and g is the constant gravitational acceleration. The presence of the magnetic field is evidenced by the Lorentz force in the momentum equation (the second term on the RHS). The current density is given by the Ampere's law

$$\mathbf{j} = \frac{1}{\mu_0} \nabla \times \mathbf{B},$$

meaning that the only current we take into account is the one that is generated by the magnetic field. Here μ_0 is the permeability of free space. The effect of the Lorentz

force on the plasma can be seen after decomposing the vectorial product following the well-known vector identity

$$\mathbf{j} \times \mathbf{B} = (\mathbf{B} \cdot \nabla) \frac{\mathbf{B}}{\mu_0} - \nabla \left(\frac{B^2}{2\mu_0} \right). \quad (2.4)$$

The first term on the right hand side of this equation represents the effect of a tension parallel to the magnetic field and the second one the gradient of a scalar magnetic pressure. The Lorentz force has therefore two effects on the plasma: to shorten magnetic field lines through the tension force and also to compress the plasma through the pressure term. It is often convenient to rearrange Eq. (2.3) taking into account this decomposition (neglecting gravity and non-inertial forces),

$$\rho \frac{D\mathbf{v}}{Dt} = -\nabla P + (\mathbf{B} \cdot \nabla) \frac{\mathbf{B}}{\mu_0}, \quad (2.5)$$

where the quantity $P = p + B^2/(2\mu_0)$ is called the total pressure (the sum of kinetic and magnetic pressures).

The equation that connects the magnetic field and fluid is the induction equation

$$\frac{\partial \mathbf{B}}{\partial t} = \nabla \times (\mathbf{v} \times \mathbf{B}) + \mathbf{R}, \quad (2.6)$$

where the quantity \mathbf{R} is the resistive term. In our analysis this will very much connected to the partial ionised character of the plasma and will be discussed later in this Chapter. In an ideal plasma $\mathbf{R} = 0$ and Eq. (2.6) reduces to a simple diffusion equation. Under these conditions, Alfvén's frozen-in flux theorem holds: in a perfectly conducting plasma, magnetic field lines behave as if they move with the plasma (by the vorticity-magnetic field analogy this is directly comparable with the classical vorticity theorem of Helmholtz and Kelvin).

The thermodynamical quantities are connected through the energy equation

$$\frac{dp}{dt} - \frac{\gamma p}{\rho} \frac{d\rho}{dt} = -(\gamma - 1)L \quad (2.7)$$

where the energy loss function L has contributions from heat flux due particle conduction, radiation, ohmic dissipation and any other sources or sinks (such as viscous

dissipation, wave heating in the corona or nuclear energy generation in the solar interior). In ideal MHD this is set to zero, which corresponds to the adiabatic approximation. In any case, this energy loss function is small compared with the other terms when the time-scale changes in pressure, density and temperature are much smaller than the time scales for radiation, conduction or heating; this is often valid for rapid changes associated with wave motions or instabilities. In Eq. (2.7) the quantity γ is the adiabatic index.

Finally, the MHD equations must be supplemented by two closure equations. One refers to the magnetic field, and it expresses the solenoidal condition

$$\nabla \cdot \mathbf{B} = 0, \quad (2.8)$$

which means that there are no magnetic charges and all magnetic field lines are closed. The second equation is the equation of state

$$p = \frac{\rho RT}{\tilde{\mu}} = nk_B T, \quad (2.9)$$

where R is the gas constant and $\tilde{\mu}$ is the mean atomic weight (the average mass per particle in units of the proton mass, which for fully ionised hydrogen takes the value 0.5, while in many coronal applications is taken as 0.6), n the particle density and k_B the Boltzmann constant.

2.2 MHD waves

Oscillations in solar structures (like prominences and sunspots) have been observed and theoretically modeled in order to understand the Sun's dynamics and physical parameters. These oscillations are interpreted in terms of MHD waves. In general, sound waves in gas, are propagating due to a pressure gradient along the direction of the medium. The gradient is negative in the direction of propagation and this propagation takes place in order to restore equilibrium. Waves can carry energy along the direction of propagation, but because of the small amplitude, the disturbance in the gas is limited. If now the gas is permeated by a magnetic field (i.e. plasma), the pressure gradient disturbs the magnetic lines. The propagating wave is then interacting

with the magnetic field, which in turn is metabolizing, exerting a restoring force, and simultaneously affecting the wave. In order to present the nature of possible waves arising in a plasma, we will consider an equilibrium state, and then we will impose a small perturbation in order to enable us to see whether linear disturbances are propagating in a wave manner. In particular, since this Thesis will deal with quiescent prominences and their small amplitude oscillations, we consider non-linear effects to be non- important. Thus the MHD equations are linearized and under specific assumptions, the linearized set can be even analytically solved.

2.2.1 Linearised ideal MHD equations

The model of consideration here is a homogeneous unbounded medium, where a uniform magnetic field is imposed along the x-axis, the equilibrium is static, and the effect of gravity is neglected . The equilibrium magnitudes ρ_0, p_0, T_0 , and \mathbf{B}_0 for the corresponding physical quantities of density, pressure, temperature and magnetic field, are all constant. Every physical parameter can be expressed as the sum of the equilibrium value and the magnitude of the linear perturbation as

$$\mathbf{B} = \mathbf{B}_0 + \mathbf{B}_1(\mathbf{r}, t), \quad (2.10)$$

$$\mathbf{v} = \mathbf{v}_1(\mathbf{r}, t), \quad (2.11)$$

$$p = p_0 + p_1(\mathbf{r}, t), \quad (2.12)$$

$$\rho = \rho_0 + \rho_1(\mathbf{r}, t), \quad (2.13)$$

$$T = T_0 + T_1(\mathbf{r}, t). \quad (2.14)$$

Here the index "1" denotes the perturbed quantities. Since perturbations are much smaller than their equilibrium counterpart, products and squares of perturbed quantities are negligibly small. Then substituting the above equations into the set of ideal MHD equations (2.1) and (2.5)–(2.9) will lead to a new set of linearized MHD equations

$$\frac{\partial \rho_1}{\partial t} + \rho_0 \nabla \cdot \mathbf{v}_1 = 0, \quad (2.15)$$

$$\rho_0 \frac{\partial \mathbf{v}_1}{\partial t} = -\nabla p_1 + \frac{1}{\mu_0} (\nabla \times \mathbf{B}_1) \times \mathbf{B}_0, \quad (2.16)$$

$$\frac{\partial p_1}{\partial t} - \frac{\gamma p_0}{\rho_0} \frac{\partial \rho_1}{\partial t} = 0, \quad (2.17)$$

$$\frac{\partial \mathbf{B}_1}{\partial t} = \nabla \times (\mathbf{v}_1 \times \mathbf{B}_0), \quad (2.18)$$

$$\nabla \cdot \mathbf{B}_1 = 0, \quad (2.19)$$

$$\frac{p_1}{p_0} - \frac{\rho_1}{\rho_0} - \frac{T_1}{T_0} = 0. \quad (2.20)$$

These equations will be combined to describe the possible oscillating modes in magnetised plasma and their properties.

2.2.2 MHD waves

In the absence of magnetic field and assuming that all changes in perturbations are adiabatic, Eq. (2.17) reduces to

$$\frac{\partial p_1}{\partial t} = c_S^2 \frac{\partial \rho_1}{\partial t}. \quad (2.21)$$

Here, c_S is the sound speed and is defined by the relation

$$c_S^2 = \frac{\gamma p_0}{\rho_0}. \quad (2.22)$$

Sound waves are propagating isotropically with the same speed c_S , and the gas surrounding the source of these waves will undergo variations in pressure, density and temperature, with motions in the gas being aligned with the direction of the wave propagation.

In a magnetized fluid the dynamics is much more complex due to the presence of magnetic fields. In a perfect conductor, the magnetic field lines and the fluid motions are frozen together, so that any attempt to initiate a sound wave will result in variations in the magnetic field. The motion of the gas, caused by the sound waves, will move the magnetic field lines, causing magnetic forces to arise. These forces may, in return, affect the gas, and so affect the propagation of sound waves. As a consequence, sound may no longer be able to propagate with the speed c_S , and the directionality of the magnetic field renders wave propagation anisotropic (see, e.g. Roberts 1991). In addition to the sound wave, the presence of the magnetic field will

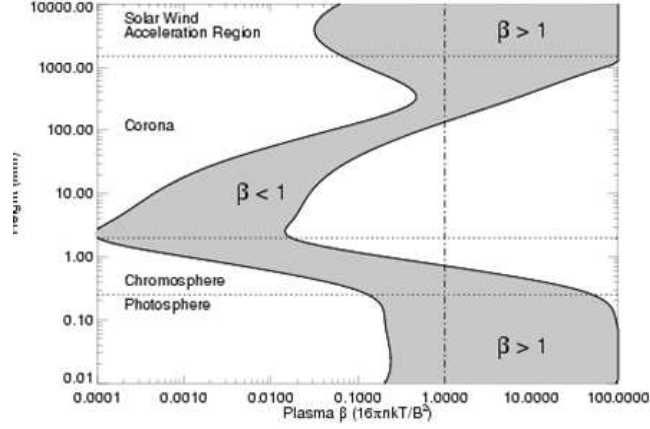


Figure 2.1: The variation of plasma-beta (defined by Eq. (2.24)) in the solar atmosphere. The plot has been adapted from Gary (2001)

generate the propagation of magnetic disturbances. The most obvious one is the so called *Alfvén wave* that are pure magnetic waves and they generate gas motions in the direction perpendicular to the ambient magnetic field, i.e. they are transversal waves. They propagate along the field with a speed v_A defined by:

$$v_A^2 = \frac{B_0^2}{\mu_0 \rho_0}. \quad (2.23)$$

The relative magnitude of these two characteristic speeds defines a key quantity in plasma physics called *the plasma- β* defined as the ratio of the kinetic and magnetic pressure, i.e.

$$\beta = \frac{p_0}{B_0^2/2\mu_0} = \frac{2c_S^2}{\gamma v_A^2}. \quad (2.24)$$

According to whether plasma beta is smaller or larger than 1, the plasma dynamics is driven mainly by thermodynamic or magnetic forces, so for plasmas where $\beta < 1$ (e.g. solar corona, prominences, top of the chromosphere) the dynamics is driven by magnetic forces, while in any region where $\beta > 1$ (bottom of the chromosphere, photosphere) the motion is controlled by thermodynamic forces (e.g. pressure gradient). The variation of this important parameter with the height in the solar atmosphere is shown in Fig. 2.1.

In addition to these two characteristic speeds, we can also define two combined

speeds that will appear in our discussion, being related to the propagation speed of mixed waves, one being the fast speed (related to the propagation of fast magnetoacoustic waves) and the other being the slow speed (or tube speed), related to the propagation of slow waves. These quantities are defined as

$$c_f^2 = c_s^2 + v_A^2, \quad c_T^2 = \frac{c_s^2 v_A^2}{c_f^2}. \quad (2.25)$$

The fast speed is both super-sonic and super-Alfvénic, while the tube speed is both sub-sonic and sub-Alfvénic.

The solar atmosphere is a highly structured and inhomogeneous medium. In order to review the possible modes arising in such plasmas, let us take a simple configuration where the ambient magnetic field is homogeneous and parallel to the z -axis. We can distinguish two directions of our dynamics, one parallel to the field and one perpendicular to it. The linearized ideal MHD equations can be reduced to two equations in the two directions (see, e.g. Roberts, 1991), i.e.

$$\rho_0 \left(\frac{\partial^2}{\partial t^2} - v_A^2 \frac{\partial^2}{\partial z^2} \right) v_{\perp} + \nabla_{\perp} \left(\frac{\partial P}{\partial t} \right) = 0, \quad (2.26)$$

and

$$\rho_0 \left(\frac{\partial^2}{\partial t^2} - c_T^2 \frac{\partial^2}{\partial z^2} \right) v_z + \frac{c_s^2}{c_f^2} \frac{\partial}{\partial z} \left(\frac{\partial P}{\partial t} \right) = 0, \quad (2.27)$$

with the total pressure varying as

$$\frac{\partial P}{\partial t} = \rho_0 v_A^2 \frac{\partial v_z}{\partial z} - \rho_0 c_f^2 \nabla \cdot \mathbf{v}. \quad (2.28)$$

Here ∇_{\perp} denotes the component of the gradient operator that is perpendicular to the direction of the magnetic field, i.e. perpendicular to the z -axis for our case and the components of the velocity vector are $\mathbf{v} = (v_{\perp}, v_z)$.

The system of equations (2.26)–(2.28) is considerably complicated, however simple solutions can be obtained in particular cases. In an incompressible plasma ($\nabla \cdot \mathbf{v} = 0$) involving no flow perturbations along the field ($v_z = 0$) and no total pressure

variations, the only remaining equation is

$$\left(\frac{\partial^2}{\partial t^2} - v_A^2 \frac{\partial^2}{\partial z^2} \right) v_{\perp} = 0. \quad (2.29)$$

This means that motions in the plane perpendicular to the ambient magnetic field are solutions of the one-dimensional wave equation and the solution of this equation are the Alfvén waves which are transverse vibrations of each field-line.

General solutions of the system (2.26)–(2.28) can be obtained after Fourier analyzing the perturbations. For a Cartesian geometry perturbations will be assumed to have the form

$$f(x, y, z, t) = f(x) \exp i(\omega t - k_y y - k_z z). \quad (2.30)$$

Here ω is the angular frequency of the waves (here assumed to be a real quantity) and k_y and k_z are the wavenumbers in the y and z directions, respectively. In this case the system (2.26)–(2.28) reduces to a single ordinary differential equation (see, e.g. Roberts 1981b)

$$\frac{d}{dx} \left[\frac{\rho_0(x)(k_z^2 v_A^2(x) - \omega^2)}{m^2(x) + k_y^2} \frac{dv_x}{dx} \right] = \rho_0(x)(k_z^2 v_A^2(x) - \omega^2) v_x \quad (2.31)$$

where

$$m^2(x) = \frac{(k_z^2 c_S^2(x) - \omega^2)(k_z^2 v_A^2(x) - \omega^2)}{c_f^2(k_z^2 c_T^2(x) - \omega^2)}, \quad (2.32)$$

where m^2 (often called the magnetoacoustic parameter) can be a negative or positive quantity (the type of the solutions of Eq. (2.31) depends on the sign of this parameter). We should mention here that all waves which we will deal with will satisfy the condition that $\omega^2 \neq k_z^2(v_A^2, c_T^2)$. If this condition is not satisfied the above equation will allow two singular points which correspond to the Alfvén and cusp singularities (see, e.g. Sakurai et al. 1991). These singularities are connected to the resonant transfer of energy between interacting systems, a mechanism that is widely used in the process of plasma heating or wave damping (see, e.g. Ruderman and Roberts 2002, Goossens et al. 2012, Goossens, Erdelyi & Ruderman (2012)).

The solution of Eq. (2.31) is a very complicated one, and only in a few cases can be analyzed analytically. In order to study realistic waves propagation we must turn

our attention to simple cases and build complex configurations based on previous knowledge.

2.2.3 Waves in a uniform atmosphere

In the case of a uniform atmosphere all equilibrium quantities are constant and therefore all characteristic speeds will be constants. This simplification will make the system (2.26)–(2.28) easily solvable (see, e.g. Lighthill 1960). Denoting $\Delta = \nabla \cdot \mathbf{v}$, the governing equations reduce to (see Roberts, (1981):

$$\frac{\partial^4 \Delta}{\partial t^4} - c_f^2 \frac{\partial^2}{\partial t^2} \nabla^2 \Delta + c_T^2 c_f^2 \frac{\partial^2}{\partial z^2} \nabla^2 \Delta = 0. \quad (2.33)$$

Applying the already-mentioned Fourier analysis we can derive the so-called *dispersion relation* that describes the wave properties and is given by

$$\omega^4 - c_f^2 k^2 \omega^2 + c_T^2 c_f^2 k_z^2 k^2 = 0, \quad (2.34)$$

where $k = (k_x^2 + k_y^2 + k_z^2)^{1/2}$ is the magnitude of the wavevector \mathbf{k} . This dispersion relation describes compressive waves ($\Delta \neq 0$) labeled as *magneto-acoustic* waves.

A much more suitable way of writing Eq. (2.34) is the form

$$(k_z^2 v_A^2 - \omega^2)(m^2 + k_x^2 + k_y^2) = 0, \quad (2.35)$$

which reveals the existence of two different set of waves. First, the solution of this equation are the Alfvén waves, corresponding to $\omega^2 = k_z^2 v_A^2$, and there are magnetoacoustic waves whose dispersion relation is given by

$$m^2 + k_x^2 + k_y^2 = 0, \quad (2.36)$$

where it is clear that for magnetoacoustic waves $m^2 < 0$ for real wavenumbers. Looking at the definition of m^2 it is obvious that the phase speed, ω^2/k_z^2 lies either between c_T^2 and the minimum of c_S^2 and v_A^2 (corresponding to slow waves) or it is greater than the maximum of c_S^2 and v_A^2 , these being the fast modes. Both fast and slow waves are driven by tension and pressure forces with density and pressure vari-

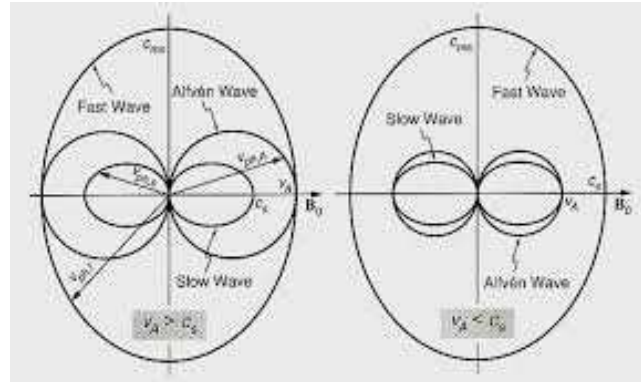


Figure 2.2: Analysis of the 3 MHD waves in a polar diagram. Adopted from Denmark Solar System school. Lectures On Space Plasma Physics 2007.

ations. Furthermore, the slow wave has much bigger temperature variations than the fast one.

Alfvén waves are incompressible (they they do not perturb density or pressure), and so $\mathbf{k} \cdot \mathbf{v} = 0$, meaning that the velocity perturbation is normal to the direction of propagation. They propagate only along the field line with the speed v_A .

Although our analysis is true for propagation along the magnetic field, similar analysis can be carried for propagation at an arbitrary angle with respect to the ambient magnetic field. The propagation properties of these three waves can be analyzed in the diagram shown in Fig. 2.2 where we plot the variation of the phase speed with respect to the propagation angle. The diagram shows that the fast mode can propagate in all directions having the maximum phase speed in the direction perpendicular to the field. The slow mode, on the other hand, has a similar diagram to the Alfvén waves, i.e. it cannot propagate in a perpendicular direction to the field. In the case of vanishing field ($v_A = 0$), the slow wave disappears and the fast wave becomes the sound wave. For more details about the properties of these waves can be found in Priest (1982).

2.3 Waves in structured media

One of the fundamental properties of magnetic fields in the solar atmosphere is that they are not diffuse, instead they tend to accumulate into individual structures that can

already be observed in a direct way. Mathematically the structuring of the magnetic field imposed on the problem of wave propagation creates some difficulty which can be solved using the property of continuity of solutions at boundaries. The present thesis contains calculations of such type, therefore we will attempt to cover the basic properties of such configurations

2.3.1 Waves at a single interface

The simplest magnetic configuration that is based on the idea of magnetic field structuring is the case of a tangential discontinuity between two uniform semi-infinite media. This idealistic structuring is realized by a density jump across an interface situated at $z = 0$. The equilibrium magnetic field is homogeneous and unidirectional having the form $\mathbf{B}_0 = B_0 \hat{\mathbf{x}}$. This problem, under solar physics conditions, was investigated by Roberts (1981a), which completed the work of previous authors including Parker (1964, 1974, 1978); Hasegawa and Chen (1974, 1976); Wentzel (1978), who studied simplifications. The key result obtained by Roberts (1981a) is that the density interface can, under certain conditions, admit two sets of surface wave. In this subsection we will closely follow the derivation given by Roberts (1981a).

Let us consider an atmosphere in a static equilibrium in the absence of gravitational forces. The continuity of stresses at the interface implies that the total pressure has to be continuous across the interface, i.e.

$$\frac{d}{dx} \left(p + \frac{B^2}{2\mu_0} \right) = 0. \quad (2.37)$$

We recall that linear perturbations about this equilibrium state are governed by the system

$$\frac{\partial \rho_1}{\partial t} + \nabla \cdot (\rho_0 \mathbf{v}) = 0, \quad (2.38)$$

$$\rho_0 \frac{\partial \mathbf{v}}{\partial t} = -\nabla \left(p_1 + \frac{1}{\mu_0} \mathbf{B}_0 \cdot \mathbf{B}_1 \right) + \frac{1}{\mu_0} (\mathbf{B}_0 \cdot \nabla) \mathbf{B}_1 + \frac{1}{\mu_0} (\mathbf{B}_1 \cdot \nabla) \mathbf{B}_0, \quad (2.39)$$

$$\frac{\partial \mathbf{B}_1}{\partial t} = \nabla \times (\mathbf{v} \times \mathbf{B}_0), \quad (2.40)$$

$$\frac{\partial p_1}{\partial t} + \mathbf{v} \cdot \nabla p_0 = c_S^2 \left(\frac{\partial \rho_1}{\partial t} + \mathbf{v} \cdot \nabla \rho_0 \right). \quad (2.41)$$

By considering the components of the momentum equation we arrive at the Eqs. (2.26)–(2.27). After Fourier analyzing the perturbations we arrive to an equation similar to (2.31)

$$\frac{d}{dz} \left[\frac{\rho_0(z)(k_z^2 v_A^2(z) - \omega^2)}{m^2(z) + k_y^2} \frac{dv_z}{dz} \right] - \rho_0(z)(k_z^2 v_A^2(z) - \omega^2)v_z = 0. \quad (2.42)$$

Let us consider that the plasma is permeated by the magnetic field of the form

$$B_0(z) = \begin{cases} B_e & z > 0, \\ B_0 & z < 0, \end{cases} \quad (2.43)$$

with $B_e \neq B_0$. Then, the continuity of the total pressure across the interface becomes

$$p_e + \frac{B_e^2}{2\mu_0} = p_0 + \frac{B_0^2}{2\mu_0}. \quad (2.44)$$

Since the plasma is piecewise uniform in the two regions, equation (2.44) applies independently on each side of the interface, as long as the solutions are continuous across $z = 0$.

We are interested in waves which propagate along the interface. In addition we suppose waveguiding at infinity. We thus impose the condition that v_z vanishes at $z \rightarrow \pm\infty$. Imposing this constraint on either side of the interface gives

$$v_z(z) = \begin{cases} \alpha_e e^{-z\sqrt{m_e^2+l^2}} & z > 0, \\ \alpha_0 e^{-z\sqrt{m_0^2+l^2}} & z < 0, \end{cases} \quad (2.45)$$

where the amplitude coefficients α_0 and α_e are determined by the boundary conditions. The quantities m_e and m_0 are the two values of m (defined by Eq. (2.32) evaluated in the two regions.

At the interface we require the continuity of total (gas plus magnetic) pressure perturbation, which now is given by

$$P = p_1 + \frac{B_0}{\mu_0} B_{1x}. \quad (2.46)$$

It is easily shown that the connection between the total pressure and the z component

of the velocity vector is given by

$$P(z) = \frac{i\rho_0}{\omega}(k^2v_A^2 - \omega^2)\frac{1}{m_0^2 + l^2}\frac{dv_z}{dz}. \quad (2.47)$$

Imposing pressure and displacement continuity across the interface gives rise to the dispersion relation for surface waves at a magnetic interface. Roberts (1981a) derived the dispersion relation describing waves at the interface in the form

$$\rho_0(k^2v_A^2 - \omega^2)\sqrt{m_e^2 + l^2} + \rho_e(k^2v_{Ae}^2 - \omega^2)\sqrt{m_0^2 + l^2} = 0. \quad (2.48)$$

This dispersion relation is already more complicated than the dispersion relation we derived for magnetoacoustic waves propagating in a uniform an un-structured medium. A detailed analysis of the properties of the dispersion relation reveals that (Roberts, 1981a)

- If one side of the interface is field free, then the interface supports a slow mode surface wave, with a phase speed less than the minimum of c_T and the sound speed in the field free region.
- If the gas in the magnetized side of the interface is cooler than the field free region then a fast mode surface wave is also supported, with a phase speed greater than the sound speed in the magnetized region and less than the minimum of the sound and Alfvén speeds in the field free region.

Without the lost of generality we can assume that $l = 0$ and equation (2.48) can be written as

$$\frac{\omega^2}{k^2} = \frac{\rho_0v_A^2m_e + \rho_ev_{Ae}^2m_0}{\rho_0m_e + \rho_em_0} \quad (2.49)$$

Our analysis will deal to a large extent with incompressible modes that correspond to the limit of $\gamma \rightarrow \infty$ (or equivalently $c_S \rightarrow \infty$), in which case the dispersion relation of the only possible Alfvén surface wave is given by

$$\frac{\omega^2}{k^2} = \frac{\rho_0v_A^2 + \rho_ev_{Ae}^2}{\rho_0 + \rho_e} \quad (2.50)$$

Very often this speed is labeled also as the "kink speed" and it is a very important

quantity for modern magnetic loop oscillations and the seismological techniques derived in the last decade.

2.3.2 Waves in magnetic slabs

The next step in building up a more complex configuration where the structuring of the magnetic field is taken into account is the case of wave propagation in a magnetic slab described in Cartesian geometry. Obviously this model is an idealistic one, but it gives good estimates for quantities of interest and highlights the effects of geometrical constrain of wave propagation (waves are guided along this slab). It is well known that once a wave is "forced" to propagate in a region with well defined geometrical size, it becomes dispersive and the dispersive character is determined by the relative size of the waveguide compared to the wavelength of the wave.

Considering a magnetic slab, which has a width z_0 , with equilibrium described by quantities with an index "0" for the plasma inside the slab ($|z| < z_0$) and by quantities having an index "e" describing the plasma outside the slab ($|z| > z_0$). The structure is taken as infinite in the y -direction, and for simplicity we restrict our analysis to two-dimensional analysis, i.e. $v_y=0$ and $l=0$. Let us consider waves that are confined to the inhomogeneity $|z| < z_0$, thus the inhomogeneity acts as a wave guide with disturbances outside the slab ($|z| > z_0$) being laterally evanescent, i.e. $v_z \rightarrow 0$ as $|z| \rightarrow \infty$. Inside and outside the slab the normal component of the velocity is determined by an equation of the type

$$\frac{\partial^2 v_z(z)}{\partial z^2} - m_{0,e}^2 v_z(z) = 0, \quad (2.51)$$

where m_0 and m_e are now referring to the internal and external regions respectively. The solution of the above equation can be written as

$$v_z(z) = \begin{cases} a_e e^{-m_e(z-z_0)} & z > z_0 \\ a_0 \cosh m_0 z + b_0 \sinh m_0 z & |z| < z_0 \\ b_e e^{m_e(z+z_0)} & z < -z_0, \end{cases} \quad (2.52)$$

and these solutions are chosen in such a way that waves are evanescent at large distances from the slab. Note that the amplitude coefficients a_0, b_0, a_e, b_e are constants

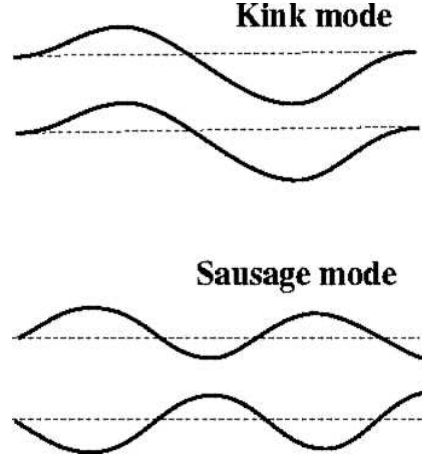


Figure 2.3: Sketch of the kink and sausage modes supported by a magnetic waveguide.

that need to be determined after applying the continuity conditions at the two interfaces.

Applying the requirement of continuity conditions of the normal component of the velocity and total pressure across the boundaries together with the requirement that the system of equations formed for the coefficients appearing in Eq. (2.52) has non-trivial solutions leads to the desired dispersion relations

$$(k^2 v_{A0}^2 - \omega^2) m_e = \frac{\rho_e}{\rho_0} \omega^2 m_0 \begin{pmatrix} \tanh \\ \coth \end{pmatrix} m_0 x_0, \quad (2.53)$$

where the two cases correspond to sausage and kink modes, respectively. Sausage modes propagate in such a way that the symmetry axis of the slab is not perturbed, while in the case of kink waves the symmetry axis of the slab is perturbed (see Fig. 2.3). Since Eq. (2.53) is a transcendental equation, it possess a wide range of solutions and within the context of solar plasma physics has been derived by Edwin and Roberts (1982, 1983). Although an extensive solution of this equation looks complicated, individual applications to, e.g. photospheric or coronal structures result to an easier configuration. According to the standard nomenclature, solutions corresponding to $m_0^2 > 0$ are labeled as surfaces waves, while waves with $m_0^2 < 0$ are body waves. There are different solutions because the waves behave spatially in a different way inside the structure; surface waves have their maximum amplitude on

the boundary and are not oscillatory inside the slab, while body waves show an oscillatory pattern inside the slab (see Fig. 2.4). Note that the $m_e^2 > 0$ restriction is

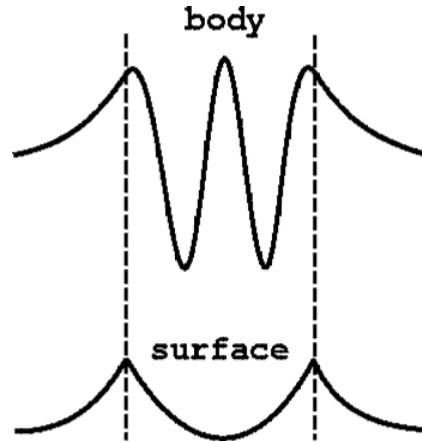


Figure 2.4: Sketch of the surface and body modes supported by a magnetic waveguide.

needed in order to have evanescent solutions outside the slab, a condition that leads to the existence of a cut-off frequency, over which the modes become leaky.

In an unstructured homogeneous plasma one expects three sort of waves, the slow magnetoacoustic waves, the fast magnetoacoustic waves, and the set of transversal Alfvén waves. During the analysis we uncoupled the transversal Alfvén waves, and thus they will not be considered further. However we should state that the slow and fast waves found in infinite plasmas are affected in a complicated procedure which depends on the relative magnitudes of sound and Alfvén speeds inside and outside the slab. In some cases, for example, that of a cold plasma (for which $v_{Ae} > v_A$, often applied for coronal structures) only two sets of body waves occur whereas under photospheric conditions where $v_{Ae} < v_A$, the slow mode can always propagate (either as a surface or body mode) but the fast mode may only propagate in a structure that is cooler than its surrounding (i.e. $c_e > c_0$).

The possible propagation modes can be discussed separately for coronal or photospheric conditions as will determine the relative magnitude of characteristic speeds. A characteristic dispersion diagram is shown in Fig. 2.5, where the possible modes arising in coronal slabs is shown (Adapted from Edwing and Roberts 1982). The dispersive character of these modes is evidenced through the dependence of their phase

2.3. WAVES IN STRUCTURED MEDIA

speed (ω/k) with the dimensionless quantity kx_0 , i.e. the wavelength of the modes (keeping the geometrical size of the slab constant). It is also remarkable that slow modes are confined in a small frequency band. This band is very narrow and close to zero when typical prominence and coronal values are used.

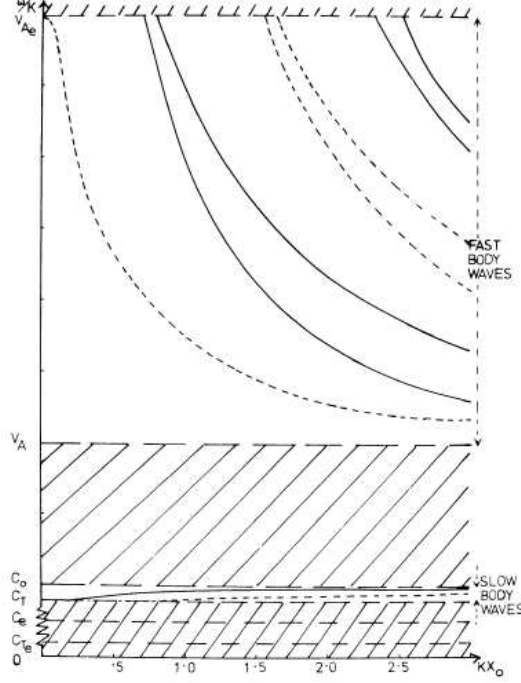


Figure 2.5: The dispersive diagram of modes arising in a coronal magnetic slab. Note that no surface modes are able to propagate in these structures (adapted from Edwin and Roberts 1982)

In the special case of $\gamma \rightarrow \infty$ (i.e. the incompressible case), then using

$$\rho_e = \frac{c_{S0}^2 + \frac{1}{2}\gamma v_{A0}^2}{c_{S_e}^2} \rho_0, \quad (2.54)$$

one can deduce that $m_0, m_e \approx k$, in which case Eq. (2.53) becomes

$$\frac{k^2 v_{A0}^2}{\omega^2} = 1 + \frac{\rho_e}{\rho_0} \begin{pmatrix} \tanh \\ \coth \end{pmatrix} m_0 x_0 k x_0. \quad (2.55)$$

As a final comment, this model can be applied to some solar structures, such as prominences, which are roughly slabs in which their length and height are much

larger than their width. In Joarder and Roberts (1992a, 1992b, 1993) and Oliver et al. (1992), a prominence is described as an infinite sheet of plasma with finite width $2a$ in the x -direction, while the y - and z -directions are Fourier-analyzed and the resulting eigenfrequencies are discussed and the output is compared with observational data. This idea has been pushed forward including more realistic prominence models (Oliver et al. 1993) and a smooth transition region (Oliver and Ballester 1996). The model has been extended to arrays of slabs modelling the multi-fibril structure of prominences by Berton and Heyvaerts 1987, Marcu et al. (2006).

Chapter 3

MHD equations in partially ionized plasma

3.1 Partially ionized plasma

At room temperature, most gases are essentially un-ionised. The particles constituting the gas are generally electrically neutral atoms and/or molecules. These particles occupy a random kinetic energy which is too small compared to the energy binding the outer shell electrons to the nucleus, and therefore, the internal electronic structure of atoms is unaffected by collisions. Nevertheless, increasing the temperature can make the collisions energetic enough to disrupt the internal structure of atoms and thus may lead to the production of free electrons and ions.

The lowest temperature at which a gas shows a significant degree of ionisation depends on the particular atom or molecule, as well as on the pressure. For example cesium becomes significantly ionised at 1,500 K, while for argon, a similar degree of ionisation can be reached at 6,000 K. At the other extreme, nearly all gases are highly ionised at temperatures in excess of about 20,000 K. It is important to note that these values are deduced assuming an equilibrium. There are many non-equilibrium situations (e.g. low pressure discharge) where a significant degree of ionisation may be present at much lower gas temperatures.

From a phenomenological point of view, an ionised gas is distinguished from a room temperature gas by its ability to conduct electricity and particles making up the

ionised gas can interact with external magnetic and/or electric fields. The possibility of coupling between fluids and electromagnetic forces gives rise to a multitude of new physical phenomena.

At temperatures we could meet deep down in the solar interior or the temperatures in flaring active regions in the solar corona, the gases are fully ionised, and the simpler gases such as H and He are completely stripped off all their electrons. The particles in such gases have no atomic structure and they interact according to simple electrostatic force laws. The description of fully ionised gases, in this respect, is considerably simplified and dynamical changes in such gases can be described within the framework of MHD, whose equations were presented in Chapter 2. Partially ionised gases consist of electrons, ions and neutral species (more precisely, a partially ionised gas contains six kinds of particles: photons, electrons, ground-level atoms, excited atoms, positive and negative ions), that is why the description of dynamical changes in such media is much more cumbersome.

In the solar atmosphere, the photosphere and lower part of the chromosphere is partially ionised plasma. Since prominences are believed to be of chromospheric origin, it is natural to assume that the plasma in these structures is also in partially ionised state. Indeed, neutral hydrogen emission lines in the Lyman continuum have been observed in prominences (the presence of neutrals will attenuate the intensity of the lines), by Chiuderi Drago et al. (2001) who have estimated that the number of neutrals in a prominence plasma may be as big as ten times the corresponding amount of electrons or as small as ten times smaller, indicating the size of variation for the ionization degree. Thus, apart from the electrical forces between electrons and ions in a prominence plasma, an important factor dominating the plasma dynamics is the collisions between electrons, neutrals and ions, and therefore, the set of MHD equations (2.1)-(2.9) should be modified, in order to accommodate this extra physical effect.

More importantly the collisions between neutrals and ions, and less importantly the collisions between electrons with ions or neutrals, are causing the Joule heating dissipation, which evidently leads the magnetoacoustic waves in the plasma to undergo a stronger frictional damping, rather than in a fully ionized plasma, where the collisions between the electrons and the ions have much smaller impact. Khodachenko et al. (2004, 2006) have shown that the effect of neutral-ion collision,

is a much stronger factor in the damping of MHD waves than viscosity or thermal conductivity effects.

In this chapter, the MHD equations will be modified to account for the ion-neutral collision effect, therefore obtaining the governing equations for partially ionized prominence plasma. The assumptions and derivation is based on an earlier study by Khodachenko et al. (2004) and Forteza et al. (2007).

Let us denote the temperature, density, number density, pressure and velocity of the electrons in a partially ionized prominence plasma by T_e, ρ_e, n_e, p_e and \mathbf{v}_e respectively. Then, the same parameters for the neutrals are denoted by T_n, ρ_n, n_n, p_n and \mathbf{v}_n , while for the ions we use T_i, ρ_i, n_i, p_i and \mathbf{v}_i . Since we are dealing with a hydrogen plasma (one electron and one ion), it is obvious that $n_i = n_e$. We can define the mass densities as $\rho_i = n_i m_i, \rho_n = n_n m_n, \rho_e = n_e m_e$, where m_i, m_e, m_n are the masses of an ion, an electron and a neutral, respectively (obviously $m_i \approx m_p$, where m_p is the proton mass). Then, the total density, total pressure and the velocity of the centre of mass are defined by

$$\rho = \rho_e + \rho_i + \rho_n \approx \rho_i + \rho_n, \quad (3.1)$$

$$p = p_e + p_i + p_n = 2p_i + p_n, \quad (3.2)$$

$$\mathbf{v} = \frac{\sum_{\alpha=e,i,n} \rho_{\alpha} \mathbf{v}_{\alpha}}{\rho} \approx \xi_i \mathbf{v}_i + \xi_n \mathbf{v}_n, \quad (3.3)$$

assuming that $\rho_e |\mathbf{v}_e| \ll \rho_i |\mathbf{v}_i|$ and that $\rho_e |\mathbf{v}_e| \ll \rho_n |\mathbf{v}_n|$. Furthermore, the relative densities of ions and neutrals are defined as

$$\xi_i = \frac{\rho_i}{\rho} \approx \frac{n_i}{n_i + n_n}, \quad (3.4)$$

$$\xi_n = \frac{\rho_n}{\rho} \approx \frac{n_n}{n_i + n_n}. \quad (3.5)$$

Then, the plasma ionization degree is defined by the ionization fraction

$$\tilde{\mu} = \frac{1}{1 + \xi_i}. \quad (3.6)$$

In reality, it represents the average mass per particle in units of the proton mass m_p . In this concept, Eq.(3.6) suggests that for a fully ionized plasma $\tilde{\mu} = 0.5$, while

for a neutral plasma $\tilde{\mu} = 1$, indicating that in a partially ionized plasma we have $0.5 < \tilde{\mu} < 1$. One may also express the relative densities in terms of the ionization factor as $\xi_i = 1/\tilde{\mu} - 1$ and $\xi_n = 2 - 1/\tilde{\mu}$.

In our analysis we assume that the number of ions, electrons and neutrals in the plasma is constant, and the effects of particle ionization and recombination will not influence the density of the plasma during the timescale of the physics we study (this is a necessary but not sufficient requirement for an ionisation equilibrium). Furthermore, assuming strong thermal coupling between ions, electrons and neutrals, their temperatures are all equal, i.e. $T_e = T_n = T_i = T$. Thus, the equations of continuity, momentum and energy conservation do not have to be separated for the 3 components (neutrals, electrons and ions), instead, a set of one-fluid MHD equations may be considered for the whole partially ionized plasma.

3.2 Continuity equation

In order to derive the continuity equation for partially ionised plasma we need to add up the partial continuity equations of the three species, i.e. the equations

$$\frac{\partial \rho_e}{\partial t} + \nabla \cdot (\rho_e \mathbf{v}_e) = 0, \quad (3.7)$$

$$\frac{\partial \rho_i}{\partial t} + \nabla \cdot (\rho_i \mathbf{v}_i) = 0, \quad (3.8)$$

$$\frac{\partial \rho_n}{\partial t} + \nabla \cdot (\rho_n \mathbf{v}_n) = 0. \quad (3.9)$$

Taking into account the definitions of density and the center of mass velocity (given by Eqs. (3.1) and (3.3), respectively), we obtain the continuity equation for partially ionized plasmas as

$$\frac{\partial \rho}{\partial t} + \nabla \cdot (\rho \mathbf{v}) = 0. \quad (3.10)$$

3.3 Momentum equation

Assuming that the lengths-scales involved in our investigation are shorter than the gravitational scale-height, we can neglect the effect of gravity, so the momentum

equation takes the general form

$$n_\alpha m_\alpha \frac{d_\alpha \mathbf{v}_\alpha}{dt} = -\nabla p_\alpha + n_\alpha Z_\alpha e (\mathbf{E} + \frac{1}{c} \mathbf{v}_\alpha \times \mathbf{B}) + \sum_\beta \mathbf{R}_{\beta\alpha}. \quad (3.11)$$

Here $\frac{d_\alpha}{dt} \equiv \frac{\partial}{\partial t} + \mathbf{v}_\alpha \cdot \nabla$ and Z_α is the charge of the particle implicated in the momentum equation (for our hydrogen plasma $Z_e = -1$, $Z_n = 0$, $Z_i = 1$). In the above equation the quantity $\mathbf{R}_{\beta\alpha}$ represents the momentum interchange between species α and β ($\alpha \neq \beta$) and is given by

$$\mathbf{R}_{\beta\alpha} = n_\alpha m_\alpha \nu'_{\alpha\beta} (\mathbf{v}_\beta - \mathbf{v}_\alpha). \quad (3.12)$$

Taking into account the principle of conservation of momentum in a collision, we arrive at

$$\mathbf{R}_{\beta\alpha} = -\mathbf{R}_{\alpha\beta}. \quad (3.13)$$

In the expression of $\mathbf{R}_{\beta\alpha}$ the quantity $\nu'_{\alpha\beta}$ is the effective collisional frequency and it can be calculated using

$$\nu'_{\alpha\beta} = \frac{m_\beta}{m_\alpha + m_\beta} \nu_{\alpha\beta}, \quad (3.14)$$

where $\nu'_{\alpha\beta} = \nu'_{\beta\alpha}$. Since $\alpha \neq \beta$, there are only six possible collisional frequencies $\nu_{\alpha\beta}$, but due to the symmetry of the problem $\nu_{\alpha\beta} = \nu_{\beta\alpha}$, therefore only three collisional frequencies need to be defined as

$$\nu_{ei} = 5.89 \times 10^{-24} \frac{n_i \ln \Lambda_C Z^2}{(k_B T)^{3/2}}, \quad (3.15)$$

$$\nu_{en} = n_n \sqrt{\frac{8k_B T}{\pi m_{en}}} \Sigma_{en}, \quad (3.16)$$

$$\nu_{in} = n_n \sqrt{\frac{8k_B T}{\pi m_{in}}} \Sigma_{in}, \quad (3.17)$$

where $\Sigma_{en} \sim 7 \times 10^{-16} \text{ cm}^2$ and $\Sigma_{in} \sim 5 \times 10^{-15} \text{ cm}^2$, denote the electron-neutral and ion-neutral collisional cross-sections, $m_{\alpha n} = m_\alpha m_n / (m_\alpha + m_n)$ with $\alpha = e, i$ and $\ln \Lambda_C$ is the Coulomb logarithm, which is usually between the values of 5 and 22, and depends weakly on temperature and density (Priest, 1984).

Let us define the quantities

$$\alpha_{\alpha\beta} = n_{\alpha}m_{\alpha}v'_{\alpha\beta}, \quad (3.18)$$

and

$$\alpha_n = \alpha_{in} + \alpha_{en}. \quad (3.19)$$

We can introduce the relative ion-neutral velocity, \mathbf{w} , and the electric current density, \mathbf{j} , as

$$\mathbf{w} = \mathbf{v}_i - \mathbf{v}_n \quad (3.20)$$

and

$$\mathbf{j} = n_i e (\mathbf{v}_i - \mathbf{v}_e), \quad (3.21)$$

respectively, then we may write three separate equations for the momentum conservation of electrons, ions and neutrals as

$$n_i m_e \frac{d_e \mathbf{v}_e}{dt} = -\nabla p_e - n_i e (\mathbf{E} + \frac{1}{c} \mathbf{v}_e \times \mathbf{B}) + (\alpha_{ei} + \alpha_{en}) \frac{\mathbf{j}}{n_i e} - \alpha_{en} \mathbf{w}, \quad (3.22)$$

$$n_i m_i \frac{d_i \mathbf{v}_i}{dt} = -\nabla p_i + n_i e (\mathbf{E} + \frac{1}{c} \mathbf{v}_i \times \mathbf{B}) - \alpha_{ei} \frac{\mathbf{j}}{n_i e} - \alpha_{in} \mathbf{w}, \quad (3.23)$$

and

$$n_n m_n \frac{d_n \mathbf{v}_n}{dt} = -\nabla p_n - \alpha_{en} \frac{\mathbf{j}}{n_i e} + (\alpha_{in} + \alpha_{en}) \mathbf{w}. \quad (3.24)$$

It should be noted that in the momentum equation of neutrals the Lorentz force does not appear, as it has effect only on charged particles. Adding together the above equations, and combining them with Eqs. (3.2), (3.20) and (3.21), we can obtain a single momentum equation describing the whole partially ionized plasma:

$$n_i m_i \frac{d_i \mathbf{v}_i}{dt} + n_n m_n \frac{d_n \mathbf{v}_n}{dt} = -\nabla p + \frac{1}{c} \mathbf{j} \times \mathbf{B}, \quad (3.25)$$

which simplifies to

$$\rho \frac{d\mathbf{v}}{dt} = -\nabla p + \frac{1}{c} \mathbf{j} \times \mathbf{B} - \nabla \cdot (\xi_i \xi_n \mathbf{w}\mathbf{w}), \quad (3.26)$$

where $d/dt \equiv \partial/\partial t + \mathbf{v} \cdot \nabla$. The last term on the RHS of Eq. (3.26) is caused by inertia

of species making up the plasma, and usually its magnitude under solar conditions is negligible. In the absence of an equilibrium flow, this term also disappears when restricting our analysis to the linear part. An expression for \mathbf{w} will be given later, when discussing Ohm's law.

3.4 The energy equation

The energy of the system is made up from the partial energies in each type of species. The energy equation for individual species (neglecting thermal conduction) can be written as

$$\frac{\partial p_\alpha}{\partial t} + \mathbf{v}_\alpha \cdot \nabla p_\alpha + \gamma p_\alpha \nabla \cdot \mathbf{v}_\alpha = (\gamma - 1)Q_\alpha, \quad \alpha = e, i, n \quad (3.27)$$

where $Q_\alpha = \sum_\beta Q_{\alpha\beta}$ with $Q_{\alpha\beta}$ being the heat generated in a gas of particles of species α as a result of collisions with particles of species β . After adding the energy equations of individual species we obtain

$$\frac{\partial p}{\partial t} + \sum_\alpha (\mathbf{v}_\alpha \cdot \nabla p_\alpha + \gamma p_\alpha \nabla \cdot \mathbf{v}_\alpha) = (\gamma - 1) \sum_\alpha Q_\alpha, \quad (3.28)$$

Combining Eqs. (3.20) and (3.21) with the relation

$$Q_{\alpha\beta} + Q_{\beta\alpha} = -\mathbf{R}_{\beta\alpha} \cdot (\mathbf{v}_\alpha \mathbf{v}_\beta), \quad (3.29)$$

we can write the sum on RHS of Eq.(3.29) as

$$Q_e + Q_i + Q_n = \frac{\alpha_e}{e^2 n_i^2} j^2 + \alpha_n w^2 - 2 \frac{\alpha_{en}}{en_i} \mathbf{w} \cdot \mathbf{j}. \quad (3.30)$$

After some algebra, the energy equation for the whole partially ionized plasma is as follows:

$$\frac{dp}{dt} + \gamma p \nabla \cdot \mathbf{v} + \gamma \nabla \cdot (2\xi_n p_i \mathbf{w} - \xi_i p_n \mathbf{w}) - \gamma \mathbf{j} \cdot \nabla \left(\frac{p_i}{en_i} \right) = (\gamma - 1) q_{Joule}, \quad (3.31)$$

and combining this with the continuity equation (3.10) yields

$$\frac{dp}{dt} - \frac{\gamma p}{\rho} \frac{d\rho}{dt} + \gamma \nabla \cdot (2\xi_n p_i \mathbf{w} - \xi_i p_n \mathbf{w}) - \gamma \mathbf{j} \cdot \nabla \left(\frac{p_i}{en_i} \right) = (\gamma - 1) q_{Joule}. \quad (3.32)$$

In practice our investigations will require only linear description in homogeneous equilibrium (i.e. the last two terms on the LHS of Eq. (3.32) will cancel) and the changes in the plasma will occur in an adiabatic way, i.e. the RHS of the above equation will also vanish.

3.5 Equation of state

This equation determines the temperature, given the number density, n , and the pressure, p , by adding the following equations of state for electrons, ions and neutrals, respectively

$$p_e = n_e k_B T = n_i k_B T, \quad (3.33)$$

$$p_i = n_i k_B T, \quad (3.34)$$

$$p_n = n_n k_B T. \quad (3.35)$$

Therefore, the equation of state for the whole partially ionized plasma becomes

$$p = p_e + p_i + p_n = (2n_i + n_n) k_B T = n k_B T. \quad (3.36)$$

3.6 Ohm's law

Traditionally, Ohm's law is the relation that connects the current density, the electric field and the contribution of the current density due to the motion of a charged particle in the presence of a magnetic field (Lorentz force contribution) written in a frame of reference that is not moving together with the charged particle. Given the particular composition of the partially ionised plasma, we can expect that the Ohm's law will be much more complex.

The momentum transfer between various species will influence the generated current density. In order to assess this contribution let us multiply Eqs. (3.22) and

(3.23) by ξ_n and Eq. (3.24) by $-\xi_i$ and add them together to obtain

$$\mathbf{w} = -\frac{\mathbf{G}}{\alpha_n} + \frac{\xi_n}{c\alpha_n} \mathbf{j} \times \mathbf{B} + \frac{\alpha_{en}}{\alpha_n} \frac{\mathbf{j}}{en_i} - \frac{\xi_n \xi_i}{\alpha_n} \rho \left(\frac{d_i \mathbf{v}_i}{dt} - \frac{d_n \mathbf{v}_n}{dt} \right), \quad (3.37)$$

where the pressure function G is defined by (Braginskii 1965)

$$\mathbf{G} = \xi_n \nabla(p_e + p_i) - \xi_i \nabla p_n. \quad (3.38)$$

Instead of using partial pressures of various components of the fluid, let us use the pressure of the mixture, so we write

$$p_e = p_i = \frac{\xi_i}{1 + \xi_i} p, \quad (3.39)$$

and

$$p_n = \frac{\xi_n}{1 + \xi_i} p, \quad (3.40)$$

which means that the pressure function can be defined as

$$\mathbf{G} = 2\xi_n \nabla \left(\frac{\xi_i}{1 + \xi_i} p \right) - \xi_i \nabla \left(\frac{\xi_n}{1 + \xi_i} p \right). \quad (3.41)$$

Furthermore, taking into account Eqs. (3.3), (3.20) and (3.21) we have

$$\mathbf{v}_e = \mathbf{v} + \xi_n \mathbf{w} - \frac{\mathbf{j}}{en_i}. \quad (3.42)$$

Now, considering together Eqs. (3.22), (3.37), and (3.42), neglecting the derivatives of \mathbf{v}_i and \mathbf{v}_n in Eq. (3.37), one can obtain

$$\begin{aligned} \mathbf{E}^* &\equiv \mathbf{E} + \frac{1}{c} \mathbf{v} \times \mathbf{B} \\ &= \frac{\varepsilon \mathbf{G} - \nabla p_e}{en_i} + \frac{\mathbf{j}}{\sigma} + \frac{1 - 2\varepsilon \xi_n}{en_i c} \mathbf{j} \times \mathbf{B} + \frac{\xi_n}{c\alpha_n} \left[\mathbf{G} \times \mathbf{B} - \frac{\xi_n}{c} (\mathbf{j} \times \mathbf{B}) \times \mathbf{B} \right] \end{aligned} \quad (3.43)$$

where $\varepsilon = \alpha_{en}/\alpha_n \ll 1$ and σ is the electrical conductivity defined as

$$\sigma = \frac{n_i e^2}{m_e [\nu'_{ei} + (1 - \varepsilon)\nu'_{en}]} \approx \frac{n_i e^2}{m_e (\nu'_{ei} + \nu'_{en})} \quad (3.44)$$

while the Joule heating term q_{Joule} appearing in Eq. (3.31) may be defined using Eq. (3.43) as

$$q_{Joule} \equiv \mathbf{E}^* \cdot \mathbf{j} = \frac{\varepsilon \mathbf{G} - \nabla p_e}{n_i} \cdot \mathbf{j} + \frac{j^2}{\sigma} + \frac{\xi_n}{c\alpha_n} (\mathbf{j} \times \mathbf{B}) \cdot \mathbf{G} + \frac{\xi_n^2}{c^2 \alpha_n} (\mathbf{j} \times \mathbf{B})^2. \quad (3.45)$$

3.7 Induction equation

The induction equation connects the magnetic field and the plasma fluid penetrated by this magnetic field. In the case of a partially ionised plasma, one has to keep in mind that only the charged particles are affected by the magnetic field, while the collective motion of the plasma is ensured by collisions between ions and neutrals. In the absence (or very low frequency) of collisions, the neutrals would fall out of the plasma.

In order to derive the induction equation, we will apply the curl operator to Eq. (3.43) and we will insert this expression into Faraday's law:

$$\nabla \times \mathbf{E} = -\frac{1}{c} \frac{\partial \mathbf{B}}{\partial t},$$

to obtain

$$\begin{aligned} \frac{\partial \mathbf{B}}{\partial t} = & \nabla \times (\mathbf{v} \times \mathbf{B}) - \frac{c}{e} \nabla \times \left(\frac{\varepsilon \mathbf{G} - \nabla p_e}{n_i} \right) - \nabla \times (\eta \nabla \times \mathbf{B}) \\ & - \nabla \times \left(\frac{\xi_n}{\alpha_n} \mathbf{G} \times \mathbf{B} \right) - \frac{c}{\mu_0 e} \nabla \times \left[\frac{1 - 2\varepsilon \xi_n}{n_i} (\nabla \times \mathbf{B}) \times \mathbf{B} \right] \\ & + \nabla \times \left\{ \frac{\xi_n^2}{\mu_0 \alpha_n} [(\nabla \times \mathbf{B}) \times \mathbf{B}] \times \mathbf{B} \right\}, \end{aligned} \quad (3.46)$$

3.8. SUMMARY OF SINGLE-FLUID MHD EQUATIONS FOR PARTIALLY IONISED PLASMA

where η is the coefficient of magnetic diffusivity, defined as

$$\eta = \frac{c^2}{\mu_0 \sigma}. \quad (3.47)$$

where c is the speed of light and σ is the electrical conductivity coefficient defined in Eq.(3.44). The coefficient appearing in the last term of Eq. (3.46) is also used as (see, e.g. Khodachenko et al. 2004)

$$\frac{\xi_n^2}{\mu_0 \alpha_n} = \frac{\eta_C - \eta}{|\mathbf{B}|^2}, \quad (3.48)$$

where η_C is the Cowling resistivity defined as

$$\eta_C = \frac{c^2 \left(1 + \frac{\xi_n^2 B_0^2 \sigma}{\alpha_n c^2}\right)}{4\pi \sigma}. \quad (3.49)$$

The RHS terms of Eq. (3.46) correspond to the convective term, Biermann's battery, Ohm's diffusion, diamagnetic current term, Hall's diffusion and ambipolar diffusion, respectively. The Biermann's battery term is negligible, unless there are big pressure gradients present. Ohm's diffusion varies with electron-ion collisions, while ambipolar diffusion is mainly based on the effect of ion-neutral collisions. Hall's diffusion is also rooted in ion-neutral collisions and it is present even in the fully ionized plasma. The diamagnetic current term represents the effect of combination between magnetic field and pressure gradient, and it is more effective for partially ionized plasma, since for neutral or full ionization, the term \mathbf{G} vanishes.

3.8 Summary of single-fluid MHD equations for partially ionised plasma

Given the nature of the plasma in which we are interested, the equations which will be used to describe the dynamics will contain information about the degree of the ionisation. Under solar conditions and in a linear regime, the quantity \mathbf{w} from Eq.(3.37) can be neglected (Khodachenko et al. 2004).

The plasma dynamics will be fully described by the linearised version of Eqs.

3.8. SUMMARY OF SINGLE-FLUID MHD EQUATIONS FOR PARTIALLY IONISED PLASMA

(3.10), (3.26), (3.32),(3.36), (3.45), and (3.46). This system contains 9 equations involving 9 quantities. In order to formulate the set of MHD equations for an ideal plasma we neglect the non-adiabatic terms. Furthermore, in a prominence the conditions of temperature and density, and the presence of strong magnetic field, bound the electrons and ions to the magnetic field, and as a result the product of ion-gyrofrequency with collision time $\omega_i\tau \gg 1$, thus turning the Hall effect into a negligible term in Ohm's law (Leake et al. 2005).

Assuming a plasma in spatially homogeneous equilibrium with no pressure gradients, and neglecting gravity, viscosity, inertia of species, the Biermann's battery and Hall's diffusion terms, the set of MHD equations for partially ionized plasma is

$$\frac{\partial \rho}{\partial t} + \nabla \cdot (\rho \mathbf{v}) = 0, \quad (3.50)$$

$$\rho \frac{d\mathbf{v}}{dt} = -\nabla p + \frac{1}{\mu_0} [(\nabla \times \mathbf{B}) \times \mathbf{B}], \quad (3.51)$$

$$\frac{dp}{dt} + \gamma p \nabla \cdot \mathbf{v} - \gamma \frac{\mathbf{j}}{en_i} \cdot \nabla p_i = -(\gamma - 1)[\rho L(\rho, T) - \nabla \cdot (\kappa \cdot \nabla T) - q_{Joule}], \quad (3.52)$$

$$\nabla \times \mathbf{B} = 0, \quad (3.53)$$

$$\begin{aligned} \frac{\partial \mathbf{B}}{\partial t} = & \nabla \times (\mathbf{v} \times \mathbf{B}) + \eta \nabla^2 \mathbf{B} - \Xi \nabla \times (\nabla p \times \mathbf{B}) \\ & + \frac{\eta_C - \eta}{|\mathbf{B}|^2} \nabla \times \{[(\nabla \times \mathbf{B}) \times \mathbf{B}] \times \mathbf{B}\}, \end{aligned} \quad (3.54)$$

$$p = \frac{\rho RT}{\tilde{\mu}}, \quad (3.55)$$

where Ξ is defined as:

$$\Xi = \frac{\xi_i \xi_n^2}{(1 + \xi_i) \alpha_n}. \quad (3.56)$$

It should be pointed out that, in order to study MHD waves in partially ionised plasmas, other approaches could be taken. For instance, Zaqrashvili et al. (2011) have considered the two-fluid approach, one fluid made of the charged particles (ions and electrons) and the other one made by neutrals. In order to obtain the set of MHD equations applicable to this case, they start from three fluid equations (Braginskii 1965; Goedbloed and Poedts 2004) plus Maxwell's equations. After neglecting the

3.8. SUMMARY OF SINGLE-FLUID MHD EQUATIONS FOR PARTIALLY IONISED PLASMA

electron inertia and viscosity effects, they derived a set of two-fluid MHD equations for partially ionised plasmas. Once derived, this set of equations can be used for the study of MHD waves in the two-fluid approach. The interest of this approach is related to the time-scales of the phenomena under study since for timescales longer than the ion-neutral collision time, the system can be considered as a single-fluid. However, when the time-scales are near or shorter than the ion-neutral collision time, two-fluid equations should be considered. Indeed considering typical prominence values $T = 10^4$ K, $n_i = 2.3 \times 10^{16} \text{ m}^{-3}$, $n_n = 1.2 \times 10^{16} \text{ m}^{-3}$ (Fontenla et al. 1990), we obtain an ion-collision time of the order of $\frac{1}{4}$ s, a time-scale much shorter than the period of any wave that we will deal with. That is why our single fluid approach is fully justified. However, instabilities can develop even at this scale, microinstabilities can develop into large scale, now observable instabilities. An illustrative example of such instability will be discussed in the following chapter.

Chapter 4

Dissipative instability in partially ionised prominence plasmas ¹

4.1 Introduction

Solar prominences are among the most enigmatic structures in the solar atmosphere whose study is made difficult by their complex evolution and the multitude of important effects appearing in them. Prominences are believed to be of chromospheric origin (Priest, 1982), and some of them show a long-term stability. When formed, prominences maintain their high density and low temperature despite being surrounded by the million degree solar corona. Their stability and thermal shielding are provided by the magnetic field. The core of almost 80% of the observed CMEs (the drivers of space weather) is made of a cold chromospheric core believed to originate from a prominence, which is why the study of the generation and evolution of prominences is necessary.

Solar prominences are complex dynamical systems whose intrinsic structure and properties make the study of these magnetic features rather complicated.

Some of the peculiar properties of prominences are listed in Chapter 1. For our analysis, the characteristic that is important is the dynamical background of prominences, flows, which are observed on all time and spatial scales. A particular feature

¹The content of this chapter is based on the publication by Ballai, Oliver and Alexandrou 2015, *Astron. Astrophys.*, 577, 82

in these observations is the presence of counter-streaming flows, i.e. oppositely directed flows (Zirker et al., 1998; Lin et al., 2003). Because of the physical conditions of the filament plasma, all these flows seem to be field-aligned. For a detailed review of the observed flows in solar prominences, see Labrosse et al. (2010) and Mackay et al. (2010).

Significant advancement in the study of prominences was made when high-resolution observations of waves, oscillations, and flows became available. Scientists were able to connect theoretical models with observations through seismological techniques in order to derive quantities and processes (structure of the magnetic field, transport mechanisms acting in prominences, internal structure, etc.) that cannot be measured directly or indirectly (for a detailed discussion of seismological techniques and results see the review by Arregui et al. 2012). There is also some evidence that velocity oscillations are more easily detected at the edges of prominences or where the material seems fainter, while they are sometimes harder to detect at the prominence main body (Tsubaki and Takeuchi, 1986; Tsubaki et al., 1988; Suematsu et al., 1990; Thompson and Schmieder, 1991; Terradas et al., 2002).

As mentioned earlier, prominences are not fully ionised gases due to their relative low temperature. In this environment the dynamics of the plasma is described by modified MHD equations, listed in Chapter 3. The ionisation degree of prominences is not well known, but there is plentiful evidence that this cannot be neglected when one studies the dynamics and stability of these structures (Patsourakos and Vial 2002, Gilbert et al. 2007, Labrosse et al. 2010, Zaqarashvili et al. 2011, Khomenko and Collados 2012, etc.).

The problem of prominence stability is paramount for other effects such as CME eruption due to the connection between these two solar atmospheric structures. In a recent series of papers Ryutova et al. (2010), Berger et al. (2010), Terradas et al. (2012) highlighted a number physical processes taking place in solar prominences that can be connected to instabilities, such as Rayleigh-Taylor instabilities (RTI) and Kelvin-Helmholtz instabilities (KHI) under the effect of plasma flows. The effect of partial ionisation on the stability of prominences was investigated earlier by, e.g. Diaz et al. (2012), who analysed the appearance of RTI in partially ionised prominence plasma. These authors found that the linear growth rate is lowered by both the compressibility of the gas and ion-neutral collisions, even though the appearance

threshold of this instability is not altered. They also found that the ion-neutral collisions have a strong impact on the RTI growth rate, which can be decreased by an order of magnitude compared to the case corresponding to the collisionless limit. They conclude that their results could explain the existence of prominence fine structure with lifetimes of the order of 30 minutes, a duration that classical theories cannot explain.

In the same year, Soler et al. (2012) investigated the KHI of compressible and partially ionised prominence plasma. They considered the stability of an interface separating two partially ionised plasmas in the presence of a shear flow. In the incompressible limit the KHI was present for any value of the flow, regardless of the degree of ionisation. When extended to a compressible limit, the instability threshold was very much sensitive to the collision frequency and density contrast between the two layers of their model. In particular the density contrast is an important parameter in their model. In classical theories the flow speed at which the KHI is set is always super-Alfvénic; however, the results of these authors show that for a high density contrast the threshold can be even sub-Alfvénic thanks to the ion-neutral coupling.

In addition to these instabilities there is another, rather unexpected instability that can arise at the interface between two media called *dissipative instability* and it is strongly connected to the phenomenon of *negative energy waves*. This instability always occurs for flows lower than the KHI value. Under normal conditions the interface between two media allows the propagation of two modes traveling in opposite directions. For flow speeds larger than a critical value, the propagation direction of the two waves becomes identical, and the wave whose phase speed is smaller becomes a negative energy wave (Ryutova, 1988). The dissipative mechanisms acting in the two regions can amplify this negative energy mode leading to *dissipative instability*, and the growth rate of this instability is proportional to the combination of dissipative coefficients. Under solar conditions the problem of negative energy waves has been studied by many authors (e.g. Ruderman and Goossens 1995, Ruderman et al. 1996, Joarder et al. 1997, Terra-Homem et al. 2003, etc). In the present study we consider this problem, but the two regions separated by the interface are the viscous corona and the partially ionised prominence plasma.

4.2. GOVERNING EQUATIONS AND BASIC ASSUMPTIONS

The concept of negative energy waves is based on the energy equation

$$\frac{dE}{dt} = -D, \quad (4.1)$$

where E is the linear part of the energy and D is the dissipative function. The two functions appearing in the above relation depend on the choice of the frame of reference. If we choose a coordinate system where $D > 0$, then the variation of the energy with time is negative, meaning that the energy of the system decays as a result of dissipation. In this case $E > 0$ for positive energy waves, and dissipation leads to the damping of the wave, i.e. to a decay in its amplitude. However, if $E < 0$ the wave is called a negative energy wave and dissipation leads to an amplification of the wave amplitude resulting to an instability.

4.2 Governing equations and basic assumptions

4.2.1 Equilibrium

We assume two semi-infinite layers of collisional and incompressible plasma separated by an interface modeling the interface between the solar prominence and solar corona.

The interface between the corona (labeled with index “1”) and the solar prominence (labeled with index “2”) is situated at $z = 0$ in a two-dimensional ($x-z$) Cartesian reference system. The homogeneous magnetic field ($\mathbf{B}_0 = B_0\mathbf{x}$) in both regions is along the x -axis with $B_{01} \neq B_{02}$ (although this is not an essential requirement, as we will deal with Alfvén speeds rather than magnetic fields). The unperturbed state is characterised by an MHD tangential discontinuity at $z = 0$, and all equilibrium quantities are constant at both sides of the discontinuity. We assume that there is an equilibrium flow in the positive x -direction ($\mathbf{v}_0 = v_0\mathbf{x}$) in the prominence (for the $z > 0$ region), while in the corona (corresponding to $z < 0$) the equilibrium is static (see Fig. 4.1). The above equilibrium describes the interface between a prominence and the surrounding quiet corona. Although these two solar regions can be neighbors for a very long time (in the case of quiescent prominences their stability is shown to be of the order of several months) they present a very different set of physical

4.2. GOVERNING EQUATIONS AND BASIC ASSUMPTIONS

parameters describing them. Solar prominences are cool and dense plasma material, thought to be of chromospheric origin that are surrounded by the very hot and very tenuous solar corona. Accordingly, it is customary to consider that the density of the prominence is two orders of magnitude larger than the density of the corona and the temperature two orders of magnitude lower than the coronal temperature. Gravity is neglected and so the RTI is not present in our problem.

4.2.2 Basic assumptions

The determination of transport mechanisms acting in solar plasmas is a very difficult task. After all, the dominant dissipative mechanism depends not only on the location where the dynamics occurs, but also on the nature of the physical mechanisms that needs describing. Under prominence conditions Ballai (2003) and Carbonell et al. (2004) showed that none of the classical dissipative processes (assuming a fully ionised plasma) are able to describe realistic damping of observed waves in prominences, except thermal conduction. Recent studies (e.g. Khodachenko et al. 2004, Arber et al. 2007, Forteza et al. 2007, 2008) also showed that the dominant transport mechanism in solar prominences is probably due to the partially ionised character of the plasma. Soler et al. (2009b) found that resonant absorption is dominant over ion-neutral effects in the damping of the kink mode in prominence threads. In the present study the appearance of resonant absorption is prevented by assuming a sharp transition between the prominence and corona.

In partially ionised plasmas the classical Coulomb resistivity is several orders of magnitude smaller than the Cowling resistivity, and the viscosity of the plasma is provided by the friction between various particles making up the plasma (neutrals, ions, protons). The second consideration also implies that the dynamics in solar prominences has to be described in a multi-fluid plasma. However, if the resistivity of the plasma is dominant (as is assumed here) the plasma is described within the framework of single-fluid MHD. In the present paper we will assume that these restrictive conditions are satisfied, i.e. we are going to use a single-fluid description.

As stated in Chapter 3, in partially ionised prominence plasmas the Coulomb resistivity is many orders of magnitude smaller than the Cowling anisotropic resistivity (see e.g. Cowling 1957, Khodachenko et al. 2004). Indeed, their difference is given

4.2. GOVERNING EQUATIONS AND BASIC ASSUMPTIONS

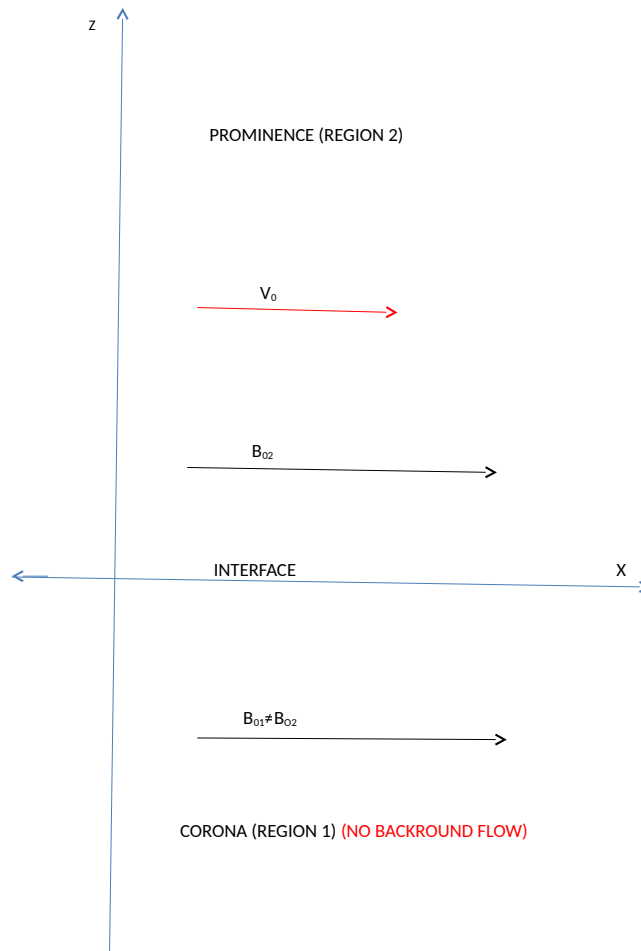


Figure 4.1: The interface between the corona (labeled with index “1”) and the solar prominence (labeled with index “2”) is situated at $z = 0$ in a two-dimensional ($x - z$) Cartesian reference system. Regions 1 and 2 correspond to $z < 0$ and $z > 0$, respectively. The equilibrium flow is denoted by v_0 for region 2 and is parallel to the interface. In region 1 equilibrium flow is static. Magnetic fields differ in magnitude in the two regions but they are both parallel to the interface

4.2. GOVERNING EQUATIONS AND BASIC ASSUMPTIONS

by η_C (the Cowling resistivity), defined by Eq. (3.49). The parameters η , μ_0 , ξ_n are all defined in section 3.7. The frictional coefficient α_n , defined by Eq. (3.19), in the case of a plasma assumed to be composed entirely of H is given by

$$\alpha_n = 2\xi_n(1 - \xi_n) \frac{\rho^2}{m_p} \sqrt{\frac{k_B T}{\pi m_p}} \Sigma_{in}, \quad (4.2)$$

where m_p is the proton (ion) mass, ρ is density, k_B is the Boltzmann constant, and $\Sigma_{in} \approx 5 \times 10^{-19} \text{ m}^2$ is the ion-neutral collisional cross-section. The number densities of electrons and ions are assumed to be approximately equal. The quantity ξ_n plays an important role in our discussion as it contains information about the ionisation degree of the plasma. By definition this quantity reflects the number of neutrals in the gas mixture, and is defined by Eq.(3.5).

The degree of ionisation can be characterised by the ionisation fraction defined by Eq. (3.6). According to this definition, a fully ionised gas corresponds to $\tilde{\mu} = 0.5$, while a neutral gas is described by $\tilde{\mu} = 1$.

Our aim here is to study the appearance and evolution of instabilities at the interface of two media, therefore we neglect the effects of particle ionisation and recombination in the solar prominence. Here we assume a strong thermal coupling between the species, which means electrons, ions, and neutrals have the same temperature (i.e. $T_e = T_i = T_n = T$). Therefore, the three-component gas can be considered as a single fluid. The concept of a three-component gas mixture will introduce new types of transport mechanisms, whose importance in the context of solar prominences was discussed in detail in the pioneering work of Forteza et al. (2007). Since we limit ourselves to linear dissipation, we will neglect effects connected to the inertia of different particles, also the transversal drift of charged particles due to the Hall term, and consider that thermodynamic quantities (pressure, temperature) are relatively smooth functions of the spatial coordinates, i.e. the relative densities of neutrals and ions are constants. Therefore, when describing the dynamics in solar prominences we will restrict our model to transport mechanisms that arise in the induction equation (see further down this chapter).

Temperatures in the solar corona can reach millions of degrees K, therefore the plasma can be considered to be completely ionised. In this important solar region

4.2. GOVERNING EQUATIONS AND BASIC ASSUMPTIONS

$\omega_{ci}\tau_i \gg 1$ (where ω_{ci} is the ion cyclotron frequency and τ_i is the ion mean collisional time), therefore ions can gyrate many times around magnetic field lines between collisions. Under typical coronal conditions this product is of the order of 10^5 . Provided the characteristic scales are larger than the mean free path of ions, viscosity in the solar corona is mainly due to ions and the viscosity gyrating around the magnetic field is given by the Braginskii's stress tensor (Braginskii 1965), whose linearized expression takes the form of a sum of 5 terms each with different physical meaning (see, e.g. Ruderman et al. 2000, Mocanu et al. 2008). The very first term in this sum is the so-called parallel (or compressional) viscosity. It controls the variation along magnetic field lines of the velocity component parallel to field lines. The parallel viscosity is due to the collision-induced random-walk diffusion of particles. The next two terms describe the perpendicular viscosity (or shear viscosity) which controls the variation perpendicular to magnetic field lines of the velocity components perpendicular to the field lines. Finally, the last two terms are known as the gyroviscosity and they do not describe viscosity at all, since the associated viscous stresses are always perpendicular to the velocity, implying that there is no dissipation (i.e. viscous heating) associated with this effect. Instead, these terms generate dispersion rather than dissipation. The value of the gyroviscosity is independent on the collisional frequency. As established by Ruderman et al. (1996), a property of the highly anisotropic viscosity is that it allows a jump in the velocity across a magnetic surface, since a strong magnetic field causes ions to rotate around the magnetic field lines, thus preventing the diffusion of particles across the field lines. This also implies that there is no momentum transport across the magnetic surfaces, and different layers of plasma can move with respect to each other without friction.

Under coronal conditions the first term, called parallel or compressional viscosity, is dominant (by several orders of magnitude) and controls the variation along magnetic field lines of the velocity component parallel to field lines. The parallel viscosity is due to the collision-induced random-walk diffusion of particles and is given by

$$\eta_0 = \frac{\rho_0 T_0 k_B \tau_i}{m_p}, \quad (4.3)$$

where ρ_0 and T_0 are the density and temperature of the medium. In practice it is more convenient to work with the kinematic coefficient of viscosity defined as $\nu = \eta_0/\rho_0$.

4.2. GOVERNING EQUATIONS AND BASIC ASSUMPTIONS

Observations show that quiescent prominences are made of chromospheric material and they live in a relatively stable position for a long time. High-resolution observations very often show that the edges of prominences are not still; small- and large-scale features appear and disappear frequently. We will explain these modifications in the interface between the two media by instabilities that develop due to the amplification of waves propagating along the interface. These instabilities can later grow into e.g. turbulence or macro-instabilities that can disrupt the interface between the two media.

4.2.3 Governing linearised equations

The equations describing the dynamics of the plasma are the incompressible dissipative and linear MHD equations. In both regions the equations

$$\nabla \cdot \mathbf{v} = 0, \quad \nabla \cdot \mathbf{b} = 0 \quad (4.4)$$

are valid (the above equations are met before in section 2.2.2 and Eq. (2.8), respectively. In the solar prominence we assume a field-aligned equilibrium flow (\mathbf{v}_0). The momentum equation (Eq. 2.3) becomes

$$\rho_2 \frac{\partial \mathbf{v}_2}{\partial t} + v_0 \frac{\partial \mathbf{v}_2}{\partial x} = -\nabla P_2 + \frac{B_{02}}{\mu_0} \frac{\partial \mathbf{b}_2}{\partial x}. \quad (4.5)$$

In the solar corona the equilibrium is static, but the momentum equation is supplemented by the viscous force, i.e.

$$\rho_1 \frac{\partial \mathbf{v}_1}{\partial t} = -\nabla P_1 + \frac{B_{02}}{\mu_0} \frac{\partial \mathbf{b}_1}{\partial x} + \mathcal{V}. \quad (4.6)$$

In the solar prominence the dominant dissipative effect is the Cowling resistivity, therefore the induction equation becomes

$$\frac{\partial \mathbf{b}_2}{\partial t} + v_0 \frac{\partial \mathbf{b}_2}{\partial x} = B_{02} \frac{\partial \mathbf{v}_2}{\partial x} + \mathcal{R}. \quad (4.7)$$

4.2. GOVERNING EQUATIONS AND BASIC ASSUMPTIONS

In the corona, the flow and dissipative effects do not modify the induction equation, so we can write

$$\frac{\partial \mathbf{b}_1}{\partial t} = B_{01} \frac{\partial \mathbf{v}_1}{\partial x}. \quad (4.8)$$

In the above equations \mathbf{v}_i and \mathbf{b}_i ($i = 1, 2$) are the perturbations of velocity and magnetic field, P_i are the total pressures (the sum of kinetic and magnetic pressures), and the dissipative terms in Eqs. (4.6) and (4.7) are given by (see, e.g. Ruderman et al. 1996)

$$\begin{aligned} \mathcal{V} &= \nu \left[\tilde{\mathbf{b}}(\tilde{\mathbf{b}} \cdot \nabla) - \frac{1}{3} \nabla \right] \left[\tilde{\mathbf{b}} \cdot \nabla(\tilde{\mathbf{b}} \cdot \mathbf{v}_1) \right], \\ \mathcal{R} &= \eta \nabla^2 \mathbf{b}_2 + \frac{(\eta_C - \eta)}{|\mathbf{B}_{02}|^2} \nabla \times \{[(\nabla \times \mathbf{b}_2) \times \mathbf{B}_{02}] \times \mathbf{B}_{02}\}, \end{aligned} \quad (4.9)$$

where $\tilde{\mathbf{b}}$ is the unit vector in the direction of the magnetic field, i.e. $\tilde{\mathbf{b}} = \mathbf{B}_{01}/B_{01}$.

Because of the orientation of the equilibrium magnetic field, the interface between the corona and solar prominence can be considered a tangential discontinuity. We write the equation of the perturbed interface as $z = \zeta(x, t)$. We assume that at $|x| \rightarrow \infty$ and $|z| \rightarrow \infty$ all perturbations vanish. At the interface surface waves will be able to propagate, as suggested in an earlier investigation by Roberts (1981). According to his results, in the absence of any equilibrium flow, incompressible Alfvén waves can propagate with a phase speed that lies between the Alfvén speeds in the two regions, which is given by

$$\frac{\omega}{k_x} = \pm \left(\frac{\rho_1 v_{A1}^2 + \rho_2 v_{A2}^2}{\rho_1 + \rho_2} \right)^{1/2} = \pm \left(\frac{v_{A1}^2 + d v_{A2}^2}{1 + d} \right)^{1/2}, \quad (4.10)$$

where $d = \rho_2/\rho_1 \gg 1$ is the density contrast parameter, k_x is the parallel component of the wavevector to the interface, and $v_{A1} = B_{01}/\sqrt{\mu_0 \rho_1}$ and $v_{A2} = B_{02}/\sqrt{\mu_0 \rho_2}$ are the Alfvén speeds in the two regions. This dispersion relation describes the propagation of the two waves along the interface in opposite directions.

For a stable interface at $z = 0$ we have to impose the linearised kinetic boundary condition and the condition of the continuity of normal component of stresses. If $\mathbf{v}_i = (v_{xi}, 0, v_{zi})$, then these conditions read

$$v_{z1} = \frac{\partial \zeta}{\partial t}, \quad v_{z2} = \frac{\partial \zeta}{\partial t} + v_0 \frac{\partial \zeta}{\partial x}, \quad (4.11)$$

4.3. DISPERSION RELATION OF SURFACE WAVES PROPAGATING AT THE TANGENTIAL DISCONTINUITY

and

$$P_1 + \rho_1 \nu \tilde{\mathbf{b}} \cdot \nabla (\tilde{\mathbf{b}} \cdot \mathbf{v}) \equiv P_1 - \rho_1 \nu \frac{\partial v_{z1}}{\partial z} = P_2. \quad (4.12)$$

We note here that at the tangential discontinuity used in the present paper there is no mass transfer between the two media, meaning that the state of the plasma in each region is not disturbed by the presence of the other medium. The system of equations (4.4)–(4.9) together with the boundary conditions at the interface will form the starting equations for our discussion on dissipative instability generated at the interface between the two media.

4.3 Dispersion relation of surface waves propagating at the tangential discontinuity

Since we are going to deal with an eigenvalue problem we will perform a normal mode analysis and take all perturbations proportional to $\exp[i(k_x x - \omega t)]$, where ω is a complex frequency that can be written as $\omega = \text{Re}(\omega) + i\text{Im}(\omega)$. This particular form of perturbations reduces the boundary conditions (see Eq. 4.11) to

$$v_{z1} = -i\omega\zeta, \quad v_{z2} = -i\Omega\zeta, \quad (4.13)$$

where $\Omega = \omega - k_x v_0$ is the Doppler-shifted frequency of waves in the solar prominence.

When computing the components of the resistive terms given by Eq. (4.9) together with the solenoidal condition (Eq. 4.4), we can obtain that all dissipative terms containing the classical Coulomb resistivity cancel for the equilibrium considered here, therefore the dissipation in the partially ionised prominence is described by the Cowling resistivity alone.

Let us introduce the viscous and resistive Reynolds numbers as

$$R_v = \frac{v_{A1}}{k_x \nu}, \quad R_r = \frac{v_{A2}}{k_x \eta_C}. \quad (4.14)$$

Under coronal and prominence conditions both Reynolds numbers are very large and therefore waves will propagate with little damping over a period, meaning that in our

4.3. DISPERSION RELATION OF SURFACE WAVES PROPAGATING AT THE TANGENTIAL DISCONTINUITY

subsequent calculations we will consider that $|Re(\omega)| \gg |Im(\omega)|$. The very large Reynolds numbers also allow us to consider dissipative terms much smaller than other terms belonging to ideal MHD, meaning that in our calculations all terms containing ν^2 or η_C^2 are neglected. The interaction between flows and waves propagating at the interface between the two media is ensured by dissipation that could play the role of energy sink. Later we will see that, contrary to our expectations, dissipation does not always act towards decreasing the wave amplitude; for specific values of flows or ionisation degree, the interplay between flows, dissipation, and waves could lead to an increase of the waves' amplitude, i.e. unstable behavior.

In region 1 the viscous MHD equations can be reduced to a system of coupled equations for the normal component of the velocity vector v_{z1} and total pressure P_1 of the form

$$\frac{dv_{z1}}{dz} = -\frac{ik_x^2\omega}{\rho_1(\mathcal{D}_{A1} + 2i\nu k_x^2\omega)}P_1, \quad (4.15)$$

$$\left(1 - \frac{i\nu\omega}{\mathcal{D}_{A1}}\frac{d^2}{dz^2}\right)v_{z1} = -\frac{i\omega}{\rho_1\mathcal{D}_{A1}}\frac{dP_1}{dz}, \quad (4.16)$$

where $\mathcal{D}_{A1} = \omega^2 - k_x^2v_{A1}^2$. Taking into account that $R_v \gg 1$, we can eliminate the total pressure from these two equations to arrive at a single relation for v_{z1} , i.e.

$$\frac{d^2v_{z1}}{dz^2} - k_x^2\left(1 - \frac{3i\nu k_x^2\omega}{\mathcal{D}_{A1}}\right)v_{z1} = 0. \quad (4.17)$$

It is easy to see that v_{z1} will vanish as $z \rightarrow -\infty$. In order to use the boundary conditions (Eqs. 4.11 and 4.12) we will also need to find the value of the total pressure. In order to calculate its expression we write the equation for the z -component of the velocity from Eq. (4.7) as

$$\frac{d^2v_{z1}}{dz^2} - \alpha^2v_{z1} = 0, \quad (4.18)$$

where

$$\alpha = k_x\left(1 - \frac{3i\nu k_x^2\omega}{\mathcal{D}_{A1}}\right)^{1/2} \approx k_x\left(1 - \frac{3i\nu k_x^2\omega}{2\mathcal{D}_{A1}}\right).$$

Equation (4.18) allows us to explicitly find the expression of the z -component of the velocity in the solar corona. With the help of Eqs. (4.11) and (4.15) we can find that the total pressure in region 1 estimated at the interface between the two regions can

4.3. DISPERSION RELATION OF SURFACE WAVES PROPAGATING AT THE TANGENTIAL DISCONTINUITY

be written as

$$P_1 = \frac{\rho_1 D_{A1}}{k_x} \left(1 - \frac{i\nu\omega k_x}{2D_{A1}} \right) \zeta. \quad (4.19)$$

For the prominence we now have an equilibrium flow in the positive x direction. Considering again the equations that relate the z -component of the velocity vector and total pressure we obtain the systems

$$\left(\mathcal{D}_{A2} + \frac{i\eta_C k_x^4 v_{A2}^2}{\Omega} \right) v_{z2} = -\frac{i\Omega}{\rho_2} \frac{dP_2}{dz}, \quad (4.20)$$

and

$$\left(\mathcal{D}_{A2} + \frac{i\eta_C k_x^4 v_{A2}^2}{\Omega} \right) \frac{dv_{z2}}{dz} = -\frac{i\Omega}{\rho_2} P_2, \quad (4.21)$$

where $\mathcal{D}_{A2} = \Omega^2 - k_x^2 v_{A2}^2$. Eliminating the total pressure from the above two expressions we obtain an equation for v_{z2} valid in the solar prominence of the form

$$\frac{d^2 v_{z2}}{dz^2} - k_x^2 v_{z2} = 0. \quad (4.22)$$

Using Eqs. (4.11) and (4.21) we can write that the total pressure at the prominence evaluated at the interface behaves as

$$P_2 = -\frac{\rho_2 (D_{A2} + i\eta_C \Omega k_x^2) \Omega \zeta}{\Omega + i\eta_C k_x^2} \approx -\frac{\rho_2 \zeta}{\Omega} (D_{A2} \Omega + ik_x^4 v_{A2}^2 \eta_C). \quad (4.23)$$

The expressions of the two total pressures in the two regions are inserted in Eq. (4.12), which leads to the dispersion relation of the form

$$D(\omega) = D_r + iD_i = 0, \quad (4.24)$$

where

$$\begin{aligned} D_r &= D_{A1} + dD_{A2}, \\ D_i &= \nu k_x^2 \omega + \frac{dk_x^4 \eta_C v_{A2}^2}{\Omega}. \end{aligned} \quad (4.25)$$

In deriving the dispersion relation (4.24) we took into account that a perturbation method is used meaning that terms proportional to ν^2 and η_C^2 are neglected.

4.3.1 Instability conditions

Since we assumed that the damping of waves propagating along the interface is weak, we can write the frequency of waves as $\omega = Re(\omega) + iIm(\omega)$ with $|Re(\omega)| \gg |Im(\omega)|$. This assumption is in line with our previous statement regarding the high Reynolds numbers of solar plasmas and the working supposition that terms containing squares and products of dissipative coefficients can be neglected. According to the dependence of perturbations on the variable t assumed earlier, $Im(\omega) > 0$ corresponds to an overstability, i.e. to a situation where the amplitude of waves propagating along the interface grows as $\exp(\omega_i t)$. Following the method developed by Cairns (1979), we write the dispersion relation as

$$D_r(\omega, k_x) = -i\nu k_x^2 \omega - \frac{idk_x^4 \eta_C v_{A2}^2}{\Omega}. \quad (4.26)$$

The solution of the equation $D_r = 0$ will result in the real part of the frequency ω . In ideal MHD the interface between the two regions is always stable; however, the introduction of dissipation may lead to instability. The dispersion relation for the ideal case leads to

$$Re(\omega)_{\pm} = \frac{k_x v_0 d}{1+d} \pm \frac{k_x}{1+d} [d(v_{KH}^2 - v_0^2)]^{1/2}. \quad (4.27)$$

Equation (4.27) describes two waves propagating along the interface in opposite directions. The quantity v_{KH} is the Kelvin-Helmholtz (KH) threshold velocity, given by

$$v_{KH}^2 = \frac{1+d}{d} (v_{A1}^2 + d v_{A2}^2), \quad (4.28)$$

and it plays a very important role in the discussion of stability of waves propagating in a flowing plasma. It is obvious from Eq. (4.27) that the plasma becomes KH unstable for flows that satisfy the condition $v_0^2 > v_{KH}^2$. We estimate the value of v_{KH} for the system under investigation. If we consider typical coronal and prominence values for density and Alfvén speeds ($d = 100$, $v_{A1} = 315 \text{ km s}^{-1}$, $v_{A2} = 28 \text{ km s}^{-1}$, all taken from Joarder and Roberts (1992)), we obtain $v_{KH} \approx 423 \text{ km s}^{-1}$. Observations in the solar prominences do not show equilibrium flows that are larger than v_{KH} ; in reality, these speeds are more likely to be of the order of a tenth of v_{KH} or smaller.

4.3. DISPERSION RELATION OF SURFACE WAVES PROPAGATING AT THE TANGENTIAL DISCONTINUITY

This means that under prominence conditions the plasma at the interface between the solar corona and solar prominences is always KH stable. In the absence of any flow, the two solutions of Eq. (4.27) describe two modes propagating in the opposite direction with equal speeds $|v_{KH}\sqrt{d}/(1+d)|$. In the presence of a flow (for our problem the flow is present in the prominence while the coronal plasma is at rest), waves are drifted by the flow. Since the flow direction points in the positive direction, the flow affects the two waves in a different way and the symmetry of the two modes is lost. It can be easily shown that the difference between the phase speeds of the two waves is $2v_0d/(1+d)$. For flow speeds larger than $v_{KH}/\sqrt{(1+d)}$, the direction of the wave propagating in the negative direction is inverted and the backward mode becomes the forward mode. The two modes can amplify each other leading to instability. If we plot the two frequencies obtained in Eq.(4.27) with respect to an increasing flow speed, we obtain that the KHI occurs when the oscillation frequencies of the forward and backward propagating surface modes merge for increasing flow velocity. The merging point then indicates the threshold of KHI for the single interface. In the present analysis we consider flows that are less than the KH threshold.

Since we assume that the damping is weak, the imaginary part of the frequency can be given by

$$Im(\omega) \approx -\frac{k_x^2}{\partial D_r / \partial Re(\omega)} \left(\nu \omega_r + \frac{dk_x^2 \eta_C v_{A2}^2}{\Omega_r} \right), \quad (4.29)$$

where $\Omega_r = Re(\omega) - k_x v_0$.

Using Eqs. (4.27) and (4.29), it is straightforward to show that the imaginary part of the frequencies is

$$Im(\omega)^+ = -\frac{\nu k_x^2}{2(1+d)} \left(\frac{v_0 d}{\Gamma} + 1 \right) + \frac{d(d+1)k_x^2 v_{A2}^2 \eta_C}{2(v_0 \Gamma - d\Gamma^2)}, \quad (4.30)$$

and

$$Im(\omega)^- = \frac{\nu k_x^2}{2(1+d)} \left(\frac{v_0 d}{\Gamma} - 1 \right) - \frac{d(d+1)k_x^2 v_{A2}^2 \eta_C}{2(v_0 \Gamma + d\Gamma^2)}, \quad (4.31)$$

where $\Gamma = \sqrt{d(v_{KH}^2 - v_0^2)}$. With the help of Eqs. (3.5), (3.6) and (3.49), we can

4.3. DISPERSION RELATION OF SURFACE WAVES PROPAGATING AT THE TANGENTIAL DISCONTINUITY

write the Cowling resistivity as

$$\eta_C = 10^9 T_2^{-3/2} + \frac{v_{A2}^2 m_n (2\mu - 1)}{2\rho_2 (1 - \mu) \Sigma_{in}} \left(\frac{\pi m_p}{k_B T_2} \right)^{1/2}. \quad (4.32)$$

The two values for the imaginary part of the frequency become

$$\begin{aligned} Im(\omega)^+ &= -\frac{\nu k_x^2}{2(1+d)} \left(\frac{v_0 d}{\Gamma} + 1 \right) + \\ &\frac{d(d+1)k_x^2 m_n (2\mu - 1) v_{A2}^4}{4(v_0 \Gamma - \Gamma^2)(1 - \mu) \rho_2 \Sigma_{in}} \left(\frac{\pi m_p}{k_B T} \right)^{1/2} \end{aligned} \quad (4.33)$$

and

$$\begin{aligned} Im(\omega)^- &= \frac{\nu k_x^2}{2(1+d)} \left(\frac{v_0 d}{\Gamma} - 1 \right) - \\ &\frac{d(d+1)k_x^2 m_n (2\mu - 1) v_{A2}^4}{4(v_0 \Gamma + \Gamma^2)(1 - \mu) \rho_2 \Sigma_{in}} \left(\frac{\pi m_p}{k_B T} \right)^{1/2}. \end{aligned} \quad (4.34)$$

We now discuss the sign of these frequencies for a range of flow speeds changing in the interval 10-60 km s⁻¹ and for an ionisation degree varied between the cases corresponding to full ionisation ($\mu = 0.5$) and neutral plasma ($\mu = 1$). A simple graphical analysis clearly shows that for the spectrum of flows considered here and for any ionisation degree, the imaginary part of the surface waves that propagate in the positive direction (i.e. in the direction of the flow) is negative, leading to a classical physical damping. In contrast, the imaginary part of the wave propagating backward (in the negative direction) can become positive for flow speeds larger than 48 km s⁻¹ (see Fig. 4.2). A positive imaginary part of the frequency is connected to an instability. A contour plot of the imaginary part of the frequency for the backward propagating wave is shown in Fig. 4.3, where the role of the partial ionisation and plasma flows becomes evident. The region above the $Im(\omega) = 0$ curve corresponds to the region where the wave is unstable, while in the region beneath the curve the wave is stable and damped. It is clear that the flow will destabilize the interface; for a given value of ionisation fraction there is a flow value at which the interface becomes unstable (a similar conclusion can be drawn from earlier studies by, e.g. Ruderman and Goossens 1995). The variation of the zero-level with respect to the ionisation fraction shows that as the plasma becomes more dominated by neutrals,

4.3. DISPERSION RELATION OF SURFACE WAVES PROPAGATING AT THE TANGENTIAL DISCONTINUITY

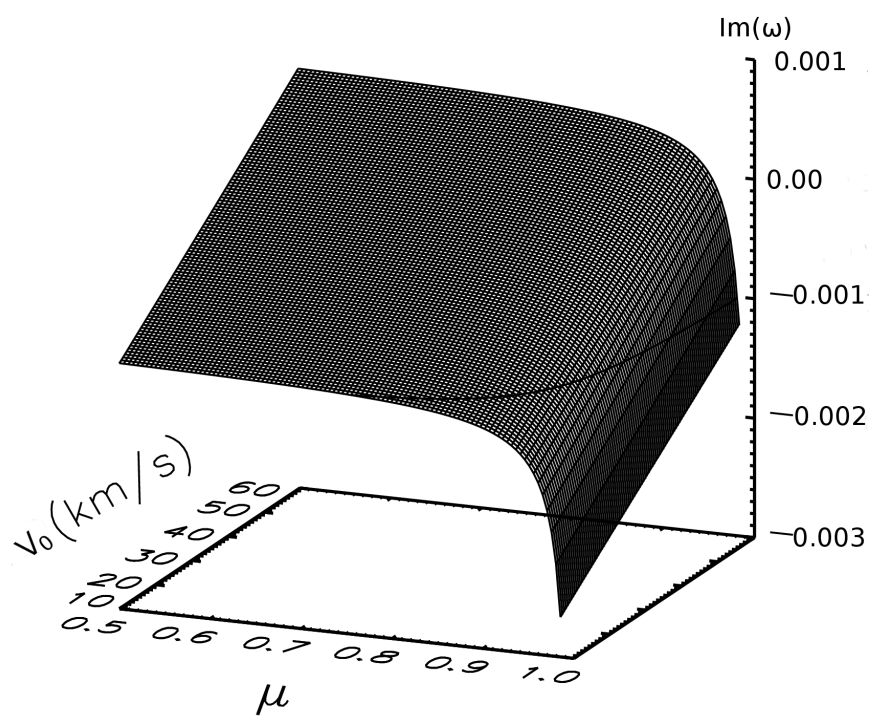


Figure 4.2: Variation of the imaginary part of the frequency for the backward propagating wave with the flow speed and the ionisation fraction. The flow changes in the interval $10\text{-}60 \text{ km s}^{-1}$ and the ionisation fraction varies between 0.5 (fully ionised plasma) and 1 (neutral gas). The horizontal curve drawn at the $Im(\omega) = 0$ helps to visualize the transition of $Im(\omega)^-$ from the positive to the negative domain.

4.3. DISPERSION RELATION OF SURFACE WAVES PROPAGATING AT
THE TANGENTIAL DISCONTINUITY

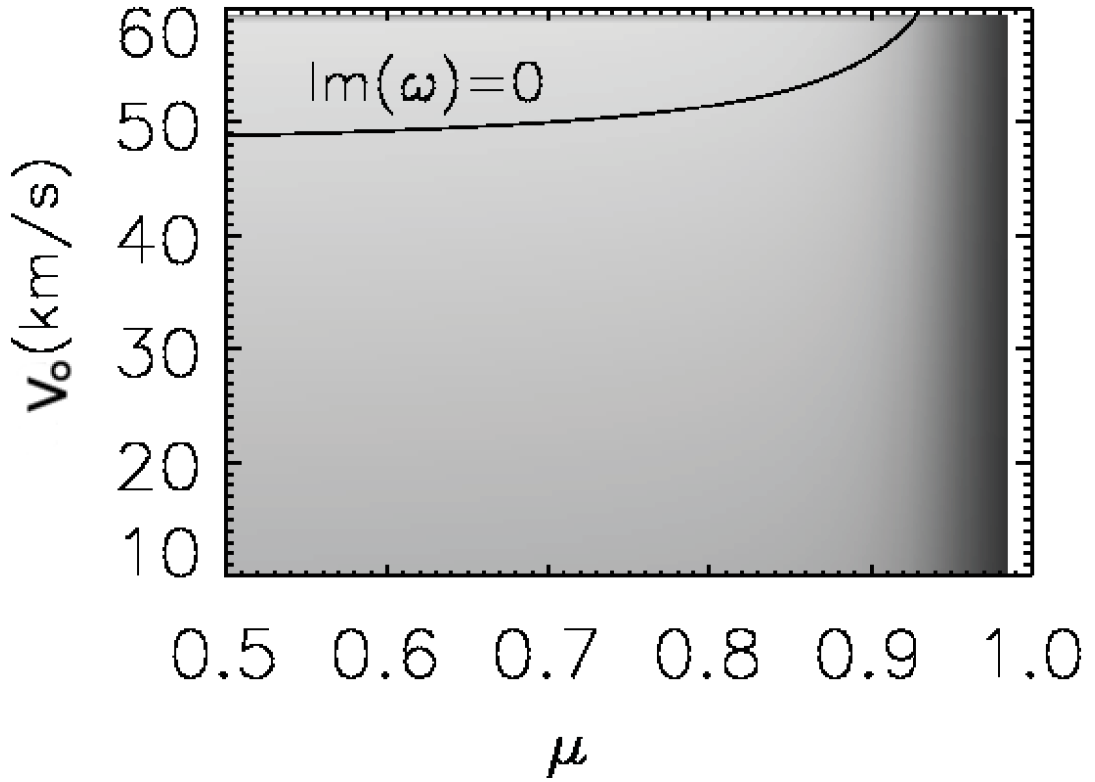


Figure 4.3: Contour plot of the variation of the imaginary part of the frequency for *backward* propagating waves. The region below the zero level curve corresponds to a stable regime and waves will have a classical damping, while the interface described by the quantities in the region above the curve is unstable.

the plasma interface becomes more stable, so that for an ionisation degree of 0.93 the interface becomes stable and waves will damp owing to dissipation. Figure 4.2 also shows that the presence of neutrals stabilizes the plasma as the instability sets in for higher values of flows (here with a density ratio of 100, $k_x = 5 \times 10^{-6} \text{ m}^{-1}$, $\nu = 10^{10} \text{ m}^2 \text{ s}^{-1}$, $T = 10^4 \text{ K}$, $\rho_2 = 5 \times 10^{-11} \text{ kg m}^{-3}$). It is instructive to identify the role of each dissipative process in the appearance of instability. While the partial ionisation in the solar prominence has the effect of stabilisation of the interface, the viscosity in the solar corona will destabilize the discontinuity and the value of the flow at which waves become unstable has little variation with the ionisation fraction and significant dependence can be observed for larger values of μ . We note that the unstable behavior of the backward wave is also connected to the very high density contrast between the solar prominence and corona. For a density contrast of one

4.3. DISPERSION RELATION OF SURFACE WAVES PROPAGATING AT THE TANGENTIAL DISCONTINUITY

order of magnitude the unstable backward wave becomes stable and the imaginary part of the dispersion relation describes classical physical damping.

Finally, we explore the connectivity between the dissipative instability discussed earlier and negative energy waves. As specified in the Introduction, the term of negative energy wave refers to the situation when the wave energy decreases with the increase of the wave amplitude. The energy of a wave with amplitude A averaged over one wavelength can be given as

$$E = \frac{1}{4} \omega \frac{\partial D_r}{\partial \omega} |A|^2, \quad (4.35)$$

where D_r is the dispersion relation of the wave. In this case the energy of the wave is the phase-averaged difference between the energy of the system when the wave is present, and its energy when the wave is absent. A criterion that can be used to determine the nature of waves is the formula suggested by Cairns (1979) where a wave is considered to have negative energy if the quantity

$$C = \text{Re}(\omega) \frac{\partial D_r}{\partial \omega} < 0. \quad (4.36)$$

The function D_r is undetermined up to a multiplicative constant whose sign has to be determined from the condition that in the absence of any flows in the system, $C > 0$. Comparing this with Eq. (4.29), it is obvious that the condition for the appearance of dissipative instability is identical with the condition of negative energy wave generation because the expression

$$\nu \text{Re}(\omega)^2 + \frac{dk_x^2 \eta_C v_{A2}^2 \text{Re}(\omega)}{\Omega_r}$$

is always positive.

Another possibility for exploiting the effect of partial ionisation on the stability at a magnetic interface is to model the interface between two partially ionised plasmas of prominences and dark plumes. Observations by Berger et al. (2010) revealed the existence of dark plumes within the prominence showing turbulent up-flows in prominences of the order of $15\text{-}30 \text{ km s}^{-1}$. These up-flows are believed to generate instabilities. In the Ca II H-line plumes are seen dark in contrast to the prominence

4.4. DISSIPATIVE INSTABILITIES IN THE TWO-FLUID APPROACH

material, which suggests that the plasma in the plumes is hotter and probably less dense than the prominence material. The width of the plumes ranges between 0.5 Mm and 6 Mm, and their maximum heights are between 11 Mm and 17 Mm. The typical plume lifetime is between 6 and 15 minutes.

Considering the same prominence/plume parameters as in Soler et al. (2012), we obtain that the interface between these two partially ionised media becomes unstable for almost all values of flows (below the KH threshold) for an ionisation degree of the prominence larger than the ionisation degree of the plume, but the growth rate of this instability is very low, meaning that the dissipative instability (at least in this simplified framework) cannot explain the generation of up-flows in plumes by instability.

4.4 Dissipative instabilities in the two-fluid approach

The problem of dissipative instability at a tangential discontinuity in a partially ionised plasma can be discussed in a different context, too. As specified in Chapter 3, for frequencies of waves that are below the ion-neutral frequencies the plasma cannot be treated as a single fluid, and a multi-fluid approach will be needed. Here we are going to treat the charge particles as an ion-electron fluid, while neutrals will be described by a set of separate equations. Neutrals will interact with the electron-ion fluid through collisions. These collisions will ensure that neutrals stay in the fluid and the constituents of the plasma have collective dynamics. As earlier, the electron inertia is neglected. The momentum transfer between particles takes place through the collisions between ions and neutrals.

Similarly the equilibrium described earlier in this Chapter, we are going to consider that the equilibrium model is composed of two partially ionised half-space plasma regions separated by a discontinuity. The plasma is permeated by a homogeneous magnetic field oriented in the x direction and the interface is situated at $z = 0$. The equilibrium plasma parameters are homogeneous and constants in both regions. We denote by the indices 1 and 2 the regions corresponding to $z < 0$ and $z > 0$, respectively (see Fig. 4.4). The equilibrium flows are denoted by \mathbf{v}_{01} and \mathbf{v}_{02} and they are parallel to the interface. The set of coupled differential equations governing the dynamics of linear waves in a two-fluid plasma in the incompressible limit is given

4.4. DISSIPATIVE INSTABILITIES IN THE TWO-FLUID APPROACH

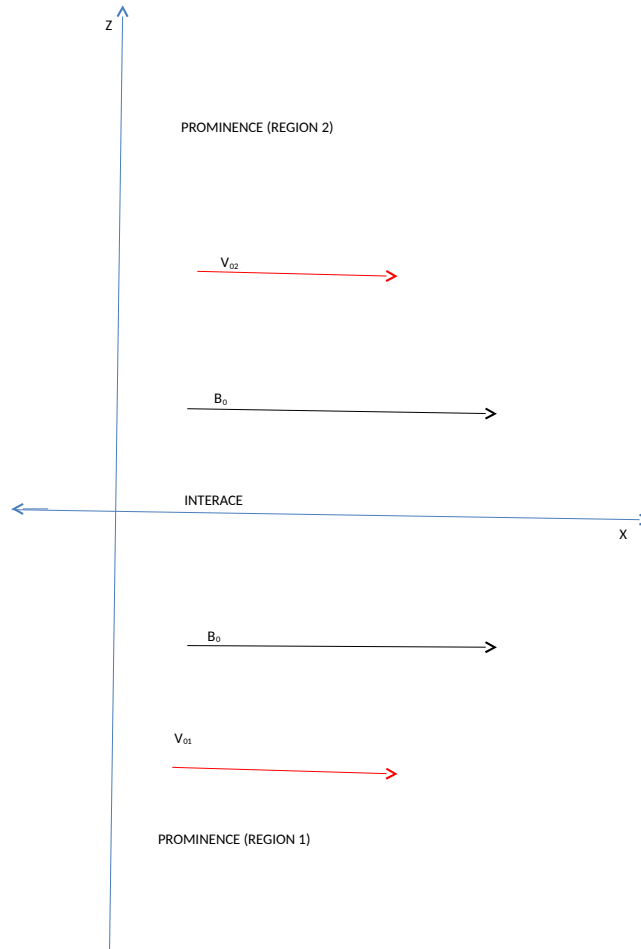


Figure 4.4: We denote by the indices 1 and 2 the regions corresponding to $z < 0$ and $z > 0$, respectively which correspond to two partially ionised plasmas of different ionisation fraction. The equilibrium flows are denoted by v_{01} and v_{02} and they are parallel to the interface. Magnetic fields are identical in the two regions and parallel to the interface.

4.4. DISSIPATIVE INSTABILITIES IN THE TWO-FLUID APPROACH

by (see, e.g. Zaqarashvili et al. 2011)

$$\rho_{0i} \left(\frac{\partial \mathbf{v}_i}{\partial t} + \mathbf{v}_0 \cdot \nabla \mathbf{v}_i \right) = -\nabla p_{ie} + \frac{1}{\mu_0} (\nabla \times \mathbf{b}) \times \mathbf{B}_0 - \alpha_{in} (\mathbf{v}_i - \mathbf{v}_n) \quad (4.37)$$

$$\rho_{0n} \left(\frac{\partial \mathbf{v}_n}{\partial t} + \mathbf{v}_0 \cdot \nabla \mathbf{v}_n \right) = -\nabla p_n - \alpha_{in} (\mathbf{v}_n - \mathbf{v}_i) \quad (4.38)$$

$$\frac{\partial \mathbf{b}}{\partial t} = \nabla \times (\mathbf{v}_0 \times \mathbf{b}) + \nabla \times (\mathbf{v}_i \times \mathbf{B}_0) \quad (4.39)$$

$$\nabla \cdot \mathbf{v}_i = \nabla \cdot \mathbf{v}_n = \nabla \cdot \mathbf{b} = 0, \quad (4.40)$$

where $\mathbf{v}_i = (v_{ix}, 0, v_{iz})$ and $\mathbf{v}_n = (v_{nx}, 0, v_{nz})$ are the components of the velocity perturbation of ions and neutrals, p_{ie} and p_n are the pressure perturbations of the ion-electron and neutral fluids, $\mathbf{b} = (b_x, 0, b_z)$ is the magnetic field perturbation, ρ_{0i} and ρ_{0n} are the equilibrium densities of ions and neutrals, while α_{in} is the ion-neutral friction coefficient. This friction ensures that collision between ions and neutrals take place. In the absence of this process, neutrals would not be able to stay in the system. Accordingly, in the absence of collisions the momentum equations would decouple. The last terms on the RHSs of Eqs. (4.37) and (4.38) express the transfer of momentum from ions to neutrals (and vice-versa) through the diffusion of one species into the other. Due to the collision and momentum transfer between species, the set of equations (4.37)–(4.40) is non-ideal, particles can loose energy through collisions.

Equations (4.37) and (4.38) are the linearized momentum equations of the ion-electron fluid and neutrals, respectively. Equation (4.39) clearly shows that the magnetic field is able to interact only with the charged part of the plasma fluid. Several simplifications were assumed in these equations. First of all, collisions of electrons with ions and neutrals are neglected because of the small momentum of electrons. We assume adiabatic perturbations and thus non-adiabatic mechanisms are neglected. In order to keep the discussion as simple as possible we are also going to neglect any dissipative mechanism that could appear in the induction equation, here we are going to concentrate on the effect of collisions on the appearance of dissipative instabilities. These simplifications will enable us to study the problem of plasma stability analytically.

4.4. DISSIPATIVE INSTABILITIES IN THE TWO-FLUID APPROACH

We express the ion-neutral friction coefficient as

$$\alpha_{in} = \rho_{0i}\rho_{0n}\gamma_{in} \quad (4.41)$$

where γ_{in} is the ion-neutral collision rate coefficient per unit mass. The friction coefficient vanishes in both the fully ionized and fully neutral cases. Instead of using γ_{in} , we are going to use the collision frequency, which has a more practical physical meaning. Thus we define the ionneutral, ν_{in} , and neutralion, ν_{ni} , collision frequencies as

$$\nu_{in} = \rho_{0i}\gamma_{in}, \quad \nu_{ni} = \rho_{0n}\gamma_{in} \quad (4.42)$$

and the two collisional frequencies are connected through $\rho_{0n}\nu_{in} = \rho_{0i}\nu_{ni}$. In consequence, in the remaining part of the present Chapter we are going to use only ν_{in} .

We employ the same normal mode analysis as in the case of single fluid description, however, here the continuity of the normal component of the momentum across the discontinuity would require an equivalent relation written for ions and neutrals. Similarly, the continuity of the stresses at the interface (see Eq. 4.12) would translate into the balance of the total pressure of charged particles and the kinetic pressure of neutrals.

The dispersion relation for waves propagating along the interface in the incompressible limit can be obtained as (see, e.g. Watson et al. 2004, Soler et al. 2012)

$$\begin{aligned} & [\rho_{0n1}\Omega_1(\Omega_1 + i\nu_{in1}) + \rho_{0n2}\Omega_2(\Omega_2 + i\nu_{in2})] \times \\ & \left\{ \rho_{0i1} \left[\Omega_1(\Omega_1 + i\chi_1\nu_{in1}) - k^2v_{A1}^2 \right] + \rho_{0i2} \left[\Omega_2(\Omega_2 + i\chi_2\nu_{in2}) - k^2v_{A2}^2 \right] \right\} = 0, \end{aligned} \quad (4.43)$$

where $\chi_{1,2} = \rho_{0n1,2}/\rho_{0i1,2}$, and $\Omega_{1,2} = \omega - kv_{01,2}$ are the Doppler-shifted frequencies in the two media. We need to mention here that, in order to obtain the above result, we assumed that the ion-neutral collisional frequencies are much smaller than the frequency of the waves, meaning that all terms containing squares or products of the collisional frequency were neglected. It can be shown that this approximation is equivalent with the assumption of weak damping.

The dispersion relation given by Eq. (4.43) allows the discussion of the entire mixture in terms of its constituents, the first parenthesis of the above equation refers

4.4. DISSIPATIVE INSTABILITIES IN THE TWO-FLUID APPROACH

to neutrals only, while the second term describes the dispersion relation of ions. We should keep in mind that an unstable behavior of any of the constituents would automatically imply the unstable behavior of the whole mixture.

Let us first discuss the neutrals. We can write the dispersion relation of neutrals as

$$\rho_{0n1}\Omega_1^2 + \rho_{0n2}\Omega_2^2 = -i(\rho_{0n1}\Omega_1\nu_{in1} + \rho_{0n2}\Omega_2\nu_{in2}) \quad (4.44)$$

Following the same procedure as in the case of a single-fluid plasma (section 4.3), first we can determine the solutions of the ideal part of the dispersion relation, i.e.

$$\omega_{1,2} = k \frac{\rho_{0n1}v_{01} + \rho_{0n2}v_{02}}{\rho_{0n1} + \rho_{0n2}} \pm ik \frac{\sqrt{\rho_{0n1}\rho_{0n2}}}{\rho_{0n1} + \rho_{0n2}} |v_{01} - v_{02}|. \quad (4.45)$$

Due to the positive imaginary part of the forward mode (the upper sign in Eq. 4.45) the neutral fluid will be unstable, while the backward propagating mode will be stable. This peculiar behavior of neutrals under prominence conditions was discussed earlier by, e.g. Soler et al. (2012) and it corresponds to the standard hydrodynamic KH instability. We should also notice that the growth rate of the instability is independent on the collision rate.

Let us now concentrate on the backward mode that is KH stable. The presence of collisions with ions will affect the propagation characteristics of the modes by attenuating their amplitude. We apply the same procedure as before and assume that the dispersion relation can be expanded in series around the value of the frequency determined by Eq. (4.45). As a result, we can obtain that the imaginary part of the frequency is given by

$$Im(\omega) = \mp \frac{\rho_{0n1}\nu_{in1} + \rho_{0n2}\nu_{in2}}{\rho_{0n1} + \rho_{0n2}}. \quad (4.46)$$

This expression is determined by the collisional rate between the two species. In the case of forward modes, the collisions will tend to damp the amplitude of the wave ($Im(\omega) < 0$) and this has to be considered together with the fact that these modes are KH unstable. Considering both effects, the growth/decay rate of the forward

4.4. DISSIPATIVE INSTABILITIES IN THE TWO-FLUID APPROACH

propagating modes becomes

$$\tilde{\omega} = k \frac{\sqrt{\rho_{0n1}\rho_{0n2}}}{\rho_{0n1} + \rho_{0n2}} |v_{01} - v_{02}| - \frac{\rho_{0n1}\nu_{in1} + \rho_{0n2}\nu_{in2}}{\rho_{0n1} + \rho_{0n2}}. \quad (4.47)$$

Let us apply this relation in connection to the modes that could appear in prominence dark plumes. Observations by Berger et al. (2008, 2011) and Ryutova et al. (2010) revealed that dark plumes are turbulent up-flows in prominences which usually develop Kelvin-Helmholtz vortex rolls. Ca II absorption lines in prominence plumes show these as dark features, in contrast to the prominence material, which suggests a hotter plasma in the plumes compared to their environment and they are also less dense than their surrounding material. The width of plumes ranges between 0.5 Mm to 6 Mm and their maximum heights are between 11 Mm and 17 Mm. The mean flow speed is about 15 km s^{-1} , although velocities up to 30 km s^{-1} are also measured. The typical plume lifetime is between 400 s and 890 s.

Let us now consider that medium 1 represents the prominence plasma and medium 2 the plume. For density, we use typical parameters for the quiescent prominence, i.e. $\rho_{01} = 5 \times 10^{-11} \text{ kg m}^{-3}$, while the density of the plume is considered to be one order of magnitude lower, i.e. $\rho_{02} = 5 \times 10^{-12} \text{ kg m}^{-3}$. The degree of the ionisation is unknown, but for illustration purposes let us assume that half of the prominence material is neutral, i.e. $\rho_{0n1} = 2.5 \times 10^{-11} \text{ kg m}^{-3}$. For the plume (being hotter plasma) we assume that a quarter of its material is still neutral, so $\rho_{0n2} = 1.25 \times 10^{-12} \text{ kg m}^{-3}$. Further, we are going to assume that the prominence plasma in equilibrium is at rest, i.e. $v_{01} = 0$, while in the plume is 20 km s^{-1} . For the collisional frequency, let us suppose that $\nu_{in2} = \alpha\nu_{in1}$. Although the rate of collisions is proportional to $T^{1/2}$ (i.e. the number of collisions in the plume is higher than in the prominence), due to the less dense material, α will be always less than 1. For prominence values ($T = 10^4 \text{ K}$ and density given above) the ion-neutral collisional frequency is 4 s^{-1} . It is easy to see that, for any value of α , the sign of Eq. (4.47) is negative, meaning that the damping due to collisions can prevent the unstable growth of the modes (due to neutrals) propagating along the interface between the prominence and dark plumes.

Let us now turn our attention to the other solution of Eq. (4.46). The imaginary part of the frequency corresponding to the backward wave is positive, meaning that these waves are subject to dissipative instability and the growth rate of the waves is

4.4. DISSIPATIVE INSTABILITIES IN THE TWO-FLUID APPROACH

independent on the value of plasma flow.

Now we consider the ions present in the system, and their dispersion relation can be written as

$$\rho_{0i1} \left(\Omega_1^2 - k^2 v_{A1}^2 \right) + \rho_{0i2} \left(\Omega_2^2 - k^2 v_{A2}^2 \right) = -i \left(\rho_{0i1} \Omega_1 \chi_1 \nu_{in1} + \rho_{0i2} \Omega_2 \chi_2 \nu_{in2} \right). \quad (4.48)$$

Once we apply the same procedure as in the case of a single fluid, we can find the root of the real part of the dispersion relation to be

$$\omega_{1,2} = k \frac{\rho_{0i1} v_{01} + \rho_{0i2} v_{02}}{\rho_{0i1} + \rho_{0i2}} \pm \frac{k \Gamma_i}{\rho_{0i1} + \rho_{0i2}}, \quad (4.49)$$

where

$$\Gamma_i = \sqrt{\rho_{0i1} \rho_{0i2} \left[v_{KH_i}^2 - (v_{01} - v_{02})^2 \right]}, \quad (4.50)$$

with the Kelvin-Helmholtz speed, v_{KH_i} defined in a similar way as earlier in the chapter. In the presence of a magnetic field, v_{KH_i} is super-Alfénic, i.e. larger than any equilibrium flow that could be observed in prominence structures. This also means that the values of $\omega_{1,2}$, defined by Eq. (4.49) are always real.

We can repeat applying the same technique in order to find the imaginary part of the frequency for ions and we obtain that

$$Im(\omega)_i = \mp \frac{1}{2\Gamma_i(\rho_{0i1} + \rho_{0i2})} \times [\rho_{0i1} \rho_{0i2} (v_{02} - v_{01})(\chi_1 \nu_{in1} - \chi_2 \nu_{in2}) \pm \Gamma_i (\rho_{0i1} \chi_1 \nu_{in1} + \rho_{0i2} \chi_2 \nu_{in2})]. \quad (4.51)$$

This increment is independent on the wavenumber. Again, a positive imaginary part of the frequency would be equivalent to an instability, while a negative $Im(\omega)$ corresponds to a physical damping. Using the characteristic values for the prominence and plume we have that $\rho_{0i1} = 2.5 \times 10^{-11} \text{ kg m}^{-3}$, $\rho_{0i2} = 3.75 \times 10^{-12} \text{ kg m}^{-3}$, $\chi_1 = 1$, $\chi_2 = 0.33$ and we investigate the variation of the imaginary part of the frequency with respect to the strength of the equilibrium flow and parameter α . Figure 4.5 shows this behavior when the flow varies in the interval $20\text{-}45 \text{ km s}^{-1}$ and the parameter α takes values 0.1 (solid line), 0.5 (dashed line) and 1 (dash-dotted line), respectively. Although these plots do not show significant variation with respect to

4.4. DISSIPATIVE INSTABILITIES IN THE TWO-FLUID APPROACH

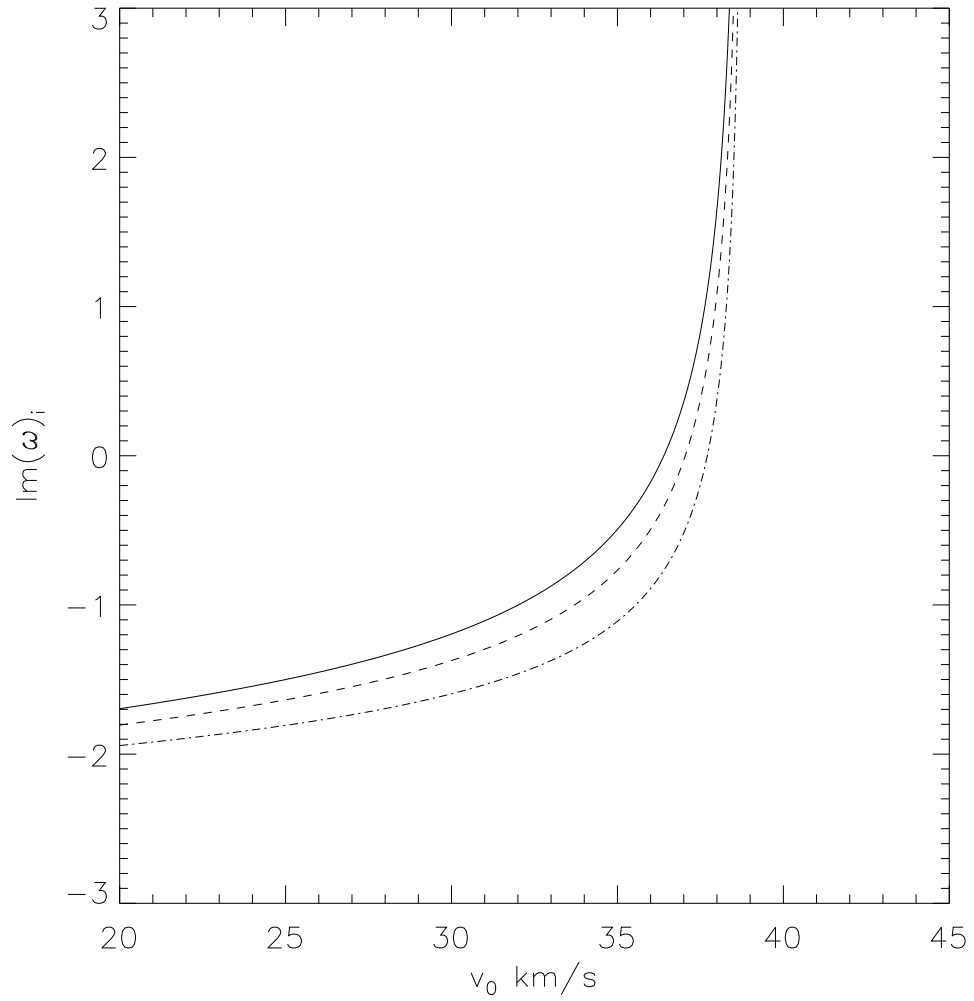


Figure 4.5: The variation of imaginary part of the frequency belonging to the ion fluid with the background flow for three different values of collisional frequency (here quantified by the parameter α). The solid line corresponds to $\alpha = 0.1$, the dashed line to $\alpha = 0.5$, and the dash-dotted line to $\alpha = 1$. Waves are unstable for those values of v_0 and α for which the imaginary part of the frequency becomes positive.

α , the imaginary part of the frequency becomes positive for flows in excess of 35 km s⁻¹. In this investigation we used $v_{A1} = 89$ km s⁻¹ and $v_{A2} = 280$ km s⁻¹, respectively. It is also clear that the higher the collisional frequency in the plume, the higher is the flow required for the backward propagating waves to become dissipative unstable.

The expression of $Im(\omega)_i$ also allows us to find that the plasma becomes unstable for any flows that satisfy the condition

$$v_0 > v_{KH_i} \frac{\rho_{0i1}\chi_1 + \alpha\rho_{0i2}\chi_2}{\left[(\chi_1 - \alpha\chi_2)^2 + (\chi_1\rho_{0i1} + \alpha\chi_2\rho_{0i2})\right]^{1/2}}. \quad (4.52)$$

Comparing Eqs. (4.47) and (4.52), we can see that the backward waves will be dissipative unstable regardless the value of the flow, because the imaginary part of the frequency corresponding to neutrals is flow independent.

The mixture of three species of plasma therefore shows a very complex pattern where the Kelvin-Helmholtz unstable behavior of neutrals is stabilized by the damping due to collisions with ions (in the case of forward propagating waves), but the whole plasma becomes unstable (due to the ions and neutrals) for flows that are rather large. However this large value of flow is not a surprise given the simplicity of our model. We are aware that the simple model employed here misses several key effects for plume dynamics. For example, the interface considered here does not allow the appearance of body waves, that could be important for the stability of plumes. Furthermore, the flow of particles not strictly parallel to the magnetic field might decrease significantly the instability threshold, as it was shown by Prialnik et al. (1986) in the case of KH instability. It remains to be seen how the effect of compressibility will change the stability criteria, bearing in mind that the effect of compressibility is to stabilize the plasma.

4.5 Conclusions

In the present Chapter we explored the stability of a tangential discontinuity. In the first instance we considered the interface between the viscous and fully ionised coronal plasma and the partially ionised solar prominence, in which the dominant

dissipative effect is the Cowling resistivity. In the second model we used a two-fluid approach modeling the interface between the prominence and a dark plume.

The magnetic fluids were assumed to be incompressible and the prominence/dark plume equilibrium was considered to be dynamical, with a homogeneous flow parallel to the interface. Assuming a weak damping, we obtained the dispersion relation of Alfvénic waves propagating along the interface. The presence of dissipative effects on both sides of the interface renders the dispersion relation to be complex with the imaginary part of this quantity describing the decay or the growth of waves. Our results show that in the first case the forward propagating wave is always stable, with the amplitude of the wave decaying because of dissipation, however, for the backward propagating wave there is a threshold of the flow (below the KHI threshold) for which the wave becomes unstable. A careful analysis proves that the partial ionisation has a stabilizing effect on the interface for any value of the ionisation fraction and the unstable behavior can be connected to the viscous nature of the coronal plasma. We also showed that partial ionisation has little effect on the threshold where waves become unstable. For a plasma where neutrals are abundant, the instability appears for higher values of flows, i.e. neutrals have a stabilizing effect. The appearance of the dissipative instability in the case of a two-fluid approach is more complex, as individual species can become unstable, leading to the instability of the whole mixture.

The above results were obtained under the strict restriction of incompressible plasma and a sharp tangential discontinuity between the two plasma layers. The first model was used to study the generation of dissipative instability at the interface of two partially ionised plasmas modeling the prominence and dark plumes. The unstable mode obtained in this case shows a very low growth rate, meaning that this type of instability (at least in this simplified model) cannot explain the appearance of turbulent up-flows in plumes that can be attributed to instability.

Chapter 5

Dissipative instability in a partially ionised prominence plasma slab²

After clarifying the problem of generation of dissipative instability at the tangential discontinuity between two media (where at least one of the media is partially ionised) we are going to extend our investigation to the problem of dissipative instability generation in a magnetic slab, i.e. structures that have at least one dimension bounded.

As presented in the Introduction, the magnetic field in the solar atmosphere tends to accumulate into entities (flux tubes, coronal loops) of finite transversal size (radius) and very often this size is determined by the balance of various forces acting upon these structures. Due to very high values of Reynolds numbers (the frozen-in condition is very well satisfied) observed waves and oscillations are perfect tracers of these magnetic structures. Once waves are "forced" to propagate in finite size waveguides, their phase speed becomes dependent on the wavelength at which they propagate, i.e. they become dispersive (in optics this phenomenon is also called waveguide dispersion). Depending on the particular dependence of the phase velocity on the wavelength, we can differentiate between positive and negative dispersion. In the first case waves propagate faster with increasing the wavelength, while in the case of waves with negative dispersion an increasing wavelength means a decreasing phase speed. The properties of dispersive waves were studied in details in a series of seminal papers by Edwin and Roberts (1982, 1983) in a static equilibrium and by

²The present chapter is based on the study by Alexandrou et al. *Dissipative instability in a partially ionised prominence plasma slab*, 2015, Astron. Astrophys. (submitted)

Terra-Homem et al. (2003) in a dynamic equilibrium. The behavior of waves was found to be different in the regimes of long and short wavelengths (compared to the vertical size of the waveguide), and different under photospheric and coronal conditions (the difference is reflected by the value of the plasma-beta in these regions).

In the present chapter we are going to investigate how the dispersion of waves will influence the dissipative instability threshold. The current discussion is a natural continuation of the previous Chapter and the same physical principles can be applied here, as well. In addition to the previous Chapter, here we investigate what is the effect of the wavelength of the waves in the generation of dissipative instability.

5.1 The equilibrium configuration

In the present Chapter the structuring of the magnetic field is modeled by a three-layer model, where a magnetic slab of thickness z_0 lying along the x -axis is sandwiched between two semi-infinite planes, with interfaces situated at $z = 0$ and $z = z_0$, respectively. The magnetic field in the three regions are taken to be identical and parallel to the x axis, i.e. $\mathbf{B}_0 = B_0 \hat{\mathbf{x}}$, where $\hat{\mathbf{x}}$ is the unit vector in the x direction. Depending on the possible roles played by different regions in the equilibrium configuration, we can study the appearance of dissipative instability in three different models (see Fig. 5.1). In the first model the equilibrium set-up describes the case of a partially ionised prominence slab fibril immersed into the fully ionised and viscous solar corona. The second and third models consist of a partially ionised prominence fibril sandwiched by an interfibril partially ionised prominence plasma and the difference between the latest two models resides in the structure of the equilibrium flow. In the second model we assume that the prominence plasma flows with a piecewise constant flow in the direction of the magnetic field, while in the third model, the interfibril prominence plasma shows a constant counterflow with respect to the flow direction in the prominence. In all models studied here the quantities describing the state of the plasma in the external medium (i.e. outside the slab) are labeled by an index "2", while inside the slab the plasma is described through quantities with an index "1". For simplicity we assume that the fluids in the two regions are incompressible in all models, a generalization of this restriction would be a rather straightforward task. A discussion on the nature of transport processes that can act

5.1. THE EQUILIBRIUM CONFIGURATION

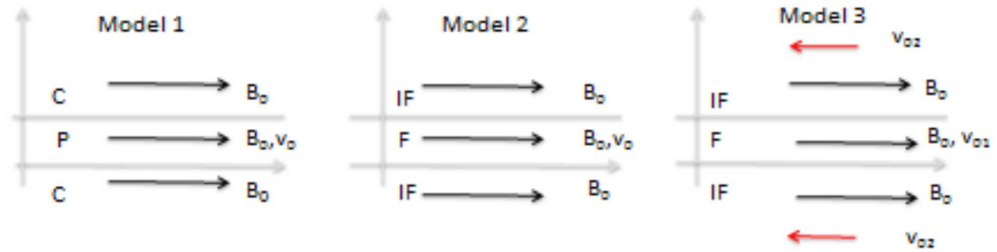


Figure 5.1: Magnetic slab of thickness z_0 lying along the x -axis lies between two semi-infinite planes, with interfaces situated at $z = 0$ and $z = z_0$. The magnetic field in the three regions are taken to be identical and parallel to the x axis. The first model represents a partially ionised prominence slab fibril (shown as P) immersed into the fully ionised and viscous solar corona (shown as C in Fig. 5.1). The second and third models consist of a partially ionised prominence fibril (shown as F in Fig. 5.1) sandwiched by an interfibril partially ionised prominence plasma (shown as IF). The latest two models engage opposite directions in their equilibrium flows.

5.1. THE EQUILIBRIUM CONFIGURATION

under these conditions was presented in an earlier study by Ballai et al. (2015) and discussed in details in Chapter 4. Here we are going to employ the same considerations and assume that the viscosity is the dominant transport mechanism in the solar corona and it is described by the first term in Braginskii's viscosity tensor, while the transport mechanisms in the prominence appear only in the induction equation, meaning that transport due to the friction of different species of particles is neglected. By assuming this simplification we supposed that the oscillations under investigation have longer periods than the ion-neutral collision time-scale.

We employ the same governing equations as in the previous chapter. Rewriting Eq.(4.15) from section 4.3 , we can deduce that inside the slab the total pressure and the z component of the velocity vector are connected by

$$(\Omega + i\eta_{C1}k^2)P_1 = \frac{i\rho_{01}}{k^2}(D_{A1} + i\eta_{C1}\Omega k^2)\frac{dv_z}{dz}, \quad (5.1)$$

where $\Omega = \omega - kv_0$ is the Doppler-shifted frequency, $D_{A1} = \Omega^2 - k^2v_{A1}^2$ and η_{C1} is the coefficient of the Cowling resistivity in region 1. In the above calculations we assumed that in the dissipative terms we can consider $d^2/dz^2 \ll k^2$. This simplification is fully justified as the plasma movement takes place in the transversal direction following the oscillatory motion of the Alfvénic wave (the plasma is incompressible).

Although we are discussing three different models, the common part of these models is that the plasma slab is filled with partially ionised prominence plasma whose dynamics is described by Eq. (4.10). In what follows we are going to discuss the equations describing the external medium separately for each model.

In model 1 (see Fig. 5.1) (prominence slab surrounded by fully ionised viscous corona) the governing equation for perturbations in the viscous and fully ionised solar corona is (see Ballai et al. 2015)

$$P_2 = \frac{i\rho_{02}(D_{A2} + 2i\nu k^2\omega)}{k^2\omega}\frac{dv_z}{dz}, \quad (5.2)$$

where $\nu = \eta_0/\rho_{02}$ is the kinematic coefficient of viscosity and the coefficient η_0 was defined earlier in Chapter 4.

For model 2 (partially ionised plasma slab surrounded by another partially ionised interfibril prominence plasma in a different state of ionisation) the governing equa-

5.1. THE EQUILIBRIUM CONFIGURATION

tion is

$$(\omega + i\eta_{C2}k^2)P_2 = \frac{i\rho_{02}}{k^2}(D_{A2} + i\eta_{C2}\omega k^2)\frac{dv_z}{dz}, \quad (5.3)$$

where now $D_{A2} = \omega^2 - k^2v_{A2}^2$ and η_{C2} is the Cowling resistivity in region 2. Finally in the case of model 3 (the interfibril partially ionised plasma exhibits counterflow) the governing equation is

$$(\tilde{\Omega} + i\eta_{C2}k^2)P_2 = \frac{i\rho_{02}}{k^2}(\tilde{D}_{A2} + i\eta_{C2}\tilde{\Omega}k^2)\frac{dv_z}{dz}, \quad (5.4)$$

where $\tilde{\Omega} = \omega + kv_0$ and $\tilde{D}_{A2} = \tilde{\Omega}^2 - k^2v_{A2}^2$.

The solutions of these equations must be connected at the boundaries of the regions. We will be concerned with those disturbances that are laterally evanescent, i.e. $v_z(z) \rightarrow 0$ as $|z| \rightarrow \infty$, meaning that the energy of the disturbance is essentially confined to the interior of the slab. As a result, the z -component of the velocity can be given as (for details see, e.g. Edwin and Roberts 1982, Ballai et al. 2015)

$$v_z = \begin{cases} \beta_e e^{-k(z-z_0)} & \text{for } z > z_0, \\ \alpha_0 \cosh(kz) + \beta_0 \sinh(kz) & \text{for } 0 < z < z_0, \\ \alpha_e e^{kz} & \text{for } z < 0. \end{cases} \quad (5.5)$$

The constant coefficients $\alpha_0, \beta_0, \alpha_e, \beta_e$ can be determined after joining the solutions at the boundaries. According to the standard classification, the only modes that can appear in this structure are surface modes, that could be sausage or kink, depending whether v_z is an odd or even function of z .

Given the particular orientation of the equilibrium magnetic field, the interfaces between the prominence slab and its environment can be considered as tangential discontinuities. Let us assume that the equation of the perturbed discontinuity is $\zeta(x, t) = 0$. The requirements that the normal component of the velocity and normal component of the stress tensor are continuous imply that the linearized kinematic boundary condition reduces to

$$[[v_z - \mathbf{v}_0 \cdot \nabla \zeta]] = 0, \quad (5.6)$$

while the continuity of the stress tensor reduces in the case of homogeneous back-

5.2. DISPERSION RELATION OF SURFACE WAVES PROPAGATING IN THE SLAB

ground to

$$[[P]] = 0, \quad (5.7)$$

where $[[,]]$ denotes the jump of a quantity across the discontinuity in the sense that the jump of an arbitrary function $g(z)$ is defined as

$$[[g(z)]] = \lim_{\epsilon \rightarrow 0^+} [g(z + \epsilon) - g(z - \epsilon)].$$

The z -component of the velocity and ζ can be related by

$$v_z = \frac{\partial \zeta}{\partial t} + \mathbf{v}_0 \cdot \nabla \zeta.$$

Using the above property, the kinematic boundary condition becomes

$$\left[\left[\frac{v_z}{\omega - \mathbf{k} \cdot \mathbf{v}_0} \right] \right] = 0 \quad (5.8)$$

In the case of models 2 and 3, the continuity of the stress tensor simplifies to the requirement that the total pressures on the two sides of the discontinuity are equal, however in the case of model 1 the viscosity of the corona is modifying this requirement, so now the continuity of the normal component of the stress tensor can be written as

$$P_1 = P_2 - 2\rho_{02}\nu \frac{\partial v_{z2}}{\partial z}, \quad (5.9)$$

that has to be evaluated at the interfaces situated at $z = 0$ and $z = z_0$.

5.2 Dispersion relation of surface waves propagating in the slab

In our derivation we assumed that all perturbations oscillate with the same frequency ω that is a complex quantity that can be written as $\omega = \text{Re}(\omega) + i\text{Im}(\omega)$. We introduce the viscous and resistive Reynolds numbers as

$$R_r = \frac{v_{A1}}{k\eta_C}, \quad R_v = \frac{v_{A2}}{k\nu}. \quad (5.10)$$

5.2. DISPERSION RELATION OF SURFACE WAVES PROPAGATING IN THE SLAB

Similarly to the method used in the previous Chapter, since both Reynolds numbers are very large and therefore waves propagating with little damping over a period, in our subsequent calculations we will consider that $|Re(\omega)| \gg |Im(\omega)|$, i.e. in our calculations all terms containing ν^2 or η_C^2 (or their product) are neglected. The interaction of flows and waves in a dissipative medium will generate the new physics our study deals with. Later we will see that, contrary to our expectations, dissipation does not always act towards decreasing the wave amplitude; for specific values of flows or ionisation degree, the interplay between flows, dissipation, and dispersion could lead to an increase of the waves' amplitude, i.e. unstable behavior.

The dispersion relation of these waves can be obtained by imposing the boundary conditions on the total pressure and normal component of velocity. For the sinh term, the dispersion relation of sausage waves reads

$$d \left(D_{A1} + \frac{i\eta_C k^4 v_{A1}^2}{\Omega} \right) + (D_{A2} + 4i\nu k^2 \omega) \tanh(kz_0) = 0, \quad (5.11)$$

while the cosh term leads to the dispersion relation of kink waves

$$d \left(D_{A1} + \frac{i\eta_C k^4 v_{A1}^2}{\Omega} \right) + (D_{A1} + 4i\nu k^2 \omega) \coth(kz_0) = 0. \quad (5.12)$$

We can rearrange these relations in the form

$$D_{A2} \left\{ \begin{array}{c} \tanh(kz_0) \\ \coth(kz_0) \end{array} \right\} + dD_{A1} + ik^2 \left[4\nu\omega \left\{ \begin{array}{c} \tanh(kz_0) \\ \coth(kz_0) \end{array} \right\} + \frac{\eta_C k^2 v_{A1}^2 d}{\Omega} \right] = 0. \quad (5.13)$$

Following the same consideration and imposing the right boundary conditions at the two interfaces, the dispersion relation for the second model becomes

$$D_{A2} \left\{ \begin{array}{c} \tanh(kz_0) \\ \coth(kz_0) \end{array} \right\} + dD_{A1} + ik^4 \left[\frac{\eta_{C1} v_{A1}^2 d}{\Omega} + \frac{\eta_{C2} v_{A2}^2}{\omega} \left\{ \begin{array}{c} \tanh(kz_0) \\ \coth(kz_0) \end{array} \right\} \right] = 0, \quad (5.14)$$

and somehow similar dispersion relation for the third model as

$$\tilde{D}_{A2} \left\{ \begin{array}{c} \tanh(kz_0) \\ \coth(kz_0) \end{array} \right\} + dD_{A1} + ik^4 \left[\frac{\eta_{C1} v_{A1}^2 d}{\Omega} + \frac{\eta_{C2} v_{A2}^2}{\tilde{\Omega}} \left\{ \begin{array}{c} \tanh(kz_0) \\ \coth(kz_0) \end{array} \right\} \right] = 0. \quad (5.15)$$

These dispersion relations will be investigated analytically and numerically in the next section to determine the range of flows and thickness of the slab for which the incompressible surface waves propagating in the slab are unstable.

5.3 Dissipative instability

Since the Reynolds numbers defined in Eq. (5.10) are very large, it is realistic to assume that the damping of waves propagating in the magnetic slab is weak. According to the chosen dependence of variables with time, a perturbation with $Im(\omega) > 0$ corresponds to an instability, i.e. to the case when the amplitude of waves grows exponentially with time according to $\exp(Im(\omega)t)$. Here we restrict ourselves to the linear phase of instabilities. Linear growth rates provide us with characteristic timescales for the instability to operate. However, nonlinear studies are needed to assess the real impact of the instability on the evolution of the plasma parameters. This topic, however, would require numerical analysis, which would be outside the scope of the present Thesis.

Following the method developed by Cairns (1979), the imaginary part of the frequency can be calculated as

$$Im(\omega) \approx -\frac{\mathcal{D}_I}{\partial \mathcal{D}_R / \partial \omega} \quad (5.16)$$

where \mathcal{D}_R and \mathcal{D}_I are the real and imaginary parts of the dispersion relations (see Eqs. 5.13–5.15) and this expression should be evaluated at the value of the frequency that corresponds to the solution of the real part of the dispersion relation, i.e. a root of the equation $\mathcal{D}_R = 0$.

Let us first concentrate on the sausage modes, the solution for kink modes being easily generated. In the first two models the difference resides only in the choice of the transport mechanism, therefore it is obvious that the real part (corresponding to

the ideal case) will be identical. In this case, it is straightforward to show that the root of real part of the dispersion relation becomes

$$\omega_{\pm} = \frac{dkv_0}{d + \tanh(kz_0)} \pm \frac{k}{d + \tanh(kz_0)} \sqrt{d \tanh(kz_0) (v_{KH}^2 - v_0^2)} = \frac{dkv_0}{d + \tanh(kz_0)} \pm \frac{k\Gamma}{d + \tanh(kz_0)}, \quad (5.17)$$

where we introduced $\Gamma = \sqrt{d \tanh(kz_0) (v_{KH}^2 - v_0^2)}$ and v_{KH} is the Kelvin-Helmholtz speed for propagation in the slab defined here as

$$v_{KH}^2 = \frac{(d + \tanh(kz_0))(v_{A1}^2 d + v_{A2}^2 \tanh kz_0)}{d \tanh(kz_0)}. \quad (5.18)$$

This speed plays a special role in the determination of the nature of instabilities that can appear in the magnetic slab. First of all, the Kelvin-Helmholtz instabilities (KHI) appear only for those flows that are greater than v_{KH} . When waves are restricted to propagate in the slab, even v_{KH} is dispersive and it varies not only with the density ratio (as in the case of an interface) but also with the relative magnitude of the wavelength compared to the transversal size of the slab. For the third model the solution of the real part of the dispersion relation reduces to

$$\omega_{\pm} = \frac{k(dv_{01} - v_{02} \tanh(kz_0))}{d + \tanh(kz_0)} \pm \frac{k\tilde{\Gamma}}{d + \tanh(kz_0)} \quad (5.19)$$

where now $\tilde{\Gamma} = \sqrt{d \tanh(kz_0) [v_{KH}^2 - (v_{01} + v_{02})^2]}$ while the Kelvin-Helmholtz (KH) speed is given by the same equation (see Eq.(5.18)).

Given the importance of v_{KH} , it is instructive to estimate the magnitude and variation of this quantity for the three models. The KH speed varies not only with the dimensionless quantity kz_0 but also with the density contrast between the plasma inside and outside the slab. Observations show that the wavenumber of waves in prominences, k , varies between 10^{-8} and 10^{-6} m^{-1} (Forteza et al. 2007). As a characteristic Alfvén speed in the prominence we choose $v_{A1} = 28 \text{ km s}^{-1}$ (see Joarder and Roberts 1982). For model 1 we assume three values of the external Alfvén speed (198 km s^{-1} , 280 km s^{-1} , 343 km s^{-1}) that - under the assumption

of identical field strength- would result in a density contrast (d) of 50, 100 and 150, respectively. For model 2 and 3 we choose the case of a dark plume where the internal Alfvén speed is $v_{A1} = 200 \text{ km s}^{-1}$ that is surrounded by the prominence with a density contract of $d = 0.05, 0.1$ and 0.5 , respectively, resulting in Alfvén speeds of 44, 63 and 141 km s^{-1} , respectively (Soler et al. 2012).

A key parameter in our discussion is the product kz_0 , where z_0 is the width of the slab. Since our analysis refers to two possible scenarios (prominence slab surrounded by coronal plasma and prominence slab surrounded by prominence plasma), the value of this parameter will be different. In the first case we are going to assume (hypothetically) that the entire prominence can be considered as one single plasma slab, in which case we are going to consider that z_0 is the width of the prominence. The typical width of prominences varies between 4 and 30 Mm (Lin 2005), meaning that the product kz_0 falls in the interval 10^{-2} and 30. For the second scenario, we are going to consider that z_0 refers to the width of a thread that has typically a thickness of 100-600 km, meaning that the dimensionless parameter kz_0 will be in the interval 10^{-3} and 6×10^{-1} .

One very important aspect to note is that regardless of the model employed, the KH speed is always super-Alfvénic. Under prominence conditions these speeds amount to values that are of the order of a few hundreds km s^{-1} . For the KHI to set in, the plasma equilibrium flow has to be larger than these speeds, however, flows of these magnitudes cannot be currently observed in solar prominences. This would also mean that in prominences the plasma is always Kelvin-Helmholtz stable. The variation of the threshold speed at which waves at propagating in the slab become KH unstable (shown here on logarithmic scale) is shown in Fig.(5.2) for model 1 with the threshold being larger for larger wavelengths for both modes. For both sort of waves the range of speeds obtained clearly show that the existence of flows larger than v_{KH} are not possible to observe, meaning that the prominence in this model is indeed KH stable. For large values of kz_0 (wide slab) the value of the Kelvin-Helmholtz speeds reaches the value obtained for a single interface (see, e.g. Ballai et al. 2015 and also in Chapter 4). It is also clear that the threshold were waves become KH unstable increases with the density contrast between the prominence and the solar corona.

In the case of models 2 and 3, the range of kz_0 is different and observations restrict us to the situation when the wavelength of waves is larger than the width of

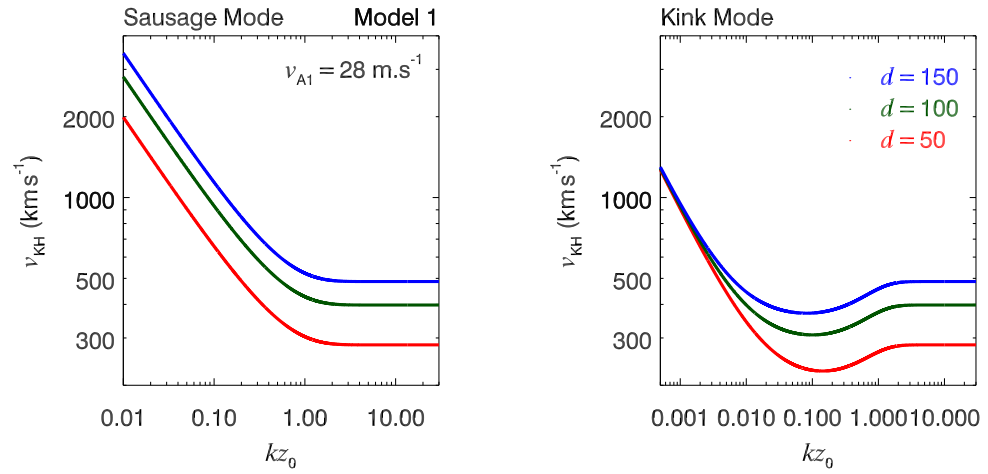


Figure 5.2: The variation of the Kelvin-Helmholtz speed with the dimensionless quantity kz_0 for model 1 on logarithmic scale for three different values of the density contrast between the solar prominence and neighboring solar corona.

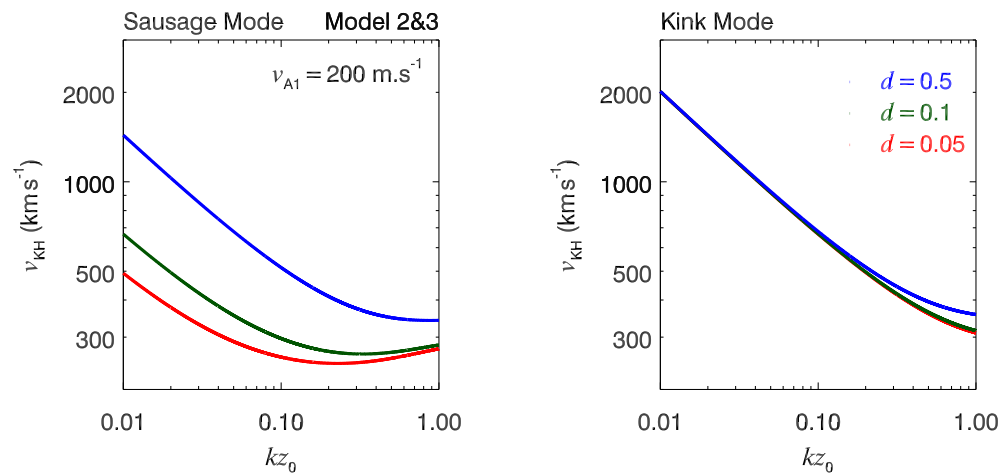


Figure 5.3: Similar to Fig 5.1, but here the variation of v_{KH} with the dimensionless quantity kz_0 refers to models 2 and 3.

5.3. DISSIPATIVE INSTABILITY

the slab (see Fig. 5.3). In the case of sausage waves v_{KH} shows a minimum in the $kx_0 \ll 1$ domain (thin slab) that is attained for $kz_0 = \tanh^{-1} v_{A1}d/v_{A2}d$ and here the threshold value is $v_{KH} = \sqrt{2(v_{A1}^2 + v_{A2}^2)}$. For kink waves the KH threshold shows a $1/kz_0$ -type monotonic decrease. For small values of the dimensionless quantity kz_0 , the KH threshold for kink waves is much larger than the corresponding value for sausage modes, while they tend to become equal for $kz_0 \approx 1$. This result shows that for long wavelengths, sausage waves can become much easily KH unstable than sausage waves, however, the range of speeds obtained here is inconsistent with the values observed for background flows, meaning that prominence threads (at least described in this model) are KH stable.

Now using the definition of $Im(\omega)$ together with the dispersion relations Eqs.(5.13) – (5.15) we can obtain, after straightforward calculations, that the imaginary parts of the frequency in the first model is given by

$$\omega_I = \mp \frac{k^2}{2\Gamma} \left[\frac{4\nu \tanh(kz_0)(dv_0 \pm \Gamma)}{d + \tanh(kz_0)} - \frac{\eta_C v_{A1}^2 d(d + \tanh(kz_0))}{v_0 \tanh(kz_0) \mp \Gamma} \right], \quad (5.20)$$

where the Cowling resistivity in the solar prominence is given by

$$\eta_C = 10^9 T_p^{-3/2} + \frac{(2\mu - 1)v_{A1}^2 m_p}{2(1 - \mu)\rho_1 \Sigma_{in}} \left(\frac{\pi m_p}{k_B T_p} \right)^{1/2}, \quad (5.21)$$

with T_p being the temperature in the prominence (inside the slab), and $\Sigma_{in} \approx 5 \times 10^{-19} \text{ m}^2$ the ion-neutral collisional cross section. Similar to Chapter 4, we assumed that the plasma is made up of hydrogen and, therefore, the mass of ions is equal to the mass of protons.

For model 2, following the same technique, the imaginary part of the frequency becomes

$$Im(\omega) \approx \mp \frac{k^2(d + \tanh(kz_0))}{2\Gamma} \left[-\frac{\eta_{C1} v_{A1}^2 d}{v_0 \tanh(kz_0) \mp \Gamma} + \frac{\eta_{C2} v_{A2}^2 \tanh(kz_0)}{dv_0 \pm \Gamma} \right], \quad (5.22)$$

while in the case of model 3, the same quantity can be written as

$$Im(\omega) \approx \mp \frac{k^2(d + \tanh(kz_0))}{2\tilde{\Gamma}} \left[-\frac{\eta_{C1}v_{A1}^2 d}{\tanh(kz_0)(v_{01} + v_{02}) \mp \tilde{\Gamma}} + \frac{\eta_{C2}v_{A2}^2 \tanh(kz_0)}{d(v_{01} + v_{02}) \pm \tilde{\Gamma}} \right]. \quad (5.23)$$

The corresponding values of the imaginary part of the frequency can be obtained for kink waves in a straightforward manner.

Now let us investigate graphically the regions where the plasma becomes unstable. As we specified earlier, the flows that are currently observed in solar prominences are of the order of a few tens of km s^{-1} . In the case of model 1 we first plot the contour plot (see Fig.(5.4)) showing the regions where the imaginary part of the frequency is changing sign for a given value of the ionisation factor (here we adopted $\nu = 0.95$). The regions on the right to the curves correspond to a combination of parameters that make the imaginary part of the frequency positive, i.e. backward propagating waves are unstable. For values of equilibrium flows that are closer to observed values (the lower end of the flow interval considered here) it is possible to obtain two values of kz_0 where $Im(\omega)$ is changing sign. In these cases, the domain of kz_0 where waves are unstable is bounded by these two values. The plots were obtained for three different values of density contrast. It is obvious that the threshold value for sausage modes depends on the value of density contrast only for larger values of flows. In the case of kink modes the instability threshold does not show any dependence on the density contrast. This behavior could be explained in terms of the internal motion of the plasma in the two wave modes. In the case of kink waves the slab oscillates without disturbing the internal structure of the slab, while in the case of sausage modes the internal plasma structure is compressed and relaxed according to the oscillating pattern of sausage modes. While the instability of sausage modes sets in for smaller values of kz_0 , i.e. long wavelength limit, kink waves become unstable only when their wavelength is comparable or shorter than the width of the slab.

Let us investigate how the instability threshold varies with the ionisation degree. We choose a particular value of the equilibrium flow of 30 km s^{-1} and let μ vary between 0.5 and 1, corresponding to the ionisation state of the plasma (see Fig 5.5). We also fix three values of density contrast ($d=50, 100, 150$) between the prominence and solar corona. It is obvious that in the case of sausage modes the threshold of

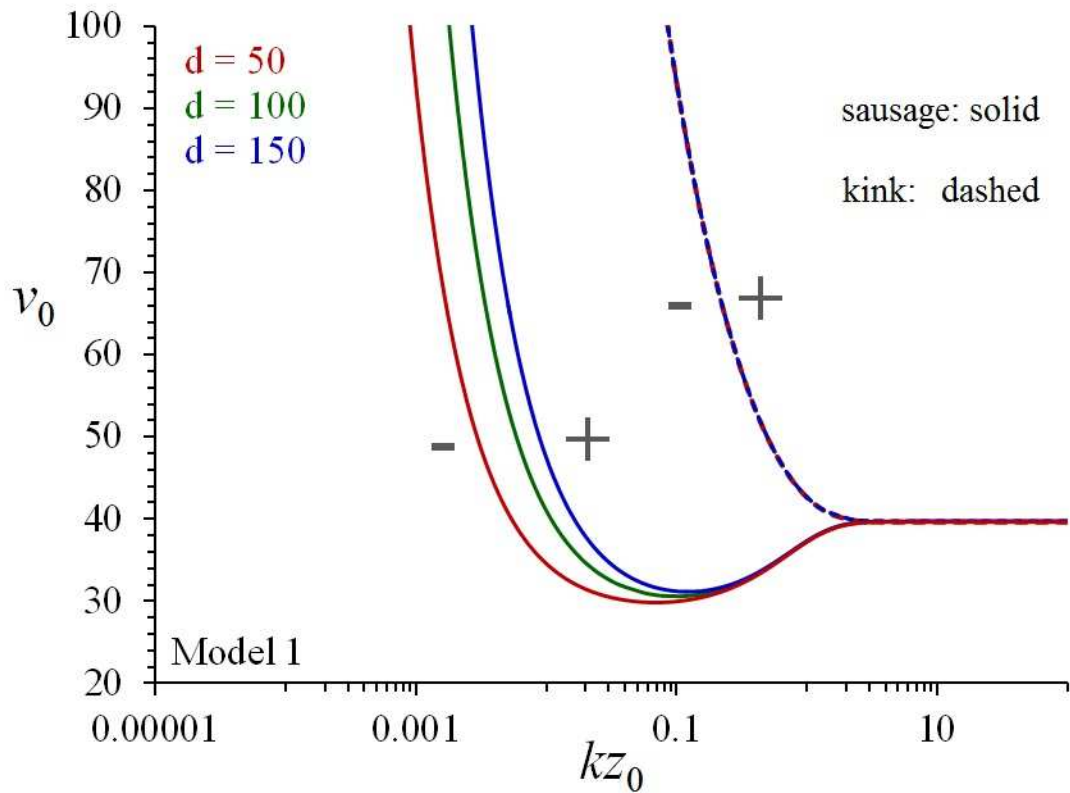


Figure 5.4: Contour plot of the variation of $Im(\omega)$ in the case of sausage (solid lines) and kink (dashed) modes in terms of background equilibrium flow and the value of the dimensionless parameter kz_0 for model 1. Here $\mu = 0.95$.

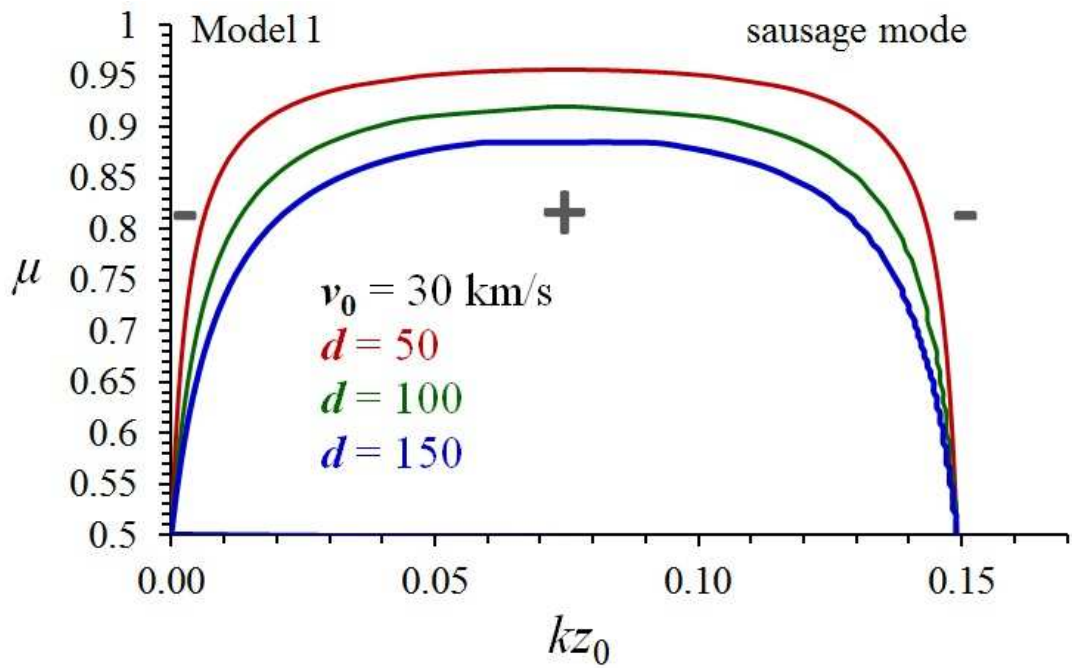


Figure 5.5: Contour plot of the variation of $Im(\omega)$ in the case of sausage (solid lines) and kink (dashed) modes in terms of ionisation degree and the value of the dimensionless parameter kz_0 for model 1. Here $v_0 = 30 \text{ km s}^{-1}$. The region where instability occurs is shown by the *plus* symbols.

instability depends on the ionisation degree for very limited interval of kz_0 . For this particular value of flow and density contrast, the backward propagating wave will be unstable only for wavelengths that are larger than the width of the slab, in particular $kz_0 < 0.15$. We can also observe that real dependence on the ionisation degree occurs only near the ends of the interval. Density differences between the two media are also influencing the instability threshold, Fig. (5.4) also shows that as the density contrast increases, the threshold moves towards the direction of increased ionisation.

Let us now discuss the second model that represents the instability of waves propagating in prominence dark plumes. In this model the plasma inside and outside the slab is partially ionised and the plasma inside the slab exhibits an equilibrium flow. These structures are hotter and less dense than their environment, therefore $d < 1$. We assume that the plasma in the plume is nearly completely ionised, therefore we choose $\mu_1 = 0.55$. The ionisation degree of the prominence (region 2) is unknown and we let the ionisation degree to vary in the interval 0.55-0.95. Let us first discuss the sausage modes appearing in these structures. The domains where the imaginary part of the frequency becomes positive is shown in Fig. (5.6). First to note is that the values of the equilibrium flow at which the backward mode is unstable for all three values of the density contrast is too high, realistic flows can be obtained only for density contrasts that are very small (of the order of 10^{-2}). Figure (5.6) shows three vertical lines corresponding to those combinations of v_0 and kz_0 for which the three quantities in the denominators of $Im(\omega)$ (given by Eq.(5.22)) become zero. The middle vertical line shows the threshold where waves start becoming KH unstable and the values of kz_0 during which these waves will continue to be KH unstable (lasts till $kz_0 \approx 0.5$). The KH instability appears only for very small values of density contrast, Although the convention for this model was that $kz_0 < 1$, we decided to plot the variation of $Im(\omega)$ for larger values in order to evidence the saturation of the threshold. Waves with very long wavelengths will be stable and they decay due to Cowling resistivity. Waves with wavelengths satisfying the condition $kz_0 \geq 0.33$ will start becoming unstable. As density increases, the domain where waves are unstable shifts towards smaller wavelengths, the maximum domain of kz_0 is reached for external plasmas with higher ionisation degree.

In the case of kink waves (see Fig. 5.7) the instability sets in again for very large values of flows. In contrast to sausage modes, the KHI threshold falls outside

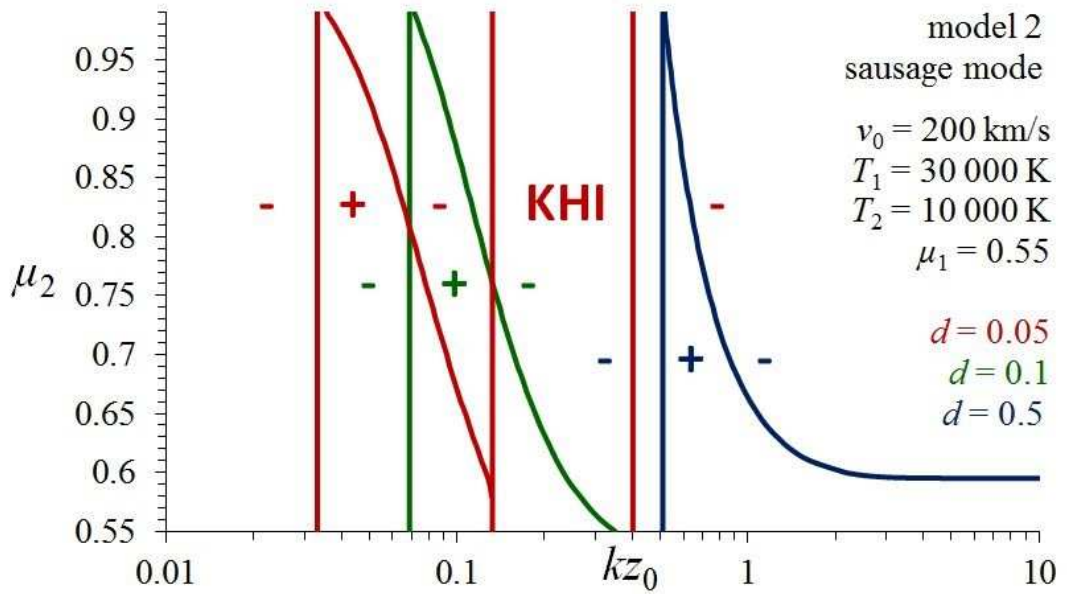


Figure 5.6: Contour plot of the variation of $Im(\omega)$ in the case of sausage modes in terms of the ionisation degree of the external medium and the value of the dimensionless parameter kz_0 for model 2. The region where instability occurs is shown by the *plus* symbols.

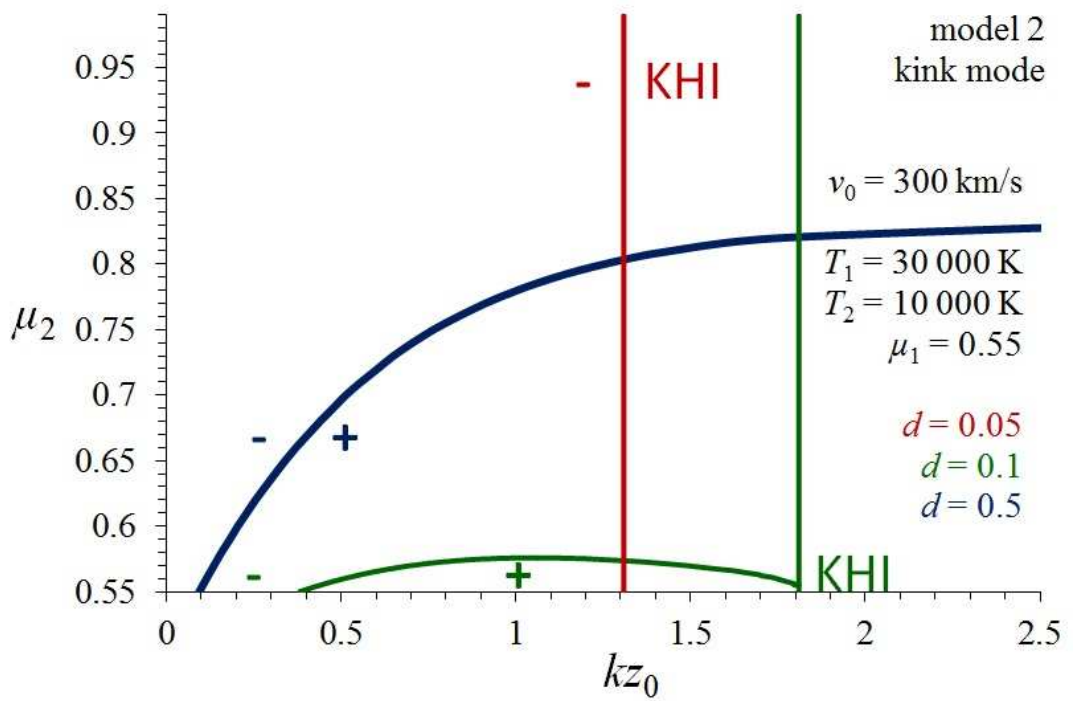


Figure 5.7: Contour plot of the variation of $Im(\omega)$ in the case of kink modes in terms of the ionisation degree of the external medium and the value of the dimensionless parameter kz_0 for model 2. The region where instability occurs is shown by the *plus* symbol.

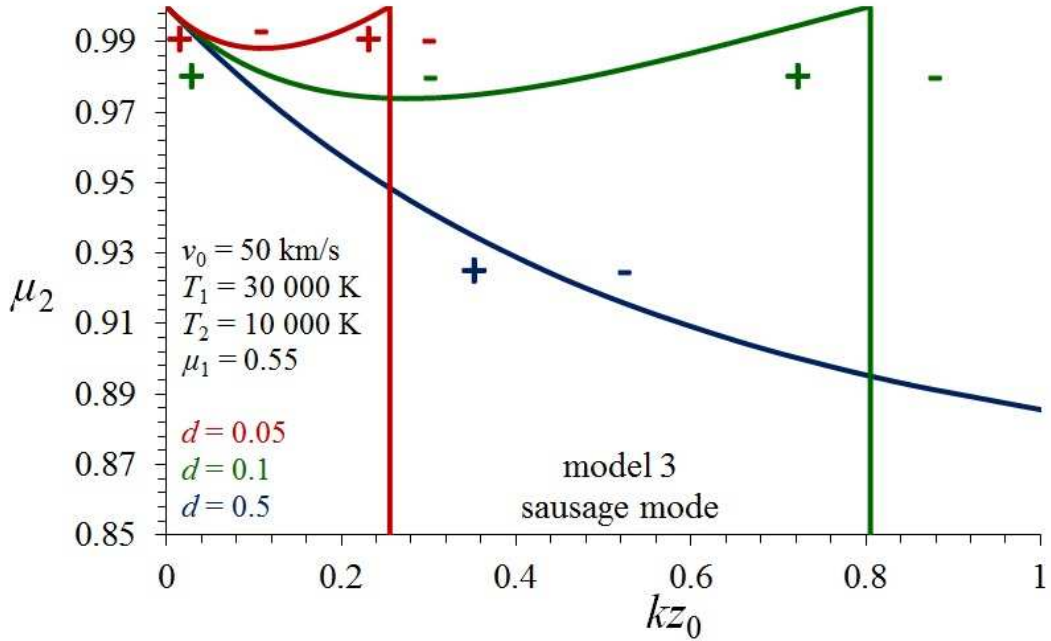


Figure 5.8: The same as in Fig. (5.5) but now the contour plots show the variation of $Im(\omega)$ in the case of sausage modes in terms of the ionisation degree of the external medium and the value of the dimensionless parameter kz_0 for model 3.

the range of kz_0 chosen for this model ($kz_0 < 1$). Figure (5.7) also shows that for a very small density contrast the plasma becomes stable, while for larger density fraction the plasma shows instability only for values of the ionisation degree that is closer to a fully ionised plasma. This means that the neutrals in the mixture will have a stabilizing effect. For very long wavelengths the backward wave is stable and waves will damp. The very high level of the flow at which these modes become unstable shows that we can safely consider these modes as stable in the realistic limit, equilibrium flows of a few hundreds of km s^{-1} are currently not observed in solar prominences.

Finally, let us look at the appearance of the dissipative instability in the case of the third model. Now the dispersion relation of the waves is given by Eq.(5.15) and the imaginary part of the frequency by Eq. (5.23). Again, we are going to discuss separately sausage and kink modes, respectively. The variation of the imaginary part of the frequency for backward modes in the case of sausage modes is shown by Fig. (5.8). Comparing the variation of $Im(\omega)$ of this model with the variation shown by

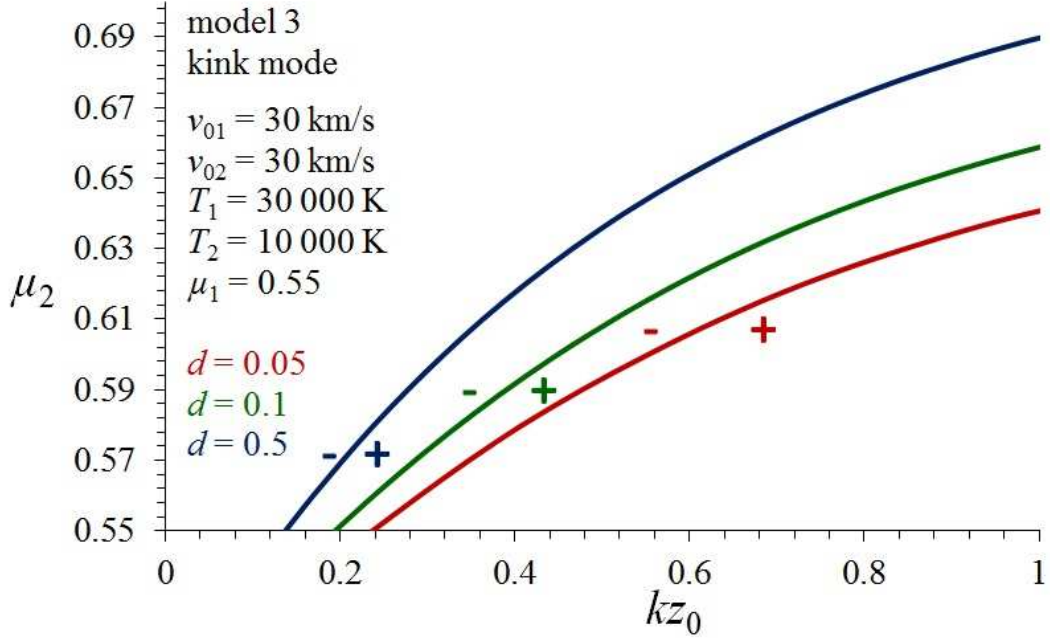


Figure 5.9: The same as in Fig. (5.5) but now the contour plots show the variation of $Im(\omega)$ in the case of kink modes in terms of the ionisation degree of the external medium and the value of the dimensionless parameter kz_0 for model 3.

Fig. (5.6) (the sausage modes corresponding to the second model), we can see that the differences are significant. First of all the plasma dynamics is below the KH threshold for any density contrast and ionisation degree. Secondly, the presence of a counterflow in the external region reduced considerably the range of flows where the Alfvénic waves propagating along the interface are dissipative unstable; in obtaining Fig. (5.6) we used an internal and external flow of 50 km s^{-1} . For very small values of density contrast ($d = 0.05$ in our case) the plasma is unstable for any ionisation degree provided the wavenumber satisfies the condition $kz_0 < 0.21$. For any wavenumber above this value, the perturbations along the tangential discontinuity will propagate under the influence of damping processes. As the density contrast increases, the threshold where the plasma becomes dissipative unstable varies with the ionisation degree and the dimensionless parameter kz_0 , so that the larger the density contrast (densities in the two regions approach each other) the easier for a system with a highly ionised plasma environment to become dissipative unstable. The variation of $Im(\omega)$ in the case of kink modes propagating in model 3 is similar to the

results obtained in the case of kink modes in model 2 (see Fig. 5.9). Again, for very large wavelengths all waves will exhibit physical damping, there is a cut-off value of the wavenumber at which these modes become dissipative unstable and this cut-off value increases with decreasing the density ratio. As the density contrast increases the domain of ionisation degree, where the backward mode is unstable, increases, however the growth of the ionisation degree is not too large. Plasmas with very large number of neutrals will be stable and modes decay due to physical damping.

5.4 Conclusions

The present Chapter focused on the conditions that need to be satisfied for the generation of dissipative instabilities for waves propagating in a partially ionised plasma slab surrounded by the corona or another partially ionised prominence environment. The geometrical restrictions imposed on waves confer them a dispersive character and different characteristics could be recovered for the symmetric and asymmetric waves (sausage and kink waves).

The nature of the dissipative instability means that it appears for flow speeds lower than the Kelvin-Helmholtz instability (KHI), the value of the Kelvin-Helmholtz speed is playing a special role in our discussion. The threshold where this instability occurs varies with the density ratio of the slab plasma and its surrounding but also with the wavelength of the waves compared to the width of the slab. Simple analysis showed that the KHI is unlikely to occur in the plasmas we dealt with, as the value of this threshold makes (especially for wavelengths that are much larger than the width of the slab) them always higher than any observed plasma background flow in the solar prominence.

We have investigated three models (a whole partially ionised prominence embedded in a viscous corona, and a partially ionised plume surrounded by a partially ionised prominence, with different dynamical equilibrium). In our analysis we focussed on the effect of three variables (values of the equilibrium flow, the dimensionless parameter kz_0 and the degree of ionisation) on the instability threshold. For model 1 we obtained that when the ionisation degree is kept constant (and close to the value of a plasma abundant in neutrals), waves with very large wavelength are damped, the unstable behavior starts at specific wavelengths. The smaller the density

ratio between the prominence and corona, the more unstable the plasma becomes for waves that have smaller wavelengths. Flows at which this transition occurs were obtained to be in line with the observed values. When fixing the value of the equilibrium flow, we found out that waves will be unstable for rather large wavelength and real dependence on the ionisation degree occurs near the end of the interval. We also obtained that the instability thresholds for kink waves are not depending on the density contrast.

For model 2 the dissipative instability occurs for rather large (thus highly unrealistic) values of the equilibrium flow, regardless of whether we are dealing with sausage or kink modes. For sausage modes the regimes where waves are dissipative unstable and KH unstable are very close. In the case of kink modes the KHI sets in only for wavelengths that are smaller than the width of the slab. Realistic values of flow speeds can be easily obtained once we assume that the surrounding plasma presents a counterflow (model 3) and here the instability threshold for both types of waves is very much dependent on the wavelength of the mode and the ionisation degree of the plasma. In the case of kink waves with very large wavelengths, the instability is inhibited, waves undergo a normal physical damping.

Obviously, the very large values of the flows required for the instability to occur in model 2 can be considerably reduced once other factors (nonparallel magnetic field, compressibility, etc.) are taken into account. However, this remains to be studied in a forthcoming work.

Chapter 6

Conclusions

The problem of prominence stability/instability is one of the most important questions in solar physics, as prominences contribute to the evolution of space weather. Given the complexity of the field in these structures, simplistic models can be constructed, that mimic the real configurations. The plasma dynamics are even more complicated by the fact that the prominence plasma is not fully ionised and it is very likely that is not even in ionisation equilibrium.

The present Thesis is dedicated to the investigation of the generation of dissipative instabilities at the interface between partially ionised prominence plasmas and their environment. These interfaces were considered to be tangential discontinuities. In the first instance we considered the interface between the viscous and fully ionised coronal plasma and the partially ionised solar prominence in which the dominant dissipative effect is the Cowling resistivity. This situation was discussed in the one-fluid and two-fluid limits. In the second model we used single fluid model to discuss the generation of dissipative instabilities in a partially ionised plasma slab surrounded by a viscous fully ionised plasma or by another partially ionised prominence plasma. The nature of the dissipative instability means that they appear for flow speeds lower than the Kelvin-Helmholtz instability (KHI), the value of the Kelvin-Helmholtz speed is playing a special role in our discussion.

The magnetic fluids were assumed to be incompressible and the prominence/dark plume equilibrium was considered to be dynamical, with a homogeneous flow parallel to the interface. Assuming a weak damping, we obtained the dispersion relation

of Alfvénic waves propagating along the interface. The presence of dissipative effects on both sides of the interface renders the dispersion relation to be complex with the imaginary part of this quantity describing the decay or the growth of waves.

Our results show that in all single models considered the forward propagating wave is always stable, with the amplitude of the wave decaying because of dissipation, however, for the backward propagating wave there is a threshold of the flow (below the KHI threshold) for which the wave becomes unstable.

In the case of a one-fluid plasma the study of the dissipative instability at a single interface reveals that:

- (i) the partial ionisation has a stabilizing effect on the interface for any value of the ionisation fraction and the unstable behavior can be connected to the viscous nature of the coronal plasma
- (ii) the partial ionisation has little effect on the threshold where waves become unstable. For a plasma where neutrals are abundant, the instability appears for higher values of flows, i.e. neutrals have a stabilizing effect
- (iii) The model was used to study the generation of dissipative instability at the interface of two partially ionised plasmas modeling the prominence and dark plumes. The unstable mode obtained in this case shows a very low growth rate, meaning that this type of instability (at least in this simplified model) cannot explain the appearance of turbulent up-flows in plumes that can be attributed to instability.

The appearance of the dissipative instability in the case of a two-fluid approach is more complex, as individual species can become unstable, leading to the instability of the whole mixture. In particular, we found that

- (i) the instability can be connected to one single species, and this makes the whole plasma unstable
- (ii) forward propagating waves belonging to neutrals are subject to a hydrodynamic KH instability, but the growth of modes can be inhibited by the damping due to the collisions between neutrals and ions
- (iii) backward propagating waves connected to ions can become dissipative unstable

The single interface model was extended to account for the effect of dispersion, i.e. when waves' propagation speed depends on their wavelength. A one fluid partially ionised plasma slab was considered to be sandwiched between two semi-infinite fully ionised plasma regions representing the solar corona, and by two

semi-infinite partially ionised prominence with different equilibrium properties than the plasma in the slab. Again, we studied the conditions that have to be satisfied in order that the dissipative instability appears in the Alfvén waves propagating along the magnetic slab. Different treatment was applied for sausage and kink modes, respectively. In our analysis we focussed on the effect of three variables (values of the equilibrium flow, the dimensionless parameter kz_0 and the degree of ionisation) on the instability threshold. Our analysis shows that

(i) the threshold where the dissipative instability occurs varies with the density ratio of the slab plasma and its surrounding but also with the wavelength of the waves compared to the width of the slab. The values of this threshold reveals that KHI will set in for very high values of flows, values that have never been observed, meaning that the plasmas discussed in our models are always KH stable

(ii) in the case of a prominence slab surrounded by the viscous corona we obtained that when the ionisation degree is kept constant (and close to the value of a plasma abundant in neutrals), waves with very large wavelength are damped, the unstable behaviour starts at specific wavelengths. The smaller is the density ratio between the prominence and corona, the plasma becomes unstable for waves that have smaller wavelengths. Flows at which this transition occurs were obtained to be in line with the observed values. When fixing the value of the equilibrium flow, we found out that waves will be unstable for rather large wavelength and real dependence on the ionisation degree occurs near the end of the interval. We also obtained that the instability thresholds for kink waves are practically independent on the density contrast.

(iii) in the case of a prominence dark plume surrounded by a cooler and denser prominence the dissipative instability occurs for rather large (thus highly unrealistic) values of the equilibrium flow, for both sausage and kink modes. For sausage modes the regimes where waves are dissipative unstable and KH unstable are very close. In the case of kink modes the KHI sets in only for wavelengths that are smaller than the width of the slab

(iv) in the case of a counterflow in the external prominence region (background flows opposite for the two regions), realistic values of flow speeds at which dissipative instability occurs can be easily obtained, and here the instability threshold for both types of waves is very much dependent on the wavelength of the mode and the ionisation degree of the plasma. In the case of kink waves with very large wavelengths,

the instability is inhibited, waves undergo a physical damping.

6.1 Future possible research avenues

The simplistic models employed in the present Thesis show that the appearance of the dissipative instability is realistic and these models can be easily expanded. First of all, compressibility can be added, especially keeping in mind that the compressibility can have a stabilizing effect on the appearance of instabilities, at least in the case of KHI (Soler et al. 2012). It remains to be seen whether this is true for the kind of instability discussed by us.

In order to keep the simplicity in mathematics, the background magnetic field was assumed to be aligned with the interface. In solar prominences this is not always the case, and a model incorporating a tilted magnetic field is another possible way to expand the present research. This obviously will alter the KH threshold and might bring especially the flows required in model 2 to a more realistic level.

Our analysis was restricted to the linear part of the instability, more particularly to the generation of the instability. A possibility to expand the present research is to perform an initial value study, and follow the generation and evolution of the instability. For this numerical investigation is needed as the amplitude of perturbations can grow to the limit where nonlinear analysis will be needed. It remains to be seen whether dissipative instability can lead to the unstable behavior of the whole prominence.

Finally, the present research can be continued by a possible study of the nature of the dissipative instability in establishing whether this instability is an absolute or convective instability.

Bibliography

- [Arber et al. (2007)] Arber, T.D., Haynes, M., & Leake, J. E., 2007, *Astrophys. J.*, 666, 541
- [Arregui et al. (2012)] Arregui, I., Oliver, R., & Ballester, J. L., 2012, *Living Rev. Sol.Phys.*, 9, 2
- [Aschwanden (2008)] Aschwanden, M. J., 2008, *Journal of Astrophysics and Astronomy* 29, 3-16.
- [Aschwanden(2004)] Aschwanden, M. J., 2004, *Physics of the Solar Corona*, Springer-Verlag, Berlin
- [Aschwanden et al. (2002)] Aschwanden, M. J., de Pontieu, B., Schrijver, C. J., & Title, A. M., 2002, *Solar Phys.*, 206, 99
- [Aschwanden et al. (2000)] Aschwanden, M. J., Nightingale, R. W., & Alexander, D., 2000, *Astrophys. J.*, 541, 1059
- [Ballai (2007)] Ballai, I., 2007, *Solar Phys.*, 246, 177-185
- [Ballai et al. (2015)] Ballai, I., Oliver, R. & Alexandrou, M., 2015, *Astron. Astrophys.* 577, 82
- [Ballai (2003)] Ballai, I., 2003, *Astron. Astrophys.*, 410, 17
- [Ballester & Priest, (1989)] Ballester, J. L. & Priest, E. R. (1989), "Model for the fibril structure of solar prominences", *Astron. Astrophys.*, 225, 213-221.
- [Balthasar et al. (1993)] Balthasar, H., Wiehr, E., Schleicher, H. & Wohl, H., 1993, *Astron. Astrophys.*, 277, 635

BIBLIOGRAPHY

- [Barceló et al. (2011)] Barceló, S., Carbonell, M. & Ballester, J.L., 2011, *Astron. Astrophys.*, 525, 60
- [Berger et al. (2008)] Berger, T.E., Shine, R.A., Slater, G.L. et al., 2008, *Astrophys. J.*, 676, 89
- [Berger et al. (2010)] Berger, T.E., Slater, G.L., Hulburt, N. et al., 2010, *Astrophys. J.*, 716, 1288
- [Berton and Heyvaerts (1987)] Berton, R. and Heyvaerts, J. (1987) *Solar Phys.*, 109, 201
- [Bonet et al. (2008)] Bonet, J. A., Márquez, I., Sánchez, J., Cabello, I. & Domingo, V. (2008). *Astrophys. J. Lett.*, 687, L131-L134
- [Boyd and Sanderson (1969)] Boyd, T. J. M. & Sanderson, J. J. (1969), *Plasma Dynamics*.
- [Braginskii (1965)] Braginskii, S. I., 1965, *Transport Processes in a Plasma, Reviews of Plasma Physics, Vol. 1 (New York: Consultants Bureau)*
- [Carbonell et al. (2010)] Carbonell, M., Forteza, P., Oliver, R. & Ballester, J.L. 2010, *Astron. Astrophys.*, 515, 80
- [Carbonell et al. (2004)] Carbonell, M., Oliver, R. & Ballester, J.L. 2004, *Astron. Astrophys.*, 415, 739
- [Cairns (1979)] Cairns, M. 1979, *J. Fluid Mech.* 92, 1
- [Chiuderi Drago et al. (2001)] Chiuderi Drago, F., Alissandrakis, C. E., Bastian, T., Bocchialini, K. & Harrison, R. A. (2001), *Solar Phys.*, Vol. 199, Issue 1, 115-132
- [Cowling (1957)] Cowling, T.G., 1957, *Magnetohydrodynamics, Monographs on Astronomical Subjects, Adam Hilger (Bristol)*
- [de Jager (1959)] de Jager, C., 1959, "Structure and dynamics of the solar atmosphere" in *Astrophysik 3: Das Sonnensystem, (Ed.) Flügge, S., Vol 52 of Handbuch der Physik, p. 80, Springer (Berlin)*

BIBLIOGRAPHY

- [De Pontieu et al. (2004)] De Pontieu, B., Erdélyi, R., & James, S.P. (2004). *Nature* 430, 536-539
- [Degenhardt & Deinzer (1993)] Degenhardt, U. & Deinzer, W. (1993), *Astron. Astrophys.*, 278, 288-292
- [Demoulin et al. (1987)] Demoulin, P., Malherbe, J. M., Schmieder, B. & Raadu, M. A. 1987, *Astron. Astrophys.*, 183, 142-150
- [Diaz et al. (2002)] Diaz, A.J., Oliver, R. & Ballester, J.L., 2002, *Astrophys. J.*, 580, 550
- [Diaz et al. (2012)] Diaz, A.J., Soler, R. & Ballester, J.L., 2012, *Astrophys. J.*, 754, 41–RT
- [Dunn et al. (1960)] Dunn, R.B., Jefferies, J.T. & Orrall, F.Q., 1960, *The Observatory* 80, 31-33
- [Edérlyi & Ballai, (2007)] Edérlyi, R. & Ballai, I. (2007), *Astronomische Nachrichten*, 318, 726-733
- [Edwin & Roberts (1982)] Edwin, P.M. & Roberts, B. (1982). *Solar Phys.*, 76, 239-259
- [Edwin & Roberts (1983)] Edwin, P.M. & Roberts, B. (1983). *Solar Phys.* 88, 179-191
- [Engvold, (2008)] Engvold, O. (2008) in *IAU Symposium*, Vol. 247, 152-157
- [Engvold, (2001)] Engvold, O. (2001) in *INTAS Workshop on MHD Waves in Astrophysical Plasmas*, ed. J. L. Ballester & B. Roberts, 123
- [Engvold, (1998)] Engvold, O. (1998). "Observations of filament structure and dynamics", in *New Perspectives in Solar Prominences*, IAU Colloq. 167, Aussois, France, April 28 - May 4, 1997.
- [Engvold et al. (1987)] Engvold, O., Kjeldseth-Moe, O., Bortoe J-D. F. & Brueckner, G.E. (1987) in *ESA Proceedings of 21st ESLAB*, p. 21-25

BIBLIOGRAPHY

- [Erdélyi and Goossens(1995)] Erdélyi, R. & Goossens, M. 1995, *Astron. Astrophys.*, 294, 575
- [Eto et al. (2002)] Eto, S., Isobe, H. & Narukage, N. (2002). *PASJ*, 54, 481
- [Fontenla et al. (1990)] Fontenla, J.M., Avrett, E.H. & Loeser, R. (1990), *Astrophys. J.*, P1, 355, 700-718
- [Forteza et al. (2007)] Forteza, P., Oliver, R., Ballester, J.L. & Khodachenko M.L., 2007, *Astron. Astrophys.*, 461, 731
- [Forteza et al. (2008)] Forteza, P., Oliver, R. & Ballester, J.L., 2008, *Astron. Astrophys.*, 492, 223
- [Foullon et al. (2004)] Foullon, C., Verwichte, E. & Nakariakov V.M., 2004, *Astron. Astrophys.*, 427, L5
- [Freij et al. (2014)] Freij, N., Scullion, E.M., Nelson, C.J., Mumford, S., Wedemeyer, S. & Erdelyi, R. 2014, *Astrophysical Journal*, 791, 61
- [Gary, (2001)] Gary, G. A. (2001), *Solar Phys.*, 203, 71-81
- [Gilbert et al. (2002)] Gilbert, H., Hansteen, V. & Holzer, T., 2002, *Astrophys. J.*, 577, 464
- [Gilbert et al. (2007)] Gilbert, H., Alexander, D. & Liu, R., 2007, *Solar Phys.*, 245, 287
- [Glatzmaier (1981)] Glatzmaier, G. A. 1981, *Solar Phys.* 125, 1-12.
- [Goedbloed and Poedts, (2004)] Goedbloed, J. P. H. & Poedts, S. 2004, *Principles of Magnetohydrodynamics*(CUP)
- [Goossens et al. 2012] Goossens, M., Soler, R., Arregui, I. & Terradas, J. 2012, *The Astrophysical Journal*, 760, 98.
- [Goossens Erdelyi and Ruderman. 2012] Goossens, M., Erdelyi, R. & Ruderman, M.S. 2012, *Space Science Rev.*

BIBLIOGRAPHY

- [Harrison, (1997)] Harrison, R. A. (1997). *Solar Phys.*175, 467-485
- [Harvey (1969)] Harvey, J., W. (1969). *PhD thesis, University of Colorado.*
- [Hasegawa and Chen, (1974)] Hasegawa, A. and Chen, L. (1974), *Physical Review Letters* 32, Issue 9, 454-456
- [Hasegawa and Chen, (1976)] Hasegawa, A. and Chen, L. (1976),*Physics of Fluids*, 19, 1924-1934
- [Heinzel & Anzer, (2006)] Heinzel, P. & Anzer, U. (2006). "On the Fine Structure of Solar Filaments", *Astrophys. J. Lett.*643, L65-L68.
- [Hyder, (1966)] Hyder, C., L. (1966), *ZAp*, 63, 78
- [Isobe & Tripathi, (2006)] Isobe, H. & Tripathi, D. (2006), *Astron. Astrophys.*, 449, L17
- [Jess et al. (2009)] Jess, D. B., Mathioudakis, M., Erdélyi, R., Crockett, P. J., Keenan, F. P. & Christian, D. J. (2009). *Science* 323,1582-
- [Jing et al. (2006)] Jing, J., Lee, J., Spirock, T. J. & Wang, H. (2006), *Solar Phys.*. 236, 97
- [Joarder& Roberts(1992a)] Joarder, P.S & Roberts, B., (1992a), *Astron. Astrophys.*, 256, 264
- [Joarder& Roberts (1992b)] Joarder, P.S & Roberts, B., (1992b), *Astron. Astrophys.*, 261,625
- [Joarder& Roberts (1993)] Joarder, P.S & Roberts, B., (1993), *Astron. Astrophys.*, 273, 642
- [Joarder et al. (1997)] Joarder, P.S., Nakariakov, V.M. & Roberts, B., 1997, *Solar Phys.*, 176, 285
- [Khodachenko et al.(2006)] Khodachenko, M.L, Rucker, H.O., Oliver, R., Arber, T. D. & Hanslmeier, A., 2006, *Advances in Space Research*, 37, 447.

BIBLIOGRAPHY

- [Khodachenko et al. (2004)] Khodachenko, M. L., Arber, T.D, Rucker, H.O. & Hanslmeier, A., 2004, *Astron. Astrophys.*, 422, 1073
- [Khomenko and Collados (2012)] Khomenko, E. & Collados, M. 2012, *Astrophys. J.*, 747, 87
- [Kippenhahn & Schlüter,(1957)] Kippenhahn, R. & Schlüter, A. (1957). *Z. Astrophys*, 43, 36-62.
- [Kleczek & Kuperus, (1969)] Kleczek, J. & Kuperus, M. (1969). *Solar Phys.*. 6, 72
- [Klimchuk,(2006)] Klimchuk, J. A. (2006). *Solar Phys.*, 234, 41-77
- [Kuperus et al. (1967)] Kuperus, M. & Tandberg-Hanssen, E., 1967, *Solar Phys.*, 2, 39
- [Labrosse et al. (2010)] Labrosse, N., Heinzel, P., Vial, J. et al., 2010, *Space Sci. Rev*, 151, 243
- [Landman et al. (1977)] Landman, D. A., Edberg, S. J, & Laney, C. D. (1977). *Astrophys. J.*, 218, 888
- [Leake et al. (2005)] Leake, J. E., Arber, T. D. & Khodachenko, M. L., 2005, *Astron. Astrophys.*, 442, 1091.
- [Lighthill, (1960)] Lighthill, M. J. (1960). *Royal Society of London Philosophical Transactions Series A* 252, 397-430.
- [Lin (2005)] Lin, Y., 2005. "Magnetic Field Topology inferred from Studies of Fine Threads in Solar Filaments", PhD thesis, University of Oslo, Oslo.
- [Lin (2010)] Lin, Y., 2010, *Space Sci. Rev*, 158, 237
- [Lin et al. (2003)] Lin, Y., Engvold, O. & Wiik, J.E., 2003, *Solar Phys.*, 216, 109
- [Lin et al. (2005)] Lin, Y., Engvold, O., Rouppe Van der Voort, L., Wiilk, J. E. & Berger, T. E. (2005), *Solar Phys.*, 226, 239
- [Mackay et al. (2010)] Mackay, D.H., Karpen, J.T., Ballester, J.L. et al., 2010, *Space Sci. Rev*, 151, 333

BIBLIOGRAPHY

- [Malville & Scindler, (1981)] Malville, J. M. & Scindler, M. (1981). *Solar Phys.*, 70, 115-128
- [Marcu et al. (2006)] Marcu, A., Ballai, I. and Pinter, B. (2006). *Astron. Astrophys.*, 449, 1193-1202.
- [Martin et al. (2008)] Martin, S. F., Lin, Y., & Engvold, O. (2008). *Solar Phys.*, 250, 31-51.
- [Menzel, (1951)] Menzel, D. H. (1951) in *Proc. Conf. on Dynamics of Ionised Media (London)*
- [Mitchener and Kruger (1973)] Mitchener, M. & Kruger, C.H. 1973, *Partially ionised gases, John Wiley & Sons (New York)*
- [Mocanu et al. (2008)] Mocanu G., Marcu, A, Ballai, I. & Orza, B., 2008, *Astroph. Nachr*, 329, 780
- [Molowny-Horas et al (1997)] Molowny-Horas, R., Oliver, R., Ballester, J. L., & Baudin, F., (1997). *Solar Phys.*. 172, 181-188.
- [Molowny-Horas et al. (1998)] Molowny-Horas, R., Baudin, F., Oliver, R., & Ballester, J. L., (1998). *J.A.*, vol. 154 of *ASP Conference series*, pp. 650-657.
- [Molowny-Horas et al. (1999)] Molowny-Horas, R., Heinzel, P., Mein, P. & Mein, N. (1999). *Astron. Astrophys.*, 345, 618.
- [Moreton & Ramsey, (1960)] Moreton, G. E. & Ramsey, H. E. (1960). *Publications of the Astronomical Society of the Pasific* 72, 357-.
- [Okamoto et al. (2004)] Okamoto, T. J., Nakai, H. & Keiyama, A. (2004). *Astrophys. J.*, 608, 1124.
- [Okamoto et al. (2007)] Okamoto, T. J., Tsuneta, S. & Berger, T. E. (2007). *Science*, 318, 1577.
- [Oliver & Ballester (1996)] Oliver, R. & Ballester, J. L. (1996). *Astrophys. J.* 456, 393-398.

BIBLIOGRAPHY

- [Oliver & Ballester (2002)] Oliver, R., & Ballester, J. L. (2002). *Solar Phys.* 206, 45.
- [Oliver et al. (1992)] Oliver, R., Ballester, J. L., Hood, A. W. & Priest, E. R. (1992). *Astrophys. J.*, 400, 369.
- [Oliver et al. (1993)] Oliver, R., Ballester, J. L., Hood, A. W. & Priest, E. R. (1993). *Astrophys. J.*, 409, 809.
- [Parenti, (2014)] Parenti, S. 2014, *Living Reviews in Solar Physics*, Vol 2, no 1.
- [Parker, (1978)] Parker, E. N. 1978, *Astrophys. J.*, 221, 368-377
- [Parker, (1974)] Parker, E. N. 1974, *Astrophysics and Space Science*, 31, 261-266.
- [Parker, (1964)] Parker, E. N. 1964, *Astrophys. J.*, 140, 1170
- [Patsourakos and Vial (2002)] Patsourakos, S., & Vial, J.-C. 2002, *Solar Phys.*, 208, 253
- [Poland & Anzer (1971)] Poland, A. & Anzer, U. (1971). *Solar Phys.* 19, 401.
- [Prialdnik et al. (1986)] Prialdnik, D., Eviatar, A. & Ershkovich, A.I., 1986, *Journal of Plasma Physics*, 35, 209
- [Priest, (1982)] Priest, E. (1982). *Solar Magneto-Hydrodynamics. Geophysics and Astrophysics Monographs*, Kluwer Academic Publishers.
- [Priest, (1984)] Priest, E. (1984). *Solar Magneto-Hydrodynamics. Geophysics and Astrophysics Monographs*, Dordrecht: Reidel.
- [Régnier et al. (2001)] Régnier, S., Solomon, J. & Vial, J.C. (2001). *Astron. Astrophys.*, 376, 292-301.
- [Roberts (1991)] Roberts, B. (1991). *Geophys. Astrophys. Fluid Dyn.* 62, 83-100.
- [Roberts (1981)] Roberts, B. *Solar Phys.*, 69, 27
- [Roberts et al. (1984)] Roberts, B., Edwin, P. M. & Benz, A. O. (1984). *Astrophys. J.*, 279, 857

BIBLIOGRAPHY

- [Roberts & Joarder (1994)] Roberts, B. & Joarder, P. S. (1994) in *Lecture Notes in Physics*, Berlin Springer Verlag, Vol. 432, *Advances in Solar Physics*, ed. G. Belvedere, M. Rodono & G. M. Simnett, 173-178.
- [Ruderman & Roberts, (2002)] Ruderman, M. S. & Roberts, B. (2002) *Astrophys. J.* 577, 475-486.
- [Ruderman and Goossens (1995)] Ruderman, M. S., & Goossens, M. 1995, *J. Plasma Phys.*, 54, 149
- [Ruderman et al. (1996)] Ruderman, M. S., Verwichte, E., Erdélyi, R. & Goossens, M. 1996, *J. Plasma Phys.*, 56, 285
- [Ruderman et al. (2000)] Ruderman, M. S., Oliver, R., Erdélyi, R., Ballester, J.L. & Goossens, M. 2000, *Astron. Astrophys.*, 354, 261
- [Ryutova (1988)] Ryutova, M. P., 1988, *Soviet Phys., JETP*, 67, 1594
- [Ryutova et al. (2010)] Ryutova, M. P., Berger, T.E., Frank, Z., Tarbell, T. & Title, A. 2010, *Solar Phys.*, 267, 75
- [Sakurai et al. (1991)] Sakurai, T., Goossens, M. & Hollweg, J.V., 1991, *Solar Phys.*, 133, 227.
- [Schmieder & Mein, (1983)] Schmieder, B. & Mein, P. (1983), *Hvar Observatory Bulletin*, Vol. 13, Issue 1, 331
- [Schmieder et al. (1990)] Schmieder, B., Raadu, M. A. & Wiik, J.E. (1990), *Journal of Plasma Physics*, Vol.44, Issue 3, 547
- [Schutgens, (1997a)] Shutgens, N.A. J. (1997a). *Astron. Astrophys.* 323, 969-985.
- [Schutgens, (1997b)] Shutgens, N.A. J. (1997b). *Astron. Astrophys.* 325, 352-359.
- [Schutgens & Toth, (1999)] Shutgens, N.A. J. & Toth, G. (1999). *Astron. Astrophys.* 345, 1038-1048.
- [Seeds, (1991)] Seeds, M. A. 1991 , "*Horizons: Exploring the Universe*", Publishers: Wodsworth Pub. Co. Belmont, California. 1991.

BIBLIOGRAPHY

- [Simon et al., (1986)] Simon, G., Gesztelyi, L., Schmieder, B. & Mein, N. 1986, *Nasa, Goddard Spaceflight Center, Coronal and Prominence Plasmas*, 229-233.
- [Sobotka, (2003)] Sobotka, M. (2003). *Astromische Nachrichten* 324, 369-373.
- [Solanski, (2003)] Solanski, S. K. (2003). *The Astronomy and Astrophysics Review* 11, 153-286.
- [Soler et al. (2009)] Soler, R., Oliver, R. & Ballester, J.L., 2009a, *Astrophys. J.*, 699, 1553
- [Soler et al. (2009)] Soler, R., Oliver, R. & Ballester, J.L., 2009b, *Astrophys. J.*, 707, 662
- [Soler et al. (2012)] Soler, R., Andries, J., & Goossens, M., 2012a, *Astron. Astrophys.*, 537, 84
- [Soler et al. (2012)] Soler, R., Diaz, A. J., Ballester, J.L. & Goossens, M., 2012, *Astrophys. J.*, 749, 163
- [Soler et al. (2013)] Soler, R., Diaz, A.J., Ballester, J.L. & Goossens, M., 2013, *Astron. Astrophys.*, 551, 86
- [Spiegel & Zahn, (1992)] Spiegel, E. A. & Zahn, J. (1992). *Astron. Astrophys.*, 265, 106.
- [Suematsu et al. (1990)] Suematsu, Y., Yoshinaga, R., Terao, N. & Tsubaki, T., 1990, *Publ. Astron. Soc. Japan*, 42, 187
- [Tandberg-Hanssen(1967)] Tandberg-Hanssen, E. 1967, *Solar Phys.*, 2, 98-105
- [Tandberg-Hanssen (1995)] Tandberg-Hanssen, E. ed. 1995, *Astrophysics and Space Science Library*, Vol. 199, The nature of solar prominences.
- [Terradas et al. (2002)] Terradas, J., Molowny-Horas, R., Wiehr, E., Balthasar, H., Oliver, R. & Ballester, J.L. (2002), *Astron. Astrophys.*, 393, 637
- [Terradas et al. (2012)] Terradas, J., Oliver, R. & Ballester, J.L., 2012, *Astron. Astrophys.*, 541, 102

BIBLIOGRAPHY

- [Terra-Homem et al. (2003)] Terra-Homem, M., Erdélyi, R. & Ballai, I. 2003, *Solar Phys.*, 217, 199
- [Thomas & Weiss, (2004)] Thomas, J. H. & Weiss, N. O. (2004). *Annual Review of Astronomy & Astrophysics* 42, 517-548.
- [Thompson and Schmieder (1991)] Thompson, W.T. & Schmieder, B. 1991, *Astron. Astrophys.*, 242, 501
- [Tripathi et al. (2009)] Tripathi, D., Isobe, H. & Jain, R. (2009), *Space Science Reviews*, 149, 283
- [Tsubaki et al. (1988)] Tsubaki, T., Toyoda, R., Suematsu, Y. & Gamboa, G.A.R. 1988, *Publ. Astron. Soc. Japan*, 40, 121
- [Tsubaki and Takeuchi. (1986)] Tsubaki, T. & Takeuchi, A. 1986, *Solar Phys.*, 104, 313
- [Uchida (1967)] Uchida, Y. 1967, *Astrophys. J.*, 147, 181
- [Van Driel-Gesztelyi & Culhane (2009)] Van Driel-Gesztelyi, L. & Culhane, J.L., (2009), *The Origin and Dynamics of Solar Magnetism, Space Sciences Series* 32, 351.
- [Vernazza et al. 1981] Vernazza, J.E., Avrett, E.H., & Loeser, R. 1981, *Astronomical Journal Supplement Series* 45, 635-721.
- [Vial, (1998)] Vial, J. C. 1998, in *Astronomical Society of the Pacific, Conference Series*, Vol. 150, IAU Colloq.167: perspectives in Solar Prominences, ed. D. F. Webb, B. Schmieder & D. M. Rust, 175.
- [Wentzel, (1978)] Wentzel, D. G. 1978, *Solar Phys.*, 58, 307-318
- [Yi & Engvold (1991)] Yi, Z. & Engvold, O. (1991) *Solar Phys.*, 134, 275
- [Yi et al. (1991)] Yi, Z., Engvold, O. & Keil, S. L. (1991) *Solar Phys.*, 132, 63
- [Zaqarashvili et al. (2012)] Zaqarashvili, T.V., Carbonell, M., Ballester, J.L. & Khodachenko, M.L., 2012, *Astron. Astrophys.*, 544, 143

BIBLIOGRAPHY

- [Zaqarashvili et al. (2011)] Zaqarashvili, T.V., Khodachenko, M.L. & Rucker, H. O., 2011, *Astron. Astrophys.*, 529, A82
- [Zirker et al. (1998)] Zirker, J.B., Engvold, O. & Martin, S.F., 1998, *Nature*, 396, 440